2012

The GluK4 Kainate Receptor Subunit Regulates Mood, Memory and Excitotoxic Neurodegeneration

Emily Rhodes Lowry

THE GLUK4 KAINATE RECEPTOR SUBUNIT REGULATES MOOD, MEMORY, AND EXCITOTOXIC NEURODEGENERATION

A Thesis Presented to the Faculty of

The Rockefeller University

in Partial Fulfillment of the Requirements for

the degree of Doctor of Philosophy

by

Emily Rhodes Lowry

June 2012

THE GLUK4 KAINATE RECEPTOR SUBUNIT REGULATES MOOD, MEMORY, AND EXCITOTOXIC NEURODEGENERATION

Emily Rhodes Lowry, Ph.D.

The Rockefeller University 2012

Though the GluK4 kainate receptor subunit shows limited homology and a restricted expression pattern relative to other kainate receptor subunits, its ablation results in distinct behavioral and molecular phenotypes.

To study the function of GluK4, I generated a global GluK4 knockout mouse line by crossing a germline-expressed cre transgenic mouse line with a GluK4-floxed mouse line in which exon 16 of GRIK4, the gene encoding GluK4, was flanked by lox-P sites (floxed). Thorough characterization of GluK4 expression in the resulting knockout mice using RT-PCR and a custom-designed anti-GluK4 antibody revealed that GRIK4 mRNA expression persisted though GluK4 protein expression was ablated.

In keeping with genome-wide studies in humans that have implicated GluK4 in bipolar disorder and schizophrenia, I found that GluK4 mice displayed reduced anxiety, increased risk-taking behavior, reduced depressive behavior, impaired sensorimotor gating, and hyperlocomotion relative to wild-type mice. GluK4 knockout mice also demonstrated impaired fear memory and spatial memory.

Furthermore, my findings indicate that GluK4 is a key mediator of excitotoxic neurodegeneration: GluK4 knockout mice showed robust neuroprotection in the Cornu Ammonis 3 (CA3) region of the hippocampus following intrahippocampal injection of kainate, a potent excitotoxin, and widespread neuroprotection throughout the hippocampus following hypoxia-ischemia. Molecular and biochemical analysis of kainate- and sham-treated wild-type and GluK4 knockout hippocampal tissue revealed that GluK4 may act through the c-Jun N-terminal Kinase (JNK) pathway to regulate the molecular cascades that lead to excitotoxicity. Finally, I found preliminary evidence to suggest that GluK4 may regulate hippocampal seizure activity following intraperitoneal injection of kainate.

Together, these findings suggest that GluK4 may be relevant to the understanding and treatment of human neuropsychiatric and neurodegenerative disorders.

To my family.

ACKNOWLEDGEMENTS

Much of the work described herein was performed in collaboration with Anna Kruyer, a fellow graduate student in the Strickland lab. Once she joined me on this project, the quality and efficiency with which experiments were executed increased exponentially. Her dynamic insight and deft bench skills were invaluable, as were her good humor and persistence in the face of disaster. Many of these experiments were two-person jobs; Anna often quietly took on the work of four.

My mentor Sid Strickland gave me the latitude that I needed to pursue far-fetched ideas, and reigned me back in if I got off-course without saying I-told-you-so. His good humor, coupled with his sincere interest in his lab members, fostered such a welcoming lab environment that I knew I wanted to join his lab very quickly after starting my rotation there. (Unfortunately, I don't think we'll ever see eye-to-eye on baseball.) I am also grateful to the other members of my faculty committee, Jeff Friedman, Leslie Voshall, and Charles Inturrisi, for adding levity along with insight to our meetings.

Zu-Lin Chen, Wei Ming Yu, Dasha Zamolodchikov, Moses Feaster, Erin Norris, and Rajani Maya – lab-mates past and present – were all wonderfully patient teachers. Jot Singh, Joe Luna, and Marta Cortes-Cantelli served as sounding boards at crucial moments.

I wouldn't be where I am today without the mentorship of Dr. Allan Basbaum, Dr. Peter Balsam, Dr. Kathleen Taylor, or Dr. Stephen Rayport, all of whom taught me about the importance of scientific rigor and lateral thinking.

Finally, I am endlessly thankful for the unwavering support of my family and friends, who saw me through the worst – and helped me appreciate the best – of my graduate career.

TABLE OF CONTENTS

LIST OF FIGURES

LIST OF TABLES

LIST OF ABBREVIATIONS

AMPA	α-amino-3-hydroxy-5-methyl-4-isoxazolepropionic acid
CA1	Cornu Ammonis 1
CA2	Cornu Ammonis 2
CA3	Cornu Ammonis 3
CNS	central nervous system
DAVID	Database for Annotation, Visualization and Integrated Discovery
DG	dentate gyrus
DRG	dorsal root ganglion
EPSC	excitatory post-synaptic current
FJC	Fluorojade C
F_R	floxed, recombined
GABA	g-Aminobutyric Acid
GSEA	Gene Set Enrichment Analysis
HI	hypoxia-ischemia
IH	intrahippocampal(ly)
IP	intraperitoneal(ly)
ISI	inter-stimulus interval
JNK	c-Jun N-terminal Kinase
LTP	long-term potentiation
MCAO	middle cerebral artery occlusion
mTLE	medial temporal lobe epilepsy
MWM	Morris Water Maze
NMDA	N-methyl-D-aspartate
PPI	prepulse inhibition
PSD-95	post-synaptic density protein 95

CHAPTER 1: INTRODUCTION

Glutamate is the principal excitatory neurotransmitter in the central nervous system (CNS), and imbalances in glutamatergic transmission have profound behavioral and physiological consequences. Hypoactivity of the glutamate system has been implicated in human affective disorders such as schizophrenia, based initially on clinical observations that glutamate antagonists can mimic certain symptoms of the disease (Krystal et al., 1994). Conversely, hyperactivity of the glutamate system can result in excitotoxic neurodegeneration, a form of neuronal cell death that often accompanies ischemic stroke (Lucas and Newhouse, 1957; Olney, 1969).

Glutamate Receptor Physiology

Both normal and pathological aspects of excitatory neurotransmission are contingent upon the interactions between glutamate and its receptors. Glutamate receptors can be broadly classified as metabotropic or ionotropic. Metabotropic receptors are G-protein-coupled, and ligand binding results in the activation of downstream signaling pathways. Ionotropic receptors are ligand-gated ion channels. Three subtypes of ionotropic receptors – N-methyl-D-aspartate (NMDA), α-amino-3-hydroxy-5-methyl-4-isoxazolepropionic acid (AMPA), and kainate receptors – were initially distinguished by the eponymous glutamate analogs for which they show the highest affinity (Lodge, 2009). Though kainate receptors were the last of the three subtypes to be identified (Bettler et al., 1990), pharmacological isolation of kainate receptor activity from that of NMDA and

AMPA receptors *in vitro,* coupled with the genetic ablation of kainate receptor subunits *in vivo,* have indicated that they play an essential role in regulating the overall excitability of neuronal networks.

Like AMPA and NMDA receptors, kainate receptors are permeable to sodium, potassium, and calcium, though permeability to the latter varies with kainate receptor subunit mRNA editing (Köhler et al., 1993). Nevertheless, kainate receptors display a distinct electrophysiological profile upon activation: they mediate excitatory post-synaptic currents (EPSCs) of smaller amplitude than AMPA or NMDA receptors, with slow decay kinetics (Castillo et al., 1997; Vignes and Collingridge, 1997). In response to repetitive stimulation, these postsynaptic kainate receptors contribute to temporal summation of synaptic input, where EPSC amplitude increases progressively after each stimulus and neuronal excitability is enhanced (Frerking and Ohliger-Frerking, 2002). Kainate receptors are also located pre-synaptically, where they act as autoreceptors. At glutamatergic synapses, presynaptic kainate receptors modulate excitatory transmission by facilitating or depressing glutamate release. At γ-Aminobutyric Acid (GABA)-ergic synapses, presynaptic kainate receptors modulate inhibitory transmission by facilitating or depressing the release of the inhibitor neurotransmitter GABA (Rodriguez-Moreno et al., 1997; Schmitz et al., 2000; Cossart et al., 2001). Furthermore, there is a growing body of evidence to suggest that kainate receptors can act in a non-canonical, metabotropic fashion. For instance, kainate receptors can control the excitability of hippocampal

pyramidal cells by inhibiting slow afterhyperpolarization (sAHP) (Melyan et al., 2002), a post-synaptic, Ca^{2+}-dependent K^+ current that occurs after burst firing to limit further action potentials. The inhibition of sAHP by kainate receptors is independent of ionotropic action, and acts through a metabotropic signaling cascade (Melyan et al., 2002; Melyan and Lancaster, 2004). Thus, through their many, disparate functions, kainate receptors serve to fine-tune network excitability, synaptic plasticity, and, potentially, cognition.

Kainate Receptor Subunits

The function of kainate receptors is further specified by their subunit composition. The five kainate receptor subunit types – GluK1-5 – assemble as tetramers and share the same general secondary structure: an extracellular N-terminal domain; a transmembrane domain (M1); a p-loop (M2) domain that begins on the cytoplasmic face of the cell membrane and penetrates the membrane without traversing it, then re-emerges on the cytoplasmic face; a second and third transmembrane domain (M3 and M4); and, finally, the cytoplasmic C-terminal domain (Oswald et al., 2007) (Figure 1.1). The ligand-binding domain is comprised of the domain (S1) that falls between the N-terminal domain and the M1 domain, and the loop (S2) between M3 and M4 (Hollmann et al., 1994; Wo and Oswald, 1994). The N-terminal domain regulates subunit assembly (Leuschner and Hoch, 1999), the p-loop forms the receptor pore (Hughes, 1994), and the C-terminal domain contains *cis*-acting regulatory elements that can promote forward trafficking in the case of GluK2 and GluK3 (Yan et al., 2004), or

endoplasmic reticulum retention in the case of GluK1 and GluK5 (Ren et al., 2003; Nasu-Nishimura et al., 2006). Depending on the subunit type, the C-terminal domain can interact with several subsets of auxiliary proteins to regulate receptor trafficking, to stabilize receptors at the synapse, or to modify channel gating (Coussen and Mulle, 2006).

Despite the similarities in their secondary structures, kainate receptor subunits differ in their agonist affinities: GluK1-3 have low-affinity agonist binding sites (K_d in the micromolar range), while GluK4 and GluK5 have high-affinity sites (K_d in the nanomolar range) (London and Coyle, 1979; Hampson et al., 1987). Furthermore, GluK4 and GluK5 share 68% sequence homology with each other, but only 45% with GluK1-3 (Werner et al., 1991; Herb et al., 1992; Sakimura et al., 1992). Low-affinity subunits can co-assemble to form functional homologous receptors, while high-affinity subunits must assemble with low-affinity subunits, as this conformation sterically hinders the endoplasmic reticulum retention motif that prevents high-affinity subunits from reaching the cell surface on their own (Herb et al., 1992; Sakimura et al., 1992).

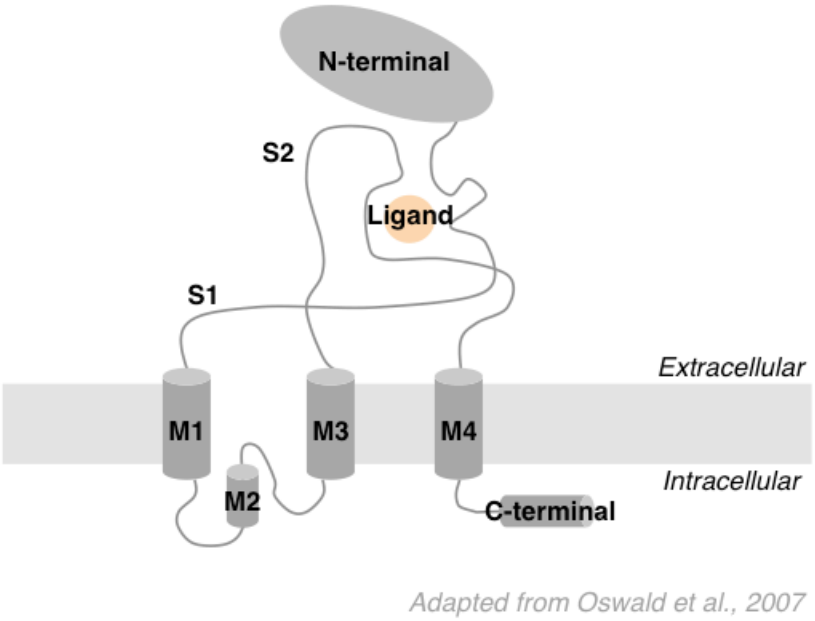

FIGURE 1.1. General kainate receptor subunit structure. Kainate receptor subunits have three transmembrane domains, M1, M2, and M3. Interspersed between M1 and M3 is the pore-forming p-loop domain, M2. S1 and S2 form the ligand-binding domain. The N-terminal regulates subunit assembly, and the C-terminal mediates receptor trafficking.

The GluK4 Kainate Receptor Subunit

Unlike the other high-affinity subunit, GluK5, which is expressed throughout the CNS (Herb et al., 1992), GluK4 mRNA and protein expression are largely restricted to the CA3 region of the hippocampus (Werner et al., 1991; Darstein et al., 2003) (Figure 1.2a). Within the CA3, GluK4 mRNA is localized to the pyramidal cell layer, while GluK4 protein is localized to the stratum lucidum (Werner et al., 1991; Darstein et al., 2003). The stratum lucidum is comprised of the axons arising from granule cells in the dentate gyrus (DG) region of the hippocampus, and their synapses onto CA3 pyramidal cell dendrites (Amaral and Witter, 1989). The association between DG granule cells and CA3 pyramidal cells is known as the mossy fiber pathway (Amaral and Witter, 1989) (Figure 1.2b). CA3 pyramidal cells then project to the Cornu Ammonis 1 (CA1) region of the hippocampus via Schaffer collaterals, or form recurrent collaterals within the stratum oriens of the CA3 (Amaral and Witter, 1989) (Figure 1.2b). Pyramidal cells within the CA3 also receive input from the entorhinal cortex (EC) through the perforant path (Lopes da Silva and Arnolds, 1978).

Outside of the CA3, GluK4 protein also shows limited expression within the polymorphic layer (hilus) of the DG region of the hippocampus, the pyramidal layer of the CA1 region of the hippocampus, Purkinje cells in the cerebellum, scattered neurons in layers II and V of the cortex, and the central terminals of dorsal root ganglion (DRG) neurons in the spinal dorsal horn (Fogarty et al., 2000; Darstein et al., 2003; Lucifora et al., 2006) (Figure 1.2a).

Within the hippocampus, GluK4 co-precipitates with GluK2, but not GluK3, and is expressed both pre- and post-synaptically (Darstein et al., 2003).

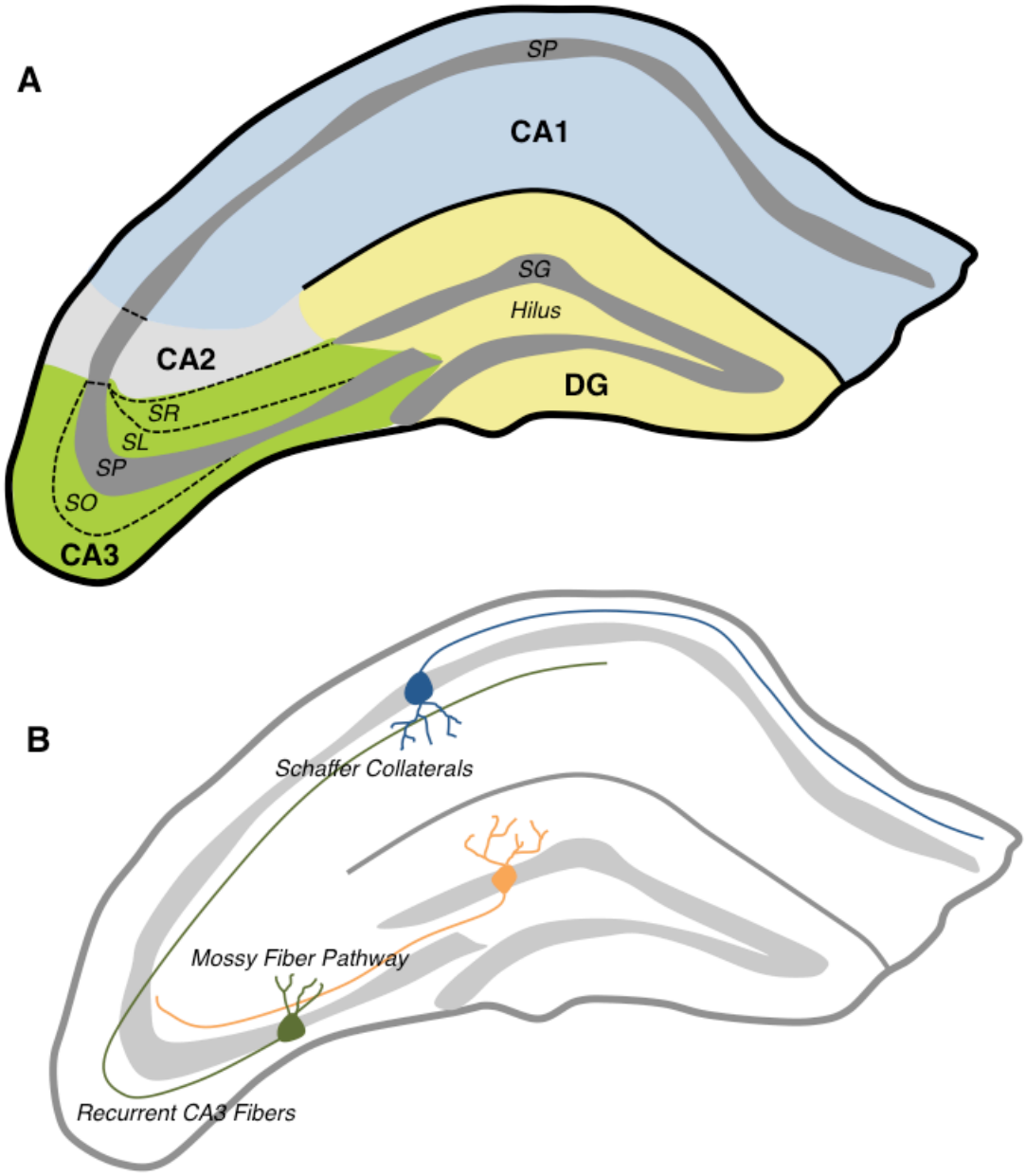

FIGURE 1.2. Hippocampal subregions and connectivity. **(A)** The hippocampus is comprised of 4 major subregions: Cornu Ammonis 1 (CA1; blue), Cornu Ammonis 2 (CA2; light gray), Cornu Ammonis 3 (CA3; green), and dentate gyrus (DG; yellow). Pyramidal cells form the stratum pyramidal (SP) of the CA1, CA2, and CA3 subregions. Dentate granule cells form the stratum granulosum (SG) of the dentate gyrus. The stratum oriens (SO), stratum lucidum (SL), and stratum radiatum (SR) are indicated for the CA3, and contain various fibers of passage. **(B)** Mossy fibers originating from the SG synapse onto pyramidal cell fibers in the SL to form the mossy fiber pathway. Pyramidal cells within the CA3 can form recurrent connections. Projections from the CA3 to the CA1 form the Schaffer collaterals.

The restricted expression pattern of GluK4 suggests that receptors containing this subunit may have distinct signaling properties and physiological functions. Initial electrophysiological studies using GluK4 knockout mice have revealed that GluK4 ablation results in both pre- and post-synaptic deficits. The mossy fiber presynaptic fiber volley induced by kainate, a strong kainate receptor agonist, is reduced in GluK4 knockout mice relative to wild-type mice (Catches et al., 2012). GluK4 knockout mice also display decreased EPSC amplitude (Fernandes et al., 2009) and impaired mossy fiber long-term potentiation (LTP) (Catches et al., 2012). Meanwhile, mossy fiber LTP is decreased in GluK4/GluK5 double-knockout mice (Fernandes et al., 2009), but unaffected in GluK5 knockout mice (Contractor et al., 2003), indicating that GluK4 plays a key role in LTP.

GluK4 in Learning and Memory

LTP, a form of synaptic plasticity, occurs when synaptic transmission is enhanced between a pre- and post-synaptic cell (Bliss and Collingridge, 1993). According to classical Hebbian theory, this process constitutes the cellular basis of learning and memory (Brown et al., 1990). LTP is typically dependent on ionotropic NMDA receptor activity (Morris, 2003); however, LTP at mossy fiber synapses within the CA3 is unique in that it is largely NMDA receptor-independent, and is instead mediated by kainate receptors (Bortolotto et al., 2003). Previous studies in which the mossy fiber pathway has been disrupted in mice by chemical inactivation or frank lesions to the CA3 have demonstrated the importance of this region to several learning and memory paradigms, including

fear conditioning and the Morris Water Maze (MWM) (Stupien et al., 2003; Florian and Roullet, 2004; Kesner, 2007).

Given the importance of GluK4 to mossy fiber LTP, and the importance of mossy fiber LTP to learning and memory, I sought to elucidate the role of GluK4 in memory. First, I generated a global GluK4 knockout mouse line by crossing a transgenic cre line in which cre is expressed in germline cells (The Jackson Laboratory), and a second mouse line in which exon 16 of *GRIK4*, the gene encoding GluK4, was floxed (a generous gift of the Contractor Laboratory at Northwestern University) (Fernandes et al., 2009). Though *GRIK4* mRNA expression persisted in this line, GluK4 protein expression was undetectable. I then compared the performance of wild-type and GluK4 knockout mice in a battery of memory-based tasks. I found, using two forms of a Y-maze task, that short-term working memory was intact in GluK4 knockout animals. However, GluK4 knockout animals showed impaired fear memory acquisition during a fear conditioning task, and impaired spatial memory acquisition and recall during a MWM task. GluK4 is therefore essential to certain types of associative, but not working, learning and memory.

GluK4 in Neuropsychiatric Disorders

Learning and memory deficits are often co-morbid with mood disorders (Palomo et al., 2008), and, indeed, there is mounting evidence from human and animal studies to suggest a role for aberrant GluK4 expression in schizophrenia and bipolar disorder. Expression of the NMDA receptor subunit NMDAR1, the AMPA

subunit GluR1, and the kainate subunits GluK3 and GluK4 were all found to be decreased at the mRNA level in post-mortem brain tissue from schizophrenics relative to tissue from normal controls (Porter et al., 1997; Sokolov, 1998). Neuroleptic treatment in schizophrenic patients restored subunit expression to normal levels (Sokolov, 1998). Additionally, a genome-wide association study identified separate single-nucleotide polymorphisms (SNPs) in *GRIK4*, the gene encoding the ionotropic glutamate kainate receptor subunit GluK4, that confer susceptibility to schizophrenia and protection against bipolar disorder, respectively (Pickard et al., 2006). This association study was initially undertaken on the basis of clinical observations in a schizophrenic patient who was found to have a chromosomal breakpoint that disrupted *GRIK4* (Pickard et al., 2006). Furthermore, a deletion mutation within the 3' untranslated region (UTR) of *GRIK4* not only confers protection against bipolar disorder (Pickard et al., 2008), but also increases GluK4 mRNA and protein expression (Pickard et al., 2008; Knight et al., 2011), and enhances hippocampal activation during a face processing task as assessed by function magnetic resonance imaging (Whalley et al., 2009a). Finally, GluK2, the kainate receptor subunit that co-precipitates with GluK4 in the CA3, has also been implicated in bipolar disorder: GluK2 knockout mice display a complex behavioral phenotype that is consistent with certain facets of the disorder.

Taken together, these data suggest that deficits in GluK4 expression may contribute to the etiology of schizophrenia and bipolar disorder. I therefore sought

to characterize the phenotype of the GluK4 knockout mouse line in behavioral tasks relating to mood and affect. I found that GluK4 knockout mice show increased exploration of the anxiogenic center zone of an open field, decreased arousal in an acoustic startle test, and decreased immobility in a forced swim test relative to wild-type mice, suggesting that GluK4 may mediate anxiety and depression. Additionally, GluK4 knockout mice showed increased locomotion relative to wild-type mice, which phenocopies the psychomotor agitation observed in schizophrenia and bipolar disorder. GluK4 mice also exhibited decreased prepulse inhibition (PPI), an indication of impaired sensorimotor gating and a hallmark of patients with schizophrenia and patients in the manic phase of bipolar disorder (Perry and Braff, 1994; Perry et al., 2001).

GluK4 in Excitotoxicity

In contrast to behavioral disorders such as schizophrenia, which are associated with insufficient glutamatergic neurotransmission, excitotoxic neurodegeneration occurs under pathological conditions where there is excessive glutamate release, such as ischemia and, on a much slower time scale, Alzheimer's disease (Jacob et al., 2007). The CA3 region of the hippocampus, where GluK4 expression is greatest, is highly – and selectively – vulnerable to cell death in some models of excitotoxicity (Nadler, 1981; Ben-Ari, 1985). Thus, I reasoned that GluK4 might be involved in excitotoxic neuronal death. Indeed, GluK4 ablation was neuroprotective in the CA3 following intrahippocampal (IH) kainate injections. Following hypoxia-ischemia (HI), a murine model of stroke in which animals are

subjected to unilateral common carotid artery transection and prolonged hypoxia, GluK4 knockout mice showed marked neuroprotection throughout the hippocampus.

Using microdissected CA3 tissue from wild-type and GluK4 knockout animals that had been injected with kainate or vehicle control (phosphate-buffered saline; PBS), I performed a microarray experiment to analyze the downstream effectors of GluK4 following excitotoxic insult, and to probe the molecular underpinnings of neuroprotection in GluK4 knockout animals. From these data and subsequent biochemical analysis, I found that several pro-apoptotic pathways, most notably the JNK pathway, were selectively up-regulated in wild-type, but not GluK4 knockout tissue, following kainate injection. The JNK pathway has been widely implicated in excitotoxic cell death. Mice deficient in JNK3, the neuronal isoform of JNK, show strong resistance to neurodegeneration following middle cerebral artery occlusion (MCAO), a murine model of ischemia, and to intraperitoneal (IP) kainate injection (Brecht et al., 2005). Peptides and small molecules that target various components of the JNK pathway are also effective in preventing neurodegeneration following MCAO (Bogoyevitch et al., 2004). Furthermore, the GluK2 and GluK5 kainate receptor subunits can directly activate the JNK pathway by forming a signaling complex with post-synaptic density protein 95 (PSD-95) and mixed lineage kinase 3 (MLK3) (Tian et al., 2005; Jiang et al., 2007). In the context of ischemia, the assembly of this signaling complex promotes MLK3 autophosphorylation and thereby initiates the kinase cascade

that leads to JNK activation (Liu et al., 2006). It is therefore likely that GluK4 activation leads to excitotoxic neurodegeneration through the JNK pathway.

Furthermore, I found that JNK pathway activation was increased following vehicle injection in GluK4 mice compared to wild-type mice, indicating that GluK4 could play a dual role in JNK pathway activation: under basal conditions, GluK4 may suppress JNK pathway activation, while under excitotoxic conditions, GluK4 may promote JNK pathway activation. The precise nature of the relationship between GluK4 and JNK pathway activation remains to be fully elucidated; however, I propose several lines of reasoning that may underlie my observations.

GluK4 in Seizure Generation

In addition to triggering excitotoxic neurodegeneration, excessive glutamate release is thought to underlie medial temporal lobe epilepsy (mTLE) (Sharma et al., 2007). Kainate administration recapitulates many of the features of mTLE, including convulsions, hippocampal lesions, and mossy fiber sprouting, suggesting that kainate receptors may play a role in the pathogenesis of this disease (Sharma et al., 2007). Furthermore, GluK2 knockout mice are resistant to kainate-induced seizures (Mulle et al., 1998). I therefore investigated seizure susceptibility in GluK4 knockout mice relative to wild-type mice, but found that the paradigm used to instigate and evaluate seizure activity was too variable to yield significant results. Nevertheless, trends in the data suggest that GluK4 knockout mice may be less susceptible to seizures than wild-type mice at high

doses of kainate, but more susceptible to seizures at low doses of kainate. These observations suggest another biphasic role for GluK4, where it may serve to suppress seizure activity under mildly seizurogenic conditions, but may promote seizure activity under highly seizurogenic conditions.

The work described herein reveals that a single glutamate receptor subunit with highly restricted expression serves as a key modulator of anxiety, depressive-like behavior, memory, and sensorimotor gating on one hand, and excitotoxic cell death cascades on the other. GluK4 may therefore provide a foothold in understanding the mechanisms – and treatment – of human neuropsychiatric and neurodegenerative disorders.

CHAPTER 2: MATERIALS AND METHODS

Animal Use

For all experiments, mice were 8 – 12 week old males maintained on a 12-hour light/dark cycle with food and water provided *ad libitum*. All animal procedures were approved by the Institutional Animal Care and Use Committee at the Rockefeller University.

Genotyping

GRIK4 recombination was assessed in DNA preparations from tail samples of wild-type and GluK4 knockout animals using the primers detailed in Table 2.1 and the following polymerase chain reaction (PCR) conditions: 3 minutes at 94˚C; 30 seconds at 94˚C, 30 seconds at 62˚C, and 30 seconds at 72˚C repeated for 35 consecutive cycles; and finally 8 minutes at 72˚C. These same primers and PCR conditions were also used to assess recombination of the *GRIK4* allele in DNA preparations of lung and hippocampus tissue.

To assess the presence of the Cre transgene in the F1 generation of GluK4 knockout animals, the primers detailed in Table 2.1 and the following PCR conditions were used: 3 minutes at 94˚C; 30 seconds at 94˚C, 1 minute at 51˚C, and 1 minute at 72˚C repeated for 35 consecutive cycles; and 2 minutes at 72˚C.

TABLE 2.1. GluK4- and cre-specific primers used to genotype GluK4 knockout mice

Primer name	Purpose	Sequence
GluK4 P1	Assessing recombination of *GRIK4* allele	GCAGGCTGAACTCTGAGTTT
GluK4 P2	Assessing recombination of *GRIK4* allele	CCAGAGACAGCACTAGGTGC
GluK4 P6	Assessing recombination of *GRIK4* allele	GCCTGGGCTAGAGTGAGAC
Cre forward	Assessing presence of Cre transgene	CCGGTGAACGTGCAAAACAGGCTCTA
Cre reverse	Assessing presence of Cre transgene	CTTCCAGGCGCGAGTTGATAGC

GRIK4 *RT-PCR*

GRIK4 mRNA expression in wild-type versus GluK4 knockout animals was expressed by quantitative (q) and non-quantitative reverse-transcriptase (RT) PCR. mRNA was extracted from fresh-dissected hippocampal tissue using TRIzol (Ambion) according to the manufacturer's instructions, and resuspended in nuclease-free water. Samples were then DNAse-treated using a DNA-free kit (Ambion). cDNA was synthesized from the purified RNA samples using a Superscript III kit (Invitrogen) according to the manufacturer's instructions, with the following specifications: for non-quantitative RT-PCR, random hexamers were used as primers, and 0.1M DTT was added to the reaction; for real-time qRT-PCR, dNTPs were used as primers and DTT was excluded from the reaction. dNTPs were used for quantitative PCR because they selectively amplify poly-adenylated (i.e., mature) RNA. Meanwhile, the purpose of the non-quantitative PCR experiment was to determine whether any RNA – mature or not – was produced in GluK4 knockout animals, so I chose to use random hexamers, which do not distinguish between immature and mature RNA in these experiments. DTT acts as an enzyme stabilizing agent in RT-PCR reactions, but

can interfere with downstream reactions involving SYBR-green and was therefore excluded from real-time qRT-PCR experiments. For both quantitative and non-quantitative reactions, the following PCR conditions were used to generate cDNA from the template RNA samples: 50 minutes at 50˚C; 5 minutes at 85˚C, after which RNAse H was added to each reaction to remove any remaining template RNA; and 20 minutes at 37˚C. Reactions in which reverse transcriptase was omitted were used as negative controls.

For non-quantitative experiments, PCR reactions were carried out using a standard PCR machine (Eppendorf). The primers used were designed to amplify distinct, 200 – 300 base pair (bp) regions of GluK4 transcript such that all regions of the transcript were represented (Table 2.2). Each primer set was used in a separate reaction mixture with wild-type or GluK4 knockout template cDNA, or negative controls. All reactions were amplified at the same time using the following PCR conditions: 3 minutes at 94˚C; 30 seconds at 94˚C, 1 minute at 55˚C, and 30 seconds at 72˚C repeated for 25 cycles; and 10 minutes at 72˚C. Reaction products were run on a 2% agarose gel and visualized by UV transillumination.

TABLE 2.2. Primers used to assess *GRIK4* expression using non-quantitative RT-PCR in wild-type and GluK4 knockout mice

Primer name	Purpose	Sequence
GluK4 exons 2 to 4 forward	Non-quantitative analysis of *GRIK4* mRNA expression, exons 2 to 4	TTCTGGTTCTCATTGTCCCG
GluK4 exons 2 to 4 reverse	Non-quantitative analysis of *GRIK4* mRNA expression, exons 2 to 4	AAGATGTCCACTTCGACCTTG
GluK4 exons 4 to 6 forward	Non-quantitative analysis of *GRIK4* mRNA expression, exons 4 to 6	AGGTCGAAGTGGACATCTTTG
GluK4 exons 4 to 6 reverse	Non-quantitative analysis of *GRIK4* mRNA expression, exons 4 to 6	GGTGAATCTCTGGAGTTGGAAC
GluK4 exons 6 to 8 forward	Non-quantitative analysis of *GRIK4* mRNA expression, exons 6 to 8	CCAGCAACACCGACATCA
GluK4 exons 6 to 8 reverse	Non-quantitative analysis of *GRIK4* mRNA expression, exons 6 to 8	GACACCATCCCCAGTTCAG
GluK4 exons 7 to 9 forward	Non-quantitative analysis of *GRIK4* mRNA expression, exons 7 to 9	CGGGATGACAAGACAGCTAC
GluK4 exons 7 to 9 reverse	Non-quantitative analysis of *GRIK4* mRNA expression, exons 7 to 9	GCATGGGATTGGTTGAAAATGG
GluK4 exons 9 to 11 forward	Non-quantitative analysis of *GRIK4* mRNA expression, exons 9 to 11	AGAACTGTGACCATGTGCC
GluK4 exons 9 to 11 reverse	Non-quantitative analysis of *GRIK4* mRNA expression, exons 9 to 11	ACCTTCCAATTCTACCATGCG
GluK4 exons 10 to 13 forward	Non-quantitative analysis of *GRIK4* mRNA expression, exons 10 to 13	CAGCCTCATGAACTACCTTCG
GluK4 exons 10 to 13 reverse	Non-quantitative analysis of *GRIK4* mRNA expression, exons 10 to 13	TCATTGCCTTCCATCTCCTG
GluK4 exons 13 to 15 forward	Non-quantitative analysis of *GRIK4* mRNA expression, exons 13 to 15	AAGGCAATGACCGATATGAGG
GluK4 exons 13 to 15 reverse	Non-quantitative analysis of *GRIK4* mRNA expression, exons 13 to 15	CTGCGTCCCATATGAACTCTG
GluK4 exons 15 to 16 forward	Non-quantitative analysis of *GRIK4* mRNA expression, exons 15 to 16	CTTCTAGCTTATCTGGCGGTC
GluK4 exons 15 to 16 reverse	Non-quantitative analysis of *GRIK4* mRNA expression, exons 15 to 16	ACACAGCGGGTAGACAAAG
GluK4 exons 16 to 17 forward	Non-quantitative analysis of *GRIK4* mRNA expression, exons 16 to 17	CGGTGTAATCTCCTGGTCAAC
GluK4 exons 16 to 17 reverse	Non-quantitative analysis of *GRIK4* mRNA expression, exons 16 to 17	ATACTCAATGGCAGTCTGGTC
GluK4 exons 18 to 20 forward	Non-quantitative analysis of *GRIK4* mRNA expression, exons 18 to 20	AAGGGCTATGGGATTGGC
GluK4 exons 18 to 20 reverse	Non-quantitative analysis of *GRIK4* mRNA expression, exons 18 to 20	CTGATGCTTCTGAGTGTCTGAG

For quantitative experiments, the PCR reactions were carried out using a Lightcycler 480 (Roche). Each reaction contained wild-type or GluK4 knockout cDNA, or negative controls. Primers used are outlined in Table 2.3, and were designed to amplify regions upstream, downstream, and surrounding exon 16 of *GRIK4* mRNA. SYBR green (Applied Biosystems) was used as an index of PCR product amplification. All reactions were performed in triplicate. Crossing threshold (CT) values were averaged between technical replicates, and normalized to reactions in which the appropriate cDNA template was amplified using primers specific for mouse β-actin (Table 2.3). All subsequent analysis of fold-change was performed using REST-MCS software (Pfaffl et al., 2002).

TABLE 2.3. Primers used to assess *GRIK4* expression using quantitative RT-PCR in wild-type and GluK4 knockout mice.

Primer name	Purpose	Sequence
GluK4 exons 3 to 4 forward	Quantitative analysis of *GRIK4* mRNA expression, exons 3 to 4	TCCTGCTTGGCTCTTGAT
GluK4 exons 3 to 4 reverse	Quantitative analysis of *GRIK4* mRNA expression, exons 3 to 4	GCGGTTGATACGGTTCTTGG
GluK4 exon 16 forward	Quantitative analysis of *GRIK4* mRNA expression, exon 16	CGGTGTAATCTCCTGGTCAAC
GluK4 exon 16 reverse	Quantitative analysis of *GRIK4* mRNA expression, exon 16	ACACAGCGGGTAGACAAAG
GluK4 exons 20 to 21 forward	Quantitative analysis of *GRIK4* mRNA expression, exons 20 to 21	TCTTTGTGGTTCTTATTTGTGGC
GluK4 exons 20 to 21 reverse	Quantitative analysis of *GRIK4* mRNA expression, exons 20 to 21	CAGTTCTGTCACCATCTCCTG
Mouse β-actin	Normalization	CTAAGGCCAACCGTGAAAAG
Mouse β-actin	Normalization	ACCAGAGGCATACAGGGACA

GRIK4 *mRNA Size Assessment and Sequencing*

Purified hippocampal cDNA from 3 wild-type and 3 GluK4 knockout animals was amplified by PCR using a forward primer targeted against the sense strand of exon 13 (see Table 2.2, primer “GluK4 exons 13 to 15 forward”), and a reverse primer targeted against the anti-sense strand of exon 20 (see Table 2.2, primer “GluK4 exons 18 to 20 reverse”). The PCR conditions were as follows: 5 minutes at 95˚C; 1 minute at 54˚C; 3 minutes at 72˚C; 30 seconds at 95˚C, 1 minute at 54˚C, and 2 minutes at 72˚C, repeated for 35 cycles; and 2 minutes at 72˚C. The resulting PCR products were run on an agarose gel to compare the size of wild-type versus GluK4 knockout transcript.

Wild-type and GluK4 knockout PCR products were also sequenced by an outside facility (Genewiz) using the forward primer, and, in separate reactions, the reverse primer to generate ~1000 bp sequences. Sequences were aligned to the known *GRIK4* mRNA sequence (RefSeq Accession number NM_175481.3) using DNASTAR software.

Generation of Custom Anti-GluK4 Antibody

A custom GluK4 antibody was generated in rabbits at an outside facility (Covance) using an immunizing peptide corresponding to amino acids 939 – 956 of the C terminal end of the mouse GluK4 protein, SPARSEESLEWDKTTNSSEPE. The resulting immune sera were purified against the immunizing peptide to ensure optimal specificity.

Western Blotting to Detect GluK4

Fresh-dissected hippocampi from wild-type and GluK4 knockout mice were homogenized in lysis buffer (25 mM Tris-Cl pH 7.4, 95 mM NaCl, 2% SDS, 10 mM EDTA) supplemented with protease and phosphatase inhibitor cocktails (Sigma). Protein concentration was determined by spectrophotometer using a bicinchonic acid (BCA) kit (Thermoscientific) according to the manufacturer's instructions. Samples were treated with mercaptoethanol and boiled for 5 minutes at 100˚C. Samples were then run on a denaturing 6% Tris-Glycine gel, transferred to a PVDF membrane, and blocked in a 5% milk solution dissolved in Tris-buffered saline with Tween-20. Blots were probed with either the custom-generated GluK4 antibody (1:2000) or an Abcam GluK4 antibody (ab10101; 1:2000). Following overnight incubation in primary antibody, blots were washed, incubated in the appropriate secondary antibody, washed again, incubated in chemiluminescent reagent (PerkinElmer), and exposed to film. Band intensity was quantified using Adobe Photoshop software and normalized to GAPDH (1:2000, 5% bovine serum albumen; Abcam) from the same blot.

Novel-arm Y-maze

For this and all subsequent behavioral trials, animals were single-housed in the room in which they were to be tested for at least 5 days prior to the initiation of the trials, and experimenters were blind to the genotype of the animals during testing and scoring.

Mice were placed in a 3-armed Y-maze in which one arm was closed off by an opaque barrier, and allowed to explore for 5 minutes. The mice were then removed from the maze and placed in their home cage for 2 minutes, during which time the barrier was removed from the third arm and the bedding in the maze was mixed. Finally, mice were placed back in the maze and observed for 5 minutes. The percent time spent in each arm once the barrier was removed was scored using Ethovision software (Noldus) and analyzed using a two-tailed Student's T-test. This and all further behavioral analyses were performed with Graph Pad Prism software.

Spontaneous Alternation Y-maze

Mice were allowed to freely explore an open-armed Y-maze for 10 minutes. The order of arm entry was scored by two independent observers, blind to the genotype of the animals. Alternation was assessed by dividing the number of arm entry triads in which each arm was visited by the total number of arm visits minus 2, and percent alternation was compared between genotypes using a two-tailed Student's T-test.

Fear Conditioning

Fear conditioning experiments took place in a conditioning chamber (MedAssociates) equipped with a speaker, a house light, and a video camera, and all trials were video-recorded for subsequent scoring. On the first day of the test (day 1), mice were placed in a conditioning chamber that had been cleaned

with an ammonia-based solution and were allowed to habituate to the chamber for 6 minutes. The final minute of the habituation period was scored to assess baseline freezing behavior. Mice then received three tone-footshock pairings (tone, 20 seconds, 85 decibels (dB), 3.5 kilohertz (kHz); footshock, 2 seconds, 0.7 milliamperes (mA)) separated by an inter-trial interval of 60 seconds. After 24 hours (day 2), mice were exposed to the context in which they had initially received the shock on day 1 ("context stimulus") for 5 minutes, and the sessions were video-recorded. The chamber environment was then altered by placing patterned contact paper on the walls, wire mesh on the floors, and yellow filters on the lights. The ammonia-based cleaning solution was replaced with an unscented disinfectant, and the chambers were scented with pure vanilla extract. Two hours after exposure to the context stimulus, mice were placed in the altered chambers and exposed to the tone ("cued stimulus") without the footshock for two minutes. Freezing behavior for all trials on days 1 and 2 was scored in 5-second bins. One-way ANOVAs were used to analyze post-shock freezing for each tone-shock pairing on day 1. Two-way ANOVAs with Bonferroni *post hoc* tests were used to compare freezing behavior between genotypes during one-minutes time bins in the contextual task on day 2, and to compare pre-tone and tone-elicited freezing behavior during the cued task on day 2.

Incremental Hot Plate

Mice were placed on an incremental hot plate apparatus (IITC Life Science) set to increase in temperature from 43˚C to 57˚C at a rate of 2.5˚C per minute. A

two-tailed Student's T-test was used to compare paw-withdrawal latency between wild-type and GluK4 knockout mice.

Morris Water Maze (MWM)

MWM experiments were performed in a 1-meter pool filled with room temperature water made opaque with non-toxic white tempera paint. Distal visual cues consisting of black and white geometric shapes were placed throughout the testing room. Mice were initially tested in four 1-minute trials per day for two consecutive days in a visual platform paradigm, where the platform was 1 cm above the water level, to assess visual acuity, swimming ability, and motivation to escape from the water. Mice were then tested in a hidden platform paradigm, where the platform was submerged 1 cm below the water level, for four trials per day for four consecutive days. Trials proceeded until mice reached the platform or, if they were unable to locate it, for 60 seconds, at which point they were placed on the platform by the experimenter. The pool quadrant in which the mice were placed was varied across trials for both the hidden and visual platform assays. Following the final trial on the 4^{th} and final day of hidden platform testing, a probe trial was carried out to assess spatial memory. The platform was removed from the pool and the mice were allowed to explore the pool for 2 minutes.

All trials were video recorded and scored using Ethovision software. For visual platform trials, the latency to reach the platform was compared between

genotypes on each testing day using a two-way analysis of variance (ANOVA) with a Bonferroni *post-hoc* correction. For hidden platform trials, path length and velocity were averaged across all trials for each mouse and compared by Student's T-test. For the probe trials, the difference in quadrant preference between genotypes was assessed by two-way ANOVA with a Bonferroni *post-hoc* test. Search strategy in hidden platform trials was assessed from traces of the trajectory from pool entry to platform for each mouse by an experimenter blind to the genotype of the mice. Assessment criteria were based on those outlined by Brody and Holtzman (2006). Strategies were categorized as spatial, non-spatial systematic, or repetitive looping. These strategies are further described in Chapter 4. Overall differences in search strategies between genotypes were assessed for each hidden platform day using a Chi-Square test.

Forced Swim Test

Mice were placed in a 4-L transparent beaker that was filled to 20 cm of its 25 cm height with room temperature water and observed for 6 minutes. All trials were video-recorded for later scoring. The total amount of time that a mouse spent immobile over the course of the 6-minute trial was scored by hand every 5 seconds from video recordings and analyzed in one-minute bins. Immobility was defined as a lack of movement, except for that which was necessary to stay afloat. The total time spent immobile over the course of the trial was analyzed by a two-tailed Student's T-test. The contribution of time, genotype, and the

interaction between time and genotype to overall variation was assessed by two-way ANOVA coupled with a Bonferroni *post-hoc* test for multiple comparisons.

Open Field Test

Two open field paradigms were used: one to assess anxiety, and one to assess locomotor behavior. In the anxiety paradigm (referred to in the text as “short / lit”), the open field test was conducted in an evenly lit 46 cm x 46 cm arena with a white floor and black walls. Mice were individually placed in the arena such that they were facing a wall, and observed for 5 minutes. The arena was cleaned with 70% ethanol between trials. All trials were tracked and scored with Ethovision software (Noldus). For scoring purposes, the arena was divided into central and peripheral zones, where the center and periphery represented 36% and 64% of the total area of the arena, respectively. Scored measures included total number of center entries, percent time spent in center *versus* periphery, total distance traveled, and average velocity. Differences in each measure between wild-type and GluK4-knockout mice were analyzed by two-tailed Student’s T-tests.

In the locomotor paradigm (referred to in the text as “long / dark”), the open field test was conducted in a completely dark room. Light meter readings indicated that ambient light levels were 0 relative light units (RLU). The open field chambers used in this paradigm (Accuscan) were equipped with a laser photobeam tracking system to assess vertical and horizontal beam breaks. The arena was divided into central and peripheral zones such that the center

represented 40% of the total area, and the periphery represented 60% of the total area (the constraints of the tracking software made it impossible to exactly reproduce the zone distributions of the short / lit paradigm). Animals were observed for 1 hour, and behavior was scored in 5-minute bins using Fusion 3.2 Software (Accuscan). Scored measures included number of center entries, percent time spent in the center zone, and distance traveled. Differences in each measure over time between wild-type and GluK4-knockout mice were assessed by a two-way repeated measures ANOVA with Bonferroni *post-hoc* analysis.

Acoustic Startle and Prepulse Inhibition (PPI)

Mice were tested in SR-LAB startle response system chambers (San Diego Instruments) equipped with a speaker and a Plexiglas restraint chamber mounted on a piezoelectric accelerometer unit. Stimuli were presented in five blocks, and each stimulus was followed by a non-stimulus period of white noise (background) of 65 dB. In the first block, animals were presented with 5 single pulses of 120 dB to test their basal startle response. In the second block, animals were presented with 4 pulses of 80, 90, 100, 110, and 120 dB, ordered pseudo-randomly, to assess startle threshold. In the third block, animals were presented with 120 dB pulses preceded by a prepulse that was 3, 6, or 12 dB louder than the background. Each prepulse / pulse combination was presented 9 times, in pseudo-random order. Single 120 dB pulses were also presented 9 times, interspersed with prepulse / pulse pairs. In the fourth block, pulse intensity was maintained at 120 dB, prepulse was maintained at 6 dB above background, and

the inter-stimulus interval (ISI) between the prepulse and pulse was varied. The ISIs assayed were 25, 50, 100, 200, and 500 milliseconds (ms), and each ISI was presented 3 times in pseudo-random order, interspersed with 120 dB single pulses. In the fifth block, animals were again presented with 5 single pulses of dB. The startle response, Vmax, was recorded using SR-LAB software (San Diego Instruments).

To assess the startle threshold, the startle response to each tone intensity in the second block was averaged for each mouse, and compared between genotypes across tones using a two-way repeated-measures ANOVA with a Bonferroni *post-hoc* test. In the third block, the percent PPI was calculated for each prepulse intensity using the following equation: 100 – ((average Vmax for prepulse intensity in question / average Vmax within block 3 for single 120 dB pulse) * 100). Percent PPI was compared between genotypes across prepulse intensity by two-way repeated-measures ANOVA with a Bonferroni *post-hoc* test. In the fourth block, the percent PPI was calculated for each ISI using the following equation: 100 – ((average Vmax for ISI in question / average Vmax within block 4 for single 120 dB pulse) * 100). Percent PPI was then compared between genotypes across ISI by two-way repeated-measures ANOVA with a Bonferroni *post-hoc* test.

Stereotaxic Injections

For IH stereotaxic injections, animals were anesthetized with 2.5% avertin (0.02 mL/g of body weight) and atropine (0.6 mg/kg of body weight). Animals were then placed in a stereotaxic apparatus (Stoetling) and injected over the course of 60 seconds with 300 nanoliters (nL) PBS or 0.15 nanomoles (nm) kainate in 300 nL PBS. Injection coordinates were as follows: -2.5 mm from Bregma on the anterior-posterior axis; 1.7 mm from the midline on the medial-lateral axis; and 1.7 mm dorsal-ventral from the surface of the skull. For stereology experiments, animals were injected unilaterally. For microarray and biochemistry experiments, animals were injected bilaterally. Injections were performed with a 2.5 µL Hamilton syringe equipped with a 33-gauge blunt needle and controlled by an automated microinjection pump (World Precision Instruments). After injection, the needle was retracted by 0.1 mm and left in place for 2 minutes to allow injected material to diffuse. Animals were then injected IP with 0.03 mL buprenex (0.03 mg/kg of body weight) for analgesia and 500 mL sterile 0.9% saline for rehydration, and they were allowed to recover on a heating pad.

Hypoxia-Ischemia (HI)

Animals were maintained under deep isoflurane anesthesia during surgery. The left common carotid artery was exposed and gently separated from the vagus nerve. The artery was then ligated at two points several millimeters apart with 6-0 silk sutures, and transected between the ligation points. Following surgery, mice were injected IP with 0.03 mL Buprenex (buprenorphine HCl; 0.03 mg/kg of body

weight) and 500 mL sterile 0.9% saline, and allowed to recover for 40 minutes on a heating pad. Animals were then transferred to a hypoxic chamber maintained at 8% O_2 and 92% N_2 for 45 minutes at 37˚C (Vannucci et al., 2001).

Stereology

24 hours after IH kainate injection or HI, animals were perfused with 15 mL ice-cold 0.9% saline followed by 15 mL of ice-cold 4% paraformaldehyde (PFA). Brains were post-fixed overnight in 4% PFA, cryoprotected for 24 hours in 30% sucrose in 0.1 M phosphate buffer, frozen in powdered dry ice, and stored at -80˚C. Thin sections were collected on a cryostat and stored at -20˚C in freezing medium (30% glycerol, 30% ethylene glycol, 40% 0.1 M phosphate buffer) until use. For tissue from IH-injected animals, 20 µm sections were collected in 12-well plates such that each plate contained a range of sections that were 240 µm apart. Extensive tissue damage sustained by HI-treated animals made it necessary to slice tissue at 30 µm, such that sections were 360 µm apart in each well of a 12-well plate.

Fixed free-floating brain sections from one well were mounted on glass slides using a gelatin-based mounting medium and dried overnight at room temperature. Sections were stained in a solution of 0.00005% Fluorojade C (FJC) and 0.0001% 4',6-Diamidino-2-Phenylindole (DAPI) (Schmued et al., 2005), and visualized using an Axiovert 200 inverted epifluorescence microscope (Carl Zeiss, Inc.). All sections were imaged at high resolution and 50x

magnification. Exposure time and gain were consistent for each stain between all sections from all animals.

Cell death was quantified using NIH Image J software. Hippocampal subregions were identified and outlined by observation of DAPI staining. Subregion outlines were overlaid onto corresponding FJC images. The FJC images were split into their component red, green, and blue color channels, and the green channel was selected for further processing. Images were calibrated in μm, and then thresholded using the triangle algorithm to highlight FJC-positive cells. This algorithm was chosen because it consistently yielded a higher signal-to-noise ratio than the other available algorithms. Image splitting, calibrating, and thresholding were all carried out using an automated macro to ensure that image processing was consistent across sections. Experimenters were blind to the genotype and treatment of the animals during image processing. The area of FJC-positive staining within each hippocampal subregion was recorded and normalized to the total number of slices quantified. Differences in FJC area between genotypes were analyzed for each subregion using a two-tailed Student's T-test.

Microarray Sample Preparation and Array Hybridization

24 hours after bilateral IH injection of PBS or kainate, animals were killed by cervical dislocation. The hippocampus from the left hemisphere was quickly removed and left intact, while the hippocampus from the right hemisphere was

microdissected with sterile tools on ice to isolate the hippocampal subfields. Tissue was immediately frozen in sterile tubes on dry ice and stored at -80˚C until use.

Total RNA and total protein were isolated simultaneously using TRIzol according to the manufacturer's instructions. Briefly, tissue samples were homogenized in TRIzol and incubated for 10 minutes at room temperature. Following the addition of chloroform, samples were centrifuged at 12,000 x g for 15 minutes at 4˚C. The aqueous layer, containing total RNA, and the organic layer, containing total protein, were collected separately for further processing. The aqueous layer was incubated at 20˚C for 1 hour in isopropanol supplemented with glycogen, centrifuged at 12,000 x g for 15 minutes at 4˚C, washed with 70% ethanol, and pelleted at 7,500 x g for 5 minutes at 4˚C. The RNA pellet was then air-dried for 5 minutes at room temperature, and resuspended in nuclease-free water at 55˚C. Meanwhile, the organic layer was cleared of DNA by ethanol precipitation followed by sedimentation at 2000 x g for 5 minutes at 4˚C. The proteins in the resulting supernatant were precipitated with isopropanol, sedimented at 12,000 x g for 10 minutes at 4˚C, and washed 3 times in 0.3 M guanidine hydrochloride in 95% ethanol. The protein pellet was then incubated in ethanol for 20 minutes at room temperature, centrifuged at 7,500 x g for 5 minutes at 4˚C, vacuum-dried for 5 minutes, and dissolved in a buffer containing 25 mM Tris-HCl, 95 mM NaCl, 2% SDS, and 10 mM EDTA supplemented with protease and phosphatase inhibitors. Protein samples were stored at -80˚C until use.

All RNA samples were purified with an RNeasy mini kit (Qiagen) according to the manufacturer's instructions. The quality and concentration of all RNA samples was determined using a Bioanalyzer (Agilent). Any sample with an RNA integrity number below 8, or a concentration below 40 nanograms (ng) / μL – the minimal criteria required for microarray analysis – was subjected to further purification with an RNeasy MinElute kit (Qiagen).

One-step RT-PCR using was performed on all hippocampal and CA3 RNA samples with primers specific to heat shock protein 27 (Hsp27; RefSeq accession number NM_103560; Table 2.4) to investigate whether the samples that were supposed to receive kainate had actually received it. Hsp27 is a heat-shock-protein-encoding gene that is highly up-regulated in the context of excitotoxicity (Hunsberger et al., 2005; van der Weerd et al., 2010). CA3 samples were further analyzed by one-step RT-PCR using CA1- and DG-specific primers (Table 2.4) to assess contamination from neighboring hippocampal sub-regions. I assessed multiple primer pairs directed against a host of region specific genes that were first identified by Lein et al. (Lein et al., 2004). These primer pairs were compared in CA3, DG, and CA1 samples, and the most robust and tissue-specific primer pairs were selected for further analysis. The CA1-specific gene selected was nephroblastoma overexpressed gene (Nov; RefSeq Accession number NM_010930), and the DG-specific gene selected was desmoplakin (Dsp; RefSeq Accession number NM_023842.2).

TABLE 2.4. Primers used to evaluate microarray RNA samples.

Primer name	Purpose	Sequence
Hsp27 forward	Semi-quantitative analysis of Hsp27 expression as indication of kainate-induced excitotoxicity	CTGGACGTCAACCACTTCG
Hsp27 reverse	Semi-quantitative analysis of Hsp27 expression as indication of kainate-induced excitotoxicity	CTGCCTTTCTTCGTGCTTG
DG forward	Semi-quantitative analysis of Dsp expression as indication of DG contamination	CCTGTGATGCGTATCAGAAAAG
DG reverse	Semi-quantitative analysis of Dsp expression as indication of DG contamination	TGTAAAGGGCTCGCATTTG
CA1 forward	Semi-quantitative analysis of Nov expression as indication of CA1 contamination	CCCGAGGAAGTAACAGACAAG
CA1 reverse	Semi-quantitative analysis of Nov expression as indication of CA1 contamination	GAGACACTGAAACTCCACCTG

One-step RT-PCR was carried out using a OneStep RT-PCR kit (Qiagen). PCR conditions were optimized for each primer pair to determine the cycle number and template RNA concentration required to achieve optimal signal. All primer pairs ultimately required 30 PCR cycles, and 25 ng of RNA. The following PCR conditions were used: 30 minutes at 50˚C; 15 minutes at 95˚C; 45 seconds at 94˚C, 45 seconds at 53˚C, and 1 minute at 72˚C, repeated for 30 cycles. The resulting PCR products were run on an agarose gel alongside a DNAladder (GeneRuler), and analyzed semiquantitatively: PCR band intensity was assessed using Photoshop, and normalized between gels using the same band on the accompanying DNA ladder. (Pilot experiments in which the one-step RT-PCR reactions were multiplexed with β-actin primers to facilitate within-sample normalization were largely unsuccessful: β-actin was far more abundant than any of the other genes amplified, and the PCR amplification of β-actin would saturate – and therefore prove useless for quantification – in far fewer cycles than the other genes.) In experiments where CA3 samples were assessed for

contamination by neighboring sub-regions, a positive control consisting of purified DG RNA or CA1 RNA amplified by the DG- or CA1-specific primer pair was included in each gel. CA3 samples with the lowest levels of contamination were selected for further processing.

Purified RNA samples that had been assessed for contamination and kainate injection as appropriate were pooled in equal proportions. 3 samples were pooled for each of the 8 conditions described in Chapter 7, and submitted to the Genomics Resource Center at the Rockefeller University for amplification, labeling, and chip hybridization. Briefly, biotin-UTP-labeled cRNA was generated and amplified by T7 linear amplification using a MessageAmp Premier RNA Amplification kit (Applied Biosystems), and hybridized to a MouseRef-8 v.20 Expression Bead Chip (Illumina). This chip includes probes for ~25,600 RefSeq transcripts, corresponding to 19,100 unique genes from the mouse genome.

Microarray Data Analysis

Raw signals from the Illumina chip were exported into Genespring software. All signals were thresholded as follows: the background was set to 70, the lower cutoff for a present call was set to 0.8, and the upper cutoff for an absent call was set to 0.6. Thresholded signals were then scaled to the median, and transformed to a $\log_2$ scale. Fold change was calculated as the ratio between conditions as appropriate.

For Database for Annotation, Visualization and Integrated Discovery (DAVID) analysis, fold change after kainate injection was calculated relative to PBS, and compared between genotypes to extract genes that were changed by greater than |2|-fold. This analysis resulted in three gene lists: genes that were changed by greater than |2|-fold in both genotypes, genes that were changed by greater than |2|-fold in wild-type samples alone, and genes that were changed by greater than |2|-fold in knockout samples alone. Each list was then input into DAVID and compared against the Kyoto Encyclopedia of Genes and Genomes (KEGG) pathway database (Huang et al., 2008).

For Gene Set Enrichment Analysis (GSEA), all probe sets meeting the threshold conditions set in Genespring were ranked for each genotype according to their fold-change after kainate injection relative to PBS. Wild-type and GluK4 knockout gene lists were analyzed separately using the GSEAPreranked setting in GSEA, and compared at 100 permutations against the Biocarta pathway database (Subramanian et al., 2005). Gene sets from the Biocarta database that were larger than 800 genes, or smaller than 6 genes, were excluded from analysis. The chip annotations file that provides the gene names associated with the microarray probe identification numbers listed in the Genespring output was downloaded from the Illumina website (MouseRef8_V2_0_R2_11278551_A). For probes that were represented more than once on the microarray chip, the instance in which it yielded the highest fold-change value was selected for analysis (max_probe setting in GSEA).

Western Blotting to Detect JNK Pathway Components

Western blotting to analyze JNK pathway components was performed as described above, with several modifications. Total protein and RNA were simultaneously extracted from fresh-dissected samples using TRIzol. 30 µg of CA3 protein per lane were treated with mercaptoethanol, boiled for 5 minutes, and loaded onto a 10% Tris-Glycine polyacrylamide gel. Proteins were transferred to a PVDF membrane, and membranes were blocked and incubated in primary as above. Anti-phosphorylated MKK4, anti-JNK, anti-phosphorylated JNK, anti-cJun, anti- phosphorylated cJun, and anti-phosphorylated ATF-2 antibodies were all purchased from Cell Signaling and used at 1:1000 in the dilution buffer recommended by the manufacturer. Anti c-Fos was purchased from Calbiochem and used at 1:250 in 5% milk. Blots were then probed with secondary antibodies, incubated in chemiluminescent reagent, and quantified as above.

Intraperitoneal (IP) Kainate Injections

10 mM kainate solution in saline was prepared fresh each day that it was administered. Up to 6 mice were injected on a given experimental day, using one of several injection paradigms: (1) an initial dose of 30 mg/kg kainate, followed by two doses of 15 mg/kg at 45 minute intervals; (2) an initial dose of 15 mg/kg kainate followed by two doses of 5 mg/kg at 10 minute intervals; (3) an initial dose of 15 mg/kg, followed by a single dose of 5 mg/kg after 20 minutes; or (4) a single dose of 15 mg/kg. In injection paradigm (1), mice were observed for 4

hours following the initial injection; in all other paradigms, mice were observed for 2 hours. After the observation period, all mice were rehydrated with 500 mL of sterile saline and allowed to recover on a heating pad overnight.

Seizures were hand-scored during the observation period using a 0 – 6 scale first developed by Racine (Racine, 1972). The scale used for the experiments herein included slight modifications as described (McKhann et al., 2003; McLin and Steward, 2006). At level 0, mice do not show any abnormal behavior; at level 1, mice cease to explore, sniff, and groom, and become motionless; at level 2, mice adopt a rigid posture, stretching their bodies out and erecting their tails; at level 3, mice begin to show myoclonic jerks of the head and neck, and may rear into a sitting position; at level 4, mice exhibit forelimb clonus, running clonus, or rearing and falling broken by periods of total stillness; at level 5, mice show continuous level 4 seizures; and at level 6, mice exhibit violent bouncing seizures that progress to a loss of posture tone and death if persisting.

Data from injection paradigms that were repeated over several days were combined for analysis. The effects of genotype and time were compared by two-way ANOVA with a Bonferroni *post-hoc* test.

CHAPTER 3: GENERATING GLUK4 KNOCKOUT ANIMALS

Mouse Crosses

GluK4 knockout animals were generated by crossing mice homozygous for a *GRIK4* allele in which exon 16 was floxed (GluK4-floxed mice; generously provided by the Contractor Laboratory at Northwestern University) (Fernandes et al., 2009) with mice homozygous for a transgene encoding cre-recombinase under the control of an EIIA promoter (Figure 3.1). The EIIA promoter is active in the early mouse embryo, allowing for cre-mediated recombination in many tissues, including germ cells. Animals resulting from this cross transmit the recombined *GRIK4* allele to their progeny in a global, cre-independent manner. All first filial generation (F1) offspring were heterozygous for the floxed, recombined (F_R) *GRIK4* allele as well as the EIIA cre transgene. Founder F1 offspring were then mated to yield the allelic frequencies outlined in Table 3.1 by the second filial (F2) generation.

F2 mice that were homozygous for the F_R *GRIK4* allele, regardless of Cre transgene status, (Table 3.1, highlighted rows) were selected for propagation of the GluK4 knockout line. All knockout animals had a mixed C57Bl/6 / 129SvE background. Animals homozygous for the wild-type (+) *GRIK4* allele but maintained on the same background as GluK4 knockout mice are referred to herein as wild-type mice.

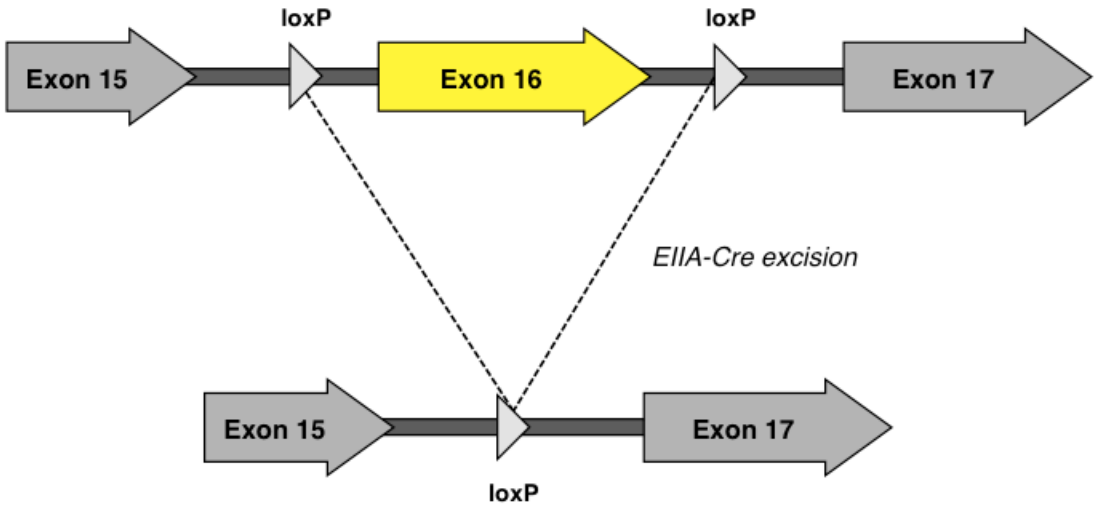

FIGURE 3.1. Schematic of GluK4 knockout strategy. Exon 16 of *GRIK4* was floxed GluK4-floxed mice. Crossing these mice with an EIIA-cre line, where cre is expressed in the germline, resulted in a global, cre-independent GluK4 knockout line.

TABLE 3.1. Expected Mendelian ratios of F2 offspring resulting from crosses of founder F1 mice.

EIIA Cre Transgene*	*GRIK4* allele**	Expected percentage of offspring
Cre/Cre	F_R/F_R	6.25%
Cre/Cre	F_R/+	12.50%
Cre/+	F_R/F_R	12.50%
Cre/+	F_R/+	25.00%
Cre/Cre	+/+	6.25%
+/+	F_R/F_R	6.25%
Cre/+	+/+	12.50%
+/+	F_R/+	12.50%
Cre/Cre	+/+	6.25%

* "+" refers to the wild-type allele, "Cre" refers to the EIIA Cre transgenic allele;

** "+" refers to the wild-type allele, "F_R" refers to the floxed, recombined allele.

Assessing Global Cre-mediated GRIK Recombination

Cre-mediated recombination of the floxed *GRIK4* allele was assessed using a three-primer PCR strategy. A forward primer, P2, and a reverse primer, P1, were designed to flank the first (downstream) loxP site, such that P2 was downstream of the loxP site and P1 was upstream. The region recognized by P1 was located between the two loxP sites, such that it would be obviated by successful cre-mediated recombination. A third reverse primer, P6, was targeted upstream of the second loxP site (Figure 3.2).

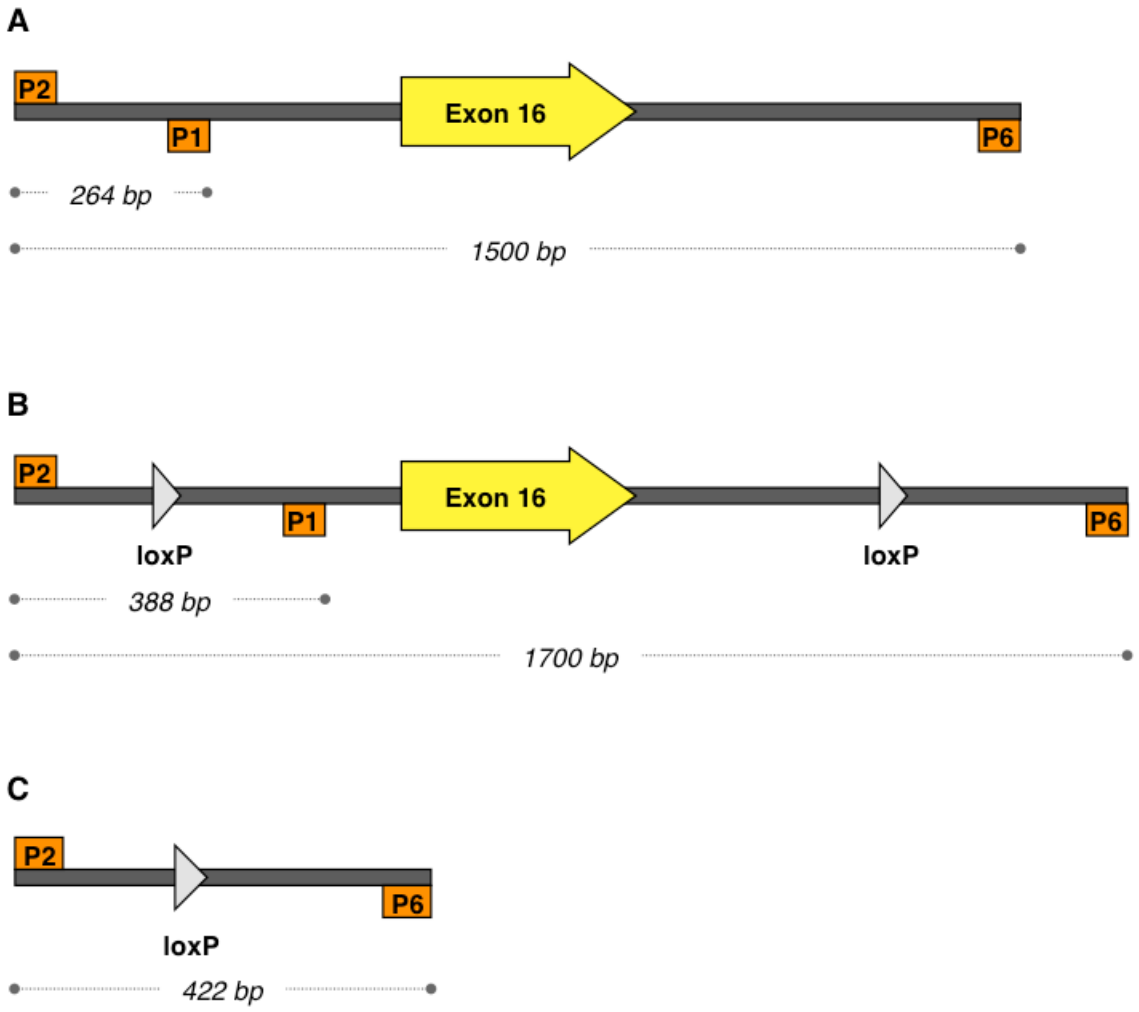

FIGURE 3.2. Schematic of genotyping strategy for GluK4 knockout mice. P2 is a forward primer, and P1 and P6 are both reverse primers. **(A)** The wild-type allele yields a 264 bp P2-P1 PCR product and a 1500 bp P2-P6 product. **(B)** The floxed, unrecombined allele yields a 388 bp P2-P1 product, and a 1700 bp P2-P6 product. **(C)** The floxed, recombined allele yields a 422 bp P2-P6 product. P1 is targeted against a region between the two loxP sites, such that successful recombination eliminates that region and, thus, the P2-P1 product.

Using this genotyping strategy, PCR products of the sizes outlined in Table 3.2 were obtained for the various genotypes assessed.

TABLE 3.2. Expected size of genotyping PCR products.

	Wild-type	**F/F** *(homozygous floxed, unrecombined)*	**GluK4 knockout** *(homozygous floxed, recombined)*
P2-P1 PCR product size	264 bp	388 bp	N/A: P1 recognition site excised
P2-P6 PCR product size	1500 bp	1700 bp	422 bp

To determine whether cre-mediated recombination of *GRIK4* had occurred globally, DNA extracts from hippocampus, cortex, lung, and tail from wild-type versus heterozygous F_R / + mice from the founder F1 generation were analyzed using the 3-primer PCR strategy described above. As predicted, the recombined *GRIK4* allele was present in all F_R / + heterozygote tissues, and absent in all wild-type tissues (Figure 3.3).

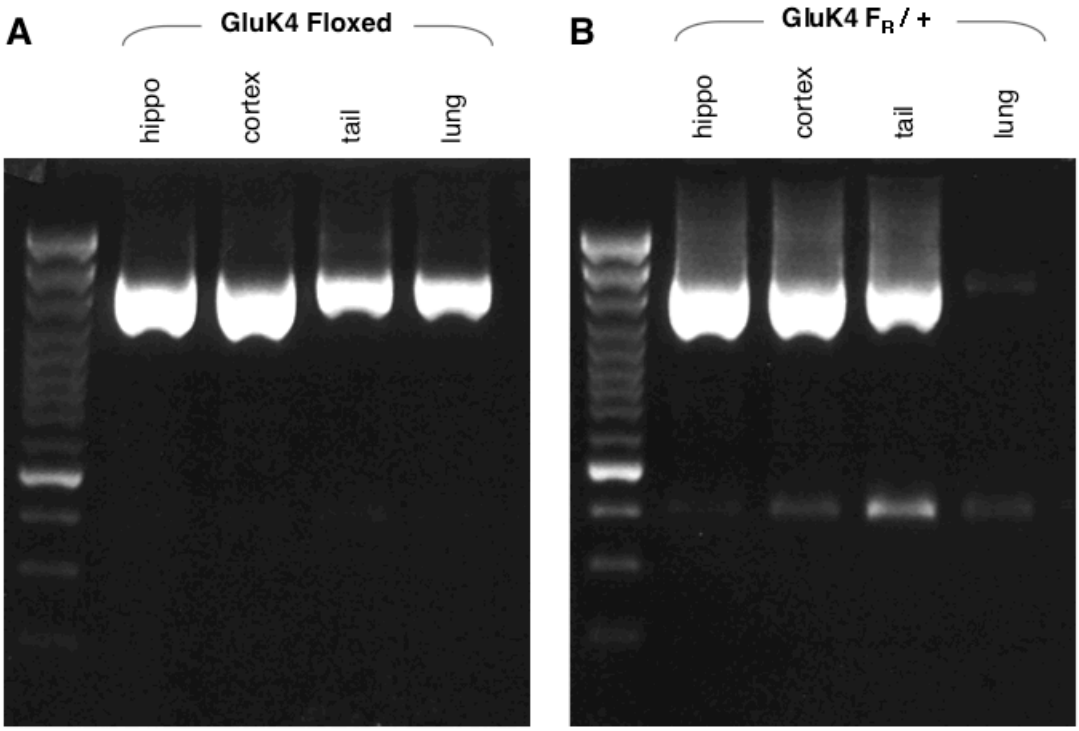

FIGURE 3.3. Assessing cre-mediated recombination of *GRIK4* in various tissues from GluK4-floxed, and GluK4 F_R / + heterozygote mice. (A) The floxed, unrecombined allele, which appears here as a ~1700 bp band corresponding to the P2-P6 PCR product, is present in all tissues assessed in GluK4-floxed mice. The faint lower band (~400 bp) represents the P2-P1 PCR product, but is not favored in this reaction. **(B)** Recombination of the floxed *GRIK4* allele has occurred in all GluK4 F_R / + heterozygote tissues assessed. The upper band (~1500 bp) represents the floxed, unrecombined allele; the lower band (~400 bp) represents the recombined allele.

Characterizing GRIK4 *mRNA Expression*

The *GRIK4* gene yields a 3488 bp transcript with 21 exons (RefSeq accession number NM_175481.5). The coding region extends from positions 201 to 3071, which overlaps with exons 3 – 21. Exon 16, which is floxed in the GluK4-floxed animals provided by the Contractor laboratory, encodes the pore-forming M2 p-loop region of GluK4 (Fernandes et al., 2009) (see Figure 1.1).

The Contractor laboratory had shown previously that a global GluK4 knockout mouse, generated using a germline-expressed cre line similar to the EIIA cre line used here, was both a transcriptional and translational null (Fernandes et al., 2009). However, they assessed *GRIK4* mRNA expression using a primer pair designed to amplify the excised exon 16, and therefore did not exclude the possibility that a *GRIK4* transcript containing the regions up- or downstream was still being expressed.

To evaluate this possibility, I designed primer sets that were targeted throughout the *GRIK4* transcript such that all exons within the coding region were represented (exons 2 – 20). I then used these primer sets to perform RT-PCR on RNA purified from wild-type and GluK4 knockout hippocampus homogenates. The PCR products were run on an agarose gel and visualized by UV illumination. Bands representing all amplified regions of *GRIK4* were present in wild-type samples. Surprisingly, the same bands were also present in GluK4 knockout samples, with the exception of those with either a forward or a reverse primer in

exon 16 (Figure 3.4a). To ensure that the presence of bands in the GluK4 knockout samples was not the result of genomic DNA contamination, I ran the same PCR reactions without including reverse transcriptase. No bands were observed in these conditions (Figure 3.4a).

To further explore *GRIK4* mRNA expression in GluK4 knockout animals, I ran RT-PCR on wild-type and GluK4 knockout hippocampal extracts using a forward primer located in exon 13, and a reverse primer in exon 20, such that the resulting PCR product would encompass exon 16. The predicted size of the PCR product from the wild-type *GRIK4* allele is 940 bp, and a band of this size was indeed observed in wild-type samples. The band observed in knockout samples was approximately 200 bp smaller, a decrease corresponding to the predicted size of exon 16 (173 bp; Figure 3.4b). PCR products from wild-type and GluK4 knockout samples were then sent to an outside facility (Genewiz) for sequencing. Aligning the resulting sequences with the predicted *GRIK4* mRNA sequence indicated that GluK4 knockout samples were indeed missing exon 16, but that the surrounding regions were intact. Furthermore, sequencing revealed that the deletion of exon 16 was in frame, and that there were no premature stop codons in the sequenced region of GluK4 knockout mRNA. Taken together, these results indicate that GluK4 knockout animals are not, in fact, transcriptional knockouts. Instead, they produce a truncated *GRIK4* mRNA product that is missing exon 16.

FIGURE 3.4. *GRIK4* mRNA is intact in GluK4 knockout mice. (A) Non-quantitative RT-PCR using primer pairs that, together, covered all coding exons of *GRIK4*, revealed that *GRIK4* mRNA was intact in GluK4 knockout mice. Only the region corresponding to the floxed exon 16 is missing. **(B)** A product encompassing the region corresponding to exon 16 was ~200 bp smaller in GluK4 knockout samples than in wild-type samples, consistent with the size of exon 16. (C) Quantitative RT-PCR using primer pairs designed to amplify exons 3-4, exons 20-21, or exon 16 indicated that *GRIK4* mRNA is expressed at the same levels in wild-type and GluK4 knockout hippocampal tissue. Once again, only the region corresponding to exon 16 appeared to be missing. Bars represent mean ± SEM. * $p < 0.05$. WT, wild-type; KO, GluK4 knockout; + RT, reactions including reverse transcriptase; - RT, reactions excluding reverse transcriptase; Ex, exons.

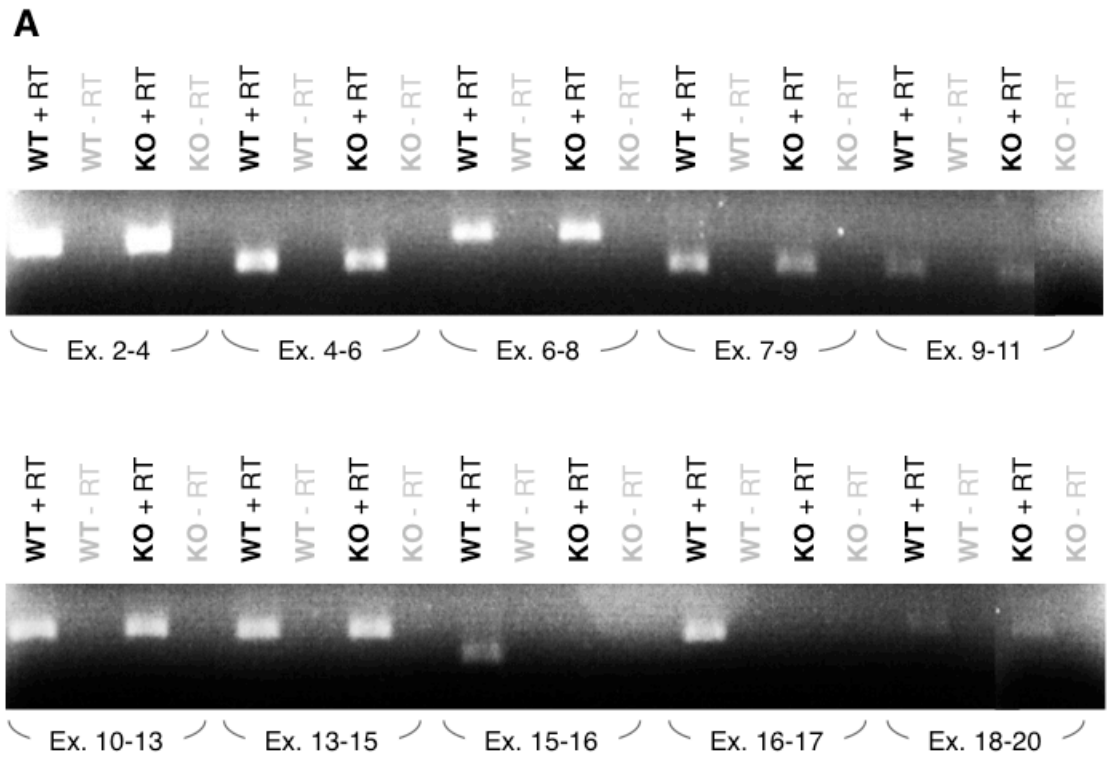
A
WT + RT
WT - RT
KO + RT
KO - RT
Ex. 2-4
Ex. 4-6
Ex. 6-8
Ex. 7-9
Ex. 9-11
Ex. 10-13
Ex. 13-15
Ex. 15-16
Ex. 16-17
Ex. 18-20

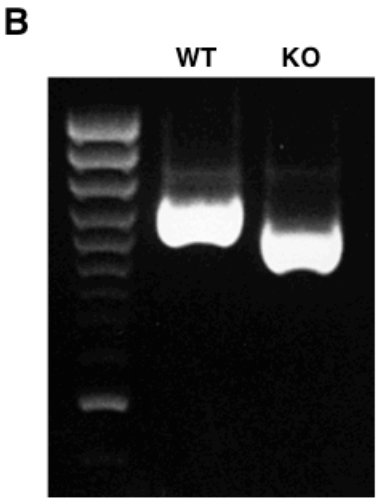
B
WT
KO

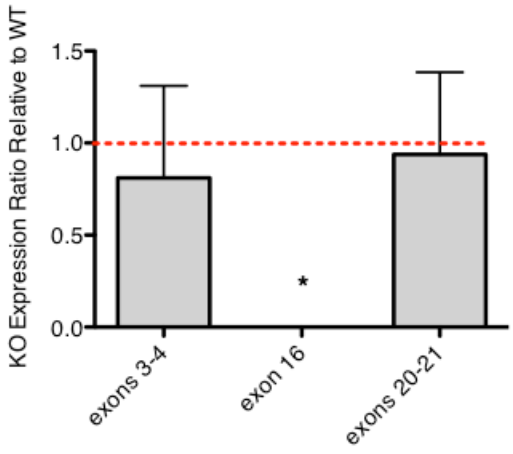
C
KO Expression Ratio Relative to WT
1.5
1.0
0.5
0.0
*
exons 3-4
exon 16
exons 20-21

The possibility remained, however, that the modified *GRIK4* mRNA produced by the GluK4 knockout animals was expressed only at very low levels, rendering the animals functional – if not true – knockouts. To address this, I performed quantitative RT-PCR on hippocampal extracts from wild-type mice and GluK4 knockout mice. Three primer sets were used in separate experiments: one set that amplified exons 3 – 4, corresponding to the coding region of the *GRIK4* transcript that is farthest downstream in the 5' direction; one set that amplified exon 16; and one set that amplified exons 20 – 21, corresponding to the coding region of the *GRIK4* transcript that is farthest upstream in the 3' direction. cDNA levels in each reaction were detected by SYBRgreen in a Roche Lightcycler 480 real time RT-PCR system. While expression of the amplified region surrounding exon 16 was significantly down-regulated ($p = 0.042$) and essentially abolished in GluK4 knockout samples relative to wild-type samples, expression of exons 3 – 4 and exons 20 – 21 did not differ significantly from wild-type levels ($p = 0.697$ and $p = 0.846$, respectively; Figure 3.4c). These data indicate that GluK4 knockout animals are not transcriptional nulls: they produce a modified *GRIK4* transcript that lacks exon 16, but is otherwise intact, and they express this modified transcript at the same levels that wild-type animals express the wild-type transcript.

Characterizing GluK4 Protein Expression

The fact that GluK4 knockout animals were not transcriptional nulls raised the possibility that they were not true translational nulls, as they were reported to be by the Contractor laboratory (Fernandes et al., 2009). Initial attempts to assess whether GluK4 knockout animals expressed GluK4 protein yielded inconsistent results: western blots using commercially available GluK4 antibodies had such high background that it was difficult to disambiguate aspecific bands from those corresponding to GluK4.

To obviate this issue, I commissioned the production of a custom, polyclonal GluK4 antibody (Covance). The immunizing peptide used to generate the antibody, SPARSEESLEWDKTTNSSEPE, corresponds to amino acids 939 – 956 of the C terminal end of the mouse GluK4 protein. This peptide had previously been used in two separate studies to generate GluK4 antibodies (Fogarty et al., 2000; Darstein et al., 2003), and was chosen because its sequence has high homology between mouse, rat, and human isoforms of GluK4, but low homology to other ionotropic glutamate receptor subunits. The resulting polyclonal antibody was affinity-purified against the immunizing peptide to remove non-specific antibody species. Using this antibody, it was possible to distinguish a band corresponding to the predicted 108 kilodalton (kDa) molecular weight of GluK4 in wild-type hippocampal extracts. However, this band was not observed in GluK4 knockout extracts, nor were any additional bands that might correspond to modified forms of GluK4 (Figure 3.5a).

Because the custom GluK4 antibody recognizes the C-terminus of the GluK4 protein, it was still possible that GluK4 knockout mice might express one or more modified forms of GluK4 in which the C-terminus was absent but other areas of the protein were intact. To assess this, western blots were performed on the same wild-type and GluK4 knockout hippocampal extracts using a commercially available antibody directed against amino acids 59 – 73 of the N-terminus of GluK4 (ab10101; Abcam). Like the other commercially available GluK4 antibodies, this antibody yielded high background. However, upon over-exposing the blots, it was possible to observe a band corresponding to the size of GluK4 in wild-type extracts that was absent in GluK4 knockout extracts. No additional bands were observed in GluK4 knockout blots using this antibody (Figure 3.5b).

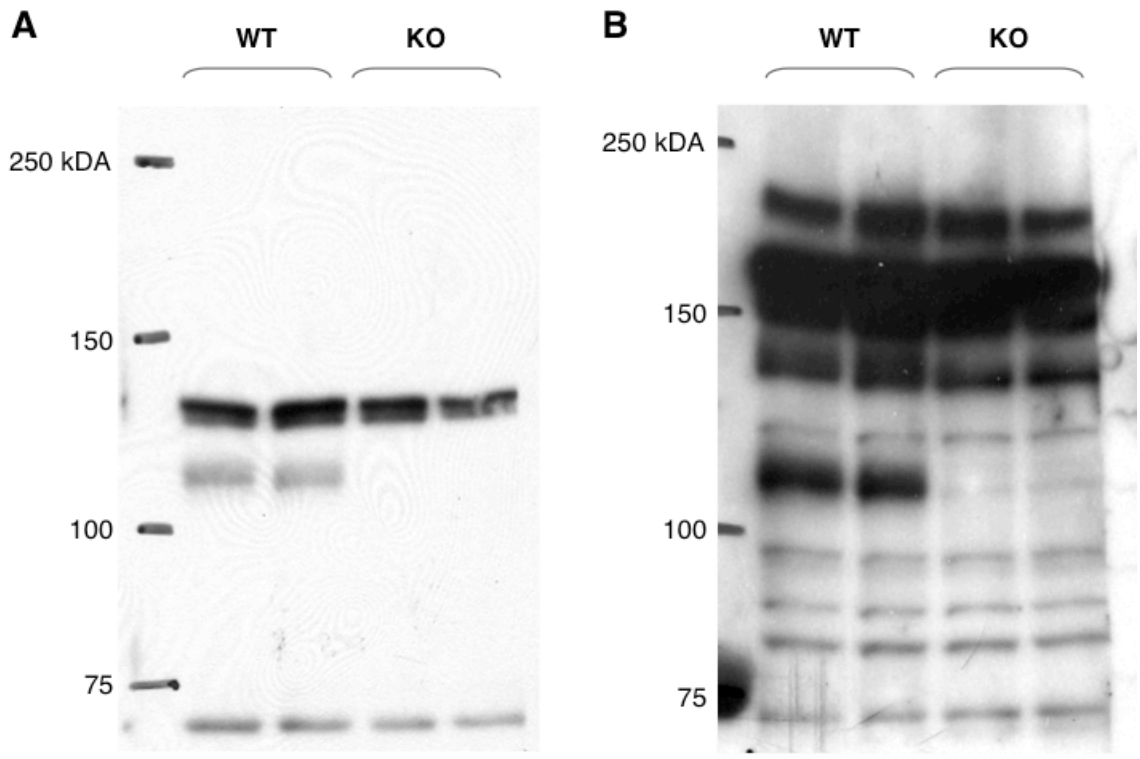

FIGURE 3.5. GluK4 protein is undetectable by western blot in GluK4 knockout animals. Western blots of wild-type and GluK4 knockout whole-hippocampus homogenates using a custom generated **(A)** or commercially available **(B)** anti-GluK4 antibody indicated that a band corresponding to the predicted size of GluK4 (108 kDa) was missing in GluK4 knockout mice.

Taken together, these results suggest that GluK4 knockout animals are ultimately translational nulls, despite the fact that they are not transcriptional nulls. It is likely that the excision of exon 16, which corresponds to the pore-forming p-loop of GluK4, results in either an unstable protein that gets targeted for degradation, or a stable protein that is unable to pass a critical checkpoint during kainate receptor assembly, and thus gets targeted for degradation.

CHAPTER 4: GLUK4 IN LEARNING AND MEMORY

GluK4 knockout mice show reduced LTP (Catches et al., 2012), a cellular process that is crucial to learning and memory. GluK4 expression is also highest within the CA3 region of the hippocampus, an area that is involved in memory acquisition and retrieval (Hunsaker et al., 2009). I therefore investigated whether GluK4-deficient animals demonstrated learning or memory impairments.

GluK4 Ablation Does Not Affect Performance in Novel-arm or Spontaneous Alternation Y-maze Tests

Working (short-term) memory was assessed by novel-arm Y-maze and spontaneous alternation Y-maze. In the novel-arm Y-maze task, mice were initially placed in a 3-armed Y-maze in which one arm was blocked, and allowed to acclimatize. The block was then removed from the third arm, thereby creating a novel environment for the mice to explore. Because mice are inherently curious about novel environments, mice with intact working memory should spend proportionally more time in the novel arm than in the two arms that had initially been open (Hughes, 2004). Both wild-type (n = 5) and GluK4 knockout (n = 6) mice favored the novel arm to the other arms, with no significant difference in the percent time spent in the novel arm (Student's T-test, $p = 0.6721$; Figure 4.1a) or either of the other arms (Student's T-test, $p = 0.8436$ and $p = 0.4399$; Figure 4.1a).

In the spontaneous alternation Y-maze task, mice were allowed to freely explore a 3-armed Y-maze. Because, once again, mice prefer novel environments, mice with intact working memory should continuously seek the least-recently-visited arm as they move about the maze, and should therefore alternate between the arms in triads – that is, arm A, followed by arm B, followed by arm C. The proportion of triads in each trial is measured as percent alternation. No significant difference in percent alternation was observed between wild-type and GluK4 knockout mice (wild-type, n = 13; GluK4 knockout, n = 12; student's T-test, p = 0.4028; Figure 4.1b).

Taken together, the data from the novel-arm Y-maze and the spontaneous alternation Y-maze suggest that GluK4 ablation does not affect working memory.

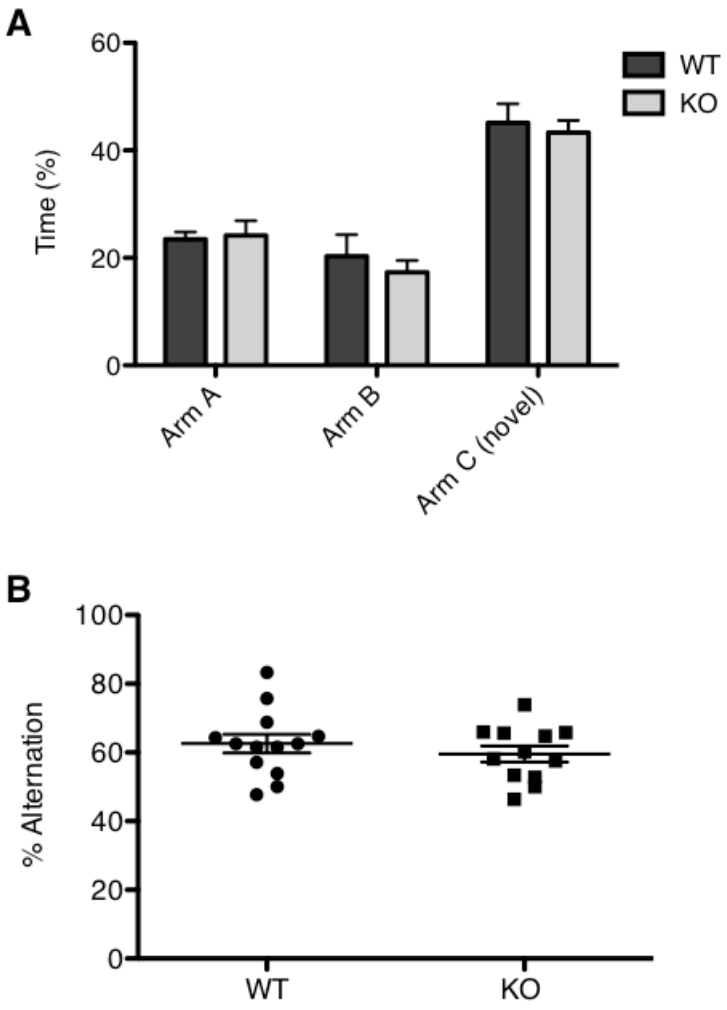

FIGURE 4.1. GluK4 knockout mice do not show working memory impairments in Y-maze tasks. (A) In a novel-arm Y-maze, wild-type (n = 5) and GluK4 knockout mice (n = 6) showed equal preference for the novel arm (Arm C; p = 0.6721). **(B)** In a spontaneous alternation Y-maze, wild-type (n = 13) and GluK4 knockout mice (n = 12) did not differ in their % alternation (p = 0.4028).

Fear Memory Acquisition is Impaired in GluK4 Knockout Mice

In Pavlovian fear conditioning paradigms, mice learn to associate a neutral conditioned stimulus (CS) and an aversive unconditioned stimulus (US), such that the CS alone evokes a fear response. The CS can be defined as a cue, such as a tone, that accompanies the US, or the context in which the mice initially receive the US. Cued and contextual fear conditioning are thought to be amygdala- and hippocampus-dependent, respectively (Maren, 2008). Targeted disruption of the afferent mossy fiber pathway in the GluK4-rich CA3 region impairs the acquisition and consolidation of contextual fear memory (Daumas et al., 2004), a finding that raises the possibility that GluK4 might be involved in contextual fear conditioning. Furthermore, ablation of the GluK2 kainate receptor disrupts cued fear memory and reduces synaptic potentiation in the lateral amygdala (Ko et al., 2005).

Based on this evidence, I investigated the role of GluK4 in both cued and contextual fear memory. The cued CS consisted of a tone (3.5 kHz, 85 dB; “cued stimulus”), and the contextual stimulus consisted of the initial environment in which the mice were presented with the US (“context stimulus”). The US consisted of a footshock delivered through floor rods connected to a shock generator. On day 1, mice were presented with three tone-shock pairings. Both wild-type and GluK4 knockout mice demonstrated immediate post-shock freezing, but while freezing behavior increased steadily during successive tone-shock pairings in the wild-type cohort, it did not increase significantly in the

knockout cohort (One-way ANOVA (tone): for wild-type mice $F = 8.455$, $p = 0.0020$, $n = 8$; for GluK4 knockout mice $F = 0.8476$, $p = 0.4426$, $n = 8$; Figure 4.2a). On day 2, mice were presented with either the context stimulus, or the cued stimulus in an altered context, both without the US. There were no significant differences in freezing between genotypes for the context stimulus paradigm (Two-way ANOVA, effect of genotype: $F = 0.35$, $p = 0.5625$; Figure 4.2b) or the cued stimulus paradigm (Two-way ANOVA, effect of genotype: $F = 0.34$, $p = 0.5701$; Figure 4.2c).

Because GluK4 shows limited expression in the dorsal root ganglia of nociceptive spinal afferent neurons (Lucifora et al., 2006), I performed an incremental hot-plate test to investigate the possibility that wild-type and GluK4 knockout animals had different pain thresholds and were therefore differentially sensitive to the footshock. Mice were tested in a hot-plate apparatus that increased in temperature at a rate of 2.5˚C/minute from 43˚ to 57˚C, and no difference in paw withdrawal latency was observed between genotypes (wild-type, $n = 3$; GluK4 knockout, $n = 5$; Student's T-test, $p = 0.3555$; Figure 4.2d) indicating that there was no difference in basal pain threshold between genotypes. Taken together, these data suggest that, while fear memory storage and retrieval are intact in GluK4 knockout mice, fear memory acquisition is significantly impaired.

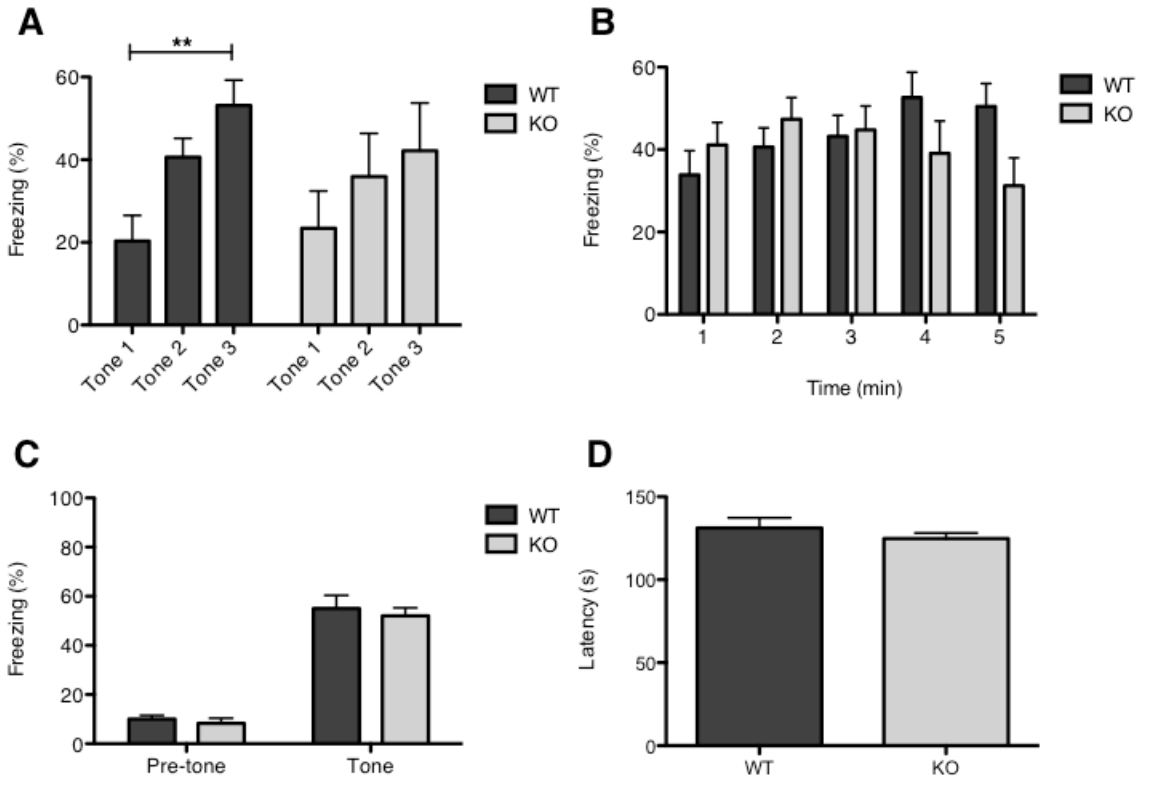

FIGURE 4.2. GluK4 knockout mice show impaired fear memory acquisition, but not recall. (A) Freezing behavior increased progressively in the wild-type cohort (n = 8) after successive tone-shock pairings on day 1 (p = 0.0020), but not in the GluK4 knockout cohort (n = 8). These findings suggest that GluK4 mice have impaired fear memory acquisition. **(B)** Freezing behavior was not significantly different between genotypes over the course of the context stimulus trial on day 2 (p = 0.5625). **(C)** Freezing behavior was not significantly different during the pre-tone or tone periods of the cued stimulus trial on day 2 (p = 0.5701). Fear memory recall was therefore intact in GluK4 knockout mice. **(D)** Wild-type and GluK4 knockout mice did not differ in their latency to withdraw their paws from an incremental hot plate, indicating that they do not have different basal pain thresholds. Bars represent mean ± SEM.

Spatial Learning and Memory are Impaired in GluK4 Knockout Mice

Spatial memory, like fear memory, is also dependent in part on the CA3 region of the hippocampus: reversible inhibition of mossy fiber transmission results in impaired spatial memory acquisition in the MWM test of spatial reference memory (Florian and Roullet, 2004). Thus, I tested wild-type and GluK4 knockout mice in the MWM to assess whether GluK4 ablation results in spatial memory deficits.

Mice were initially tested in a visual platform paradigm, where the platform was raised above the water surface, and no basal differences in visual or swimming abilities were observed between the genotypes (wild-type n = 13; GluK4 knockout n = 12; two-way ANOVA for latency to reach platform, effect of genotype, $F= 1.15$, $p = 0.2946$; Figure 4.3a).

Mice were then trained for 4 days in a hidden platform paradigm, where the platform was submerged below the water level, and, thus, no longer visible to the mice, such that they had to navigate to the platform location using distal spatial cues. Throughout hidden platform testing the GluK4 knockout cohort performed significantly worse than the wild-type cohort, demonstrating increased path length between the point of water entry and the escape platform (Student's T-test, $p = 0.0231$, Figure 4.3b) without any concomitant changes in velocity (Student's T-test, $p = 0.2407$; Figure 4.3c).

FIGURE 4.3. MWM performance is impaired in GluK4 knockout mice during hidden platform trials. (A) The latency to reach the platform during the trials when the platform was visible above the waterline did not differ between wild-type (n = 13) and GluK4 knockout mice (n = 12; p = 0.2946), indicating that vision, swimming ability, and motivation to escape the water were all equal between genotypes. (B) Pathlength to reach the hidden platform was increased in GluK4 knockout mice relative to wild-type mice over the course of the hidden platform trials (p = 0.0231), indicating that spatial memory is impaired in GluK4 knockout mice. (C) There was no difference between genotypes in swimming velocity (p = 0.2407), suggesting that the increase in pathlength observed in the GluK4 knockout mice was not an artifact of hyperactivity. Bars represent mean ± SEM. VP, visual platform.

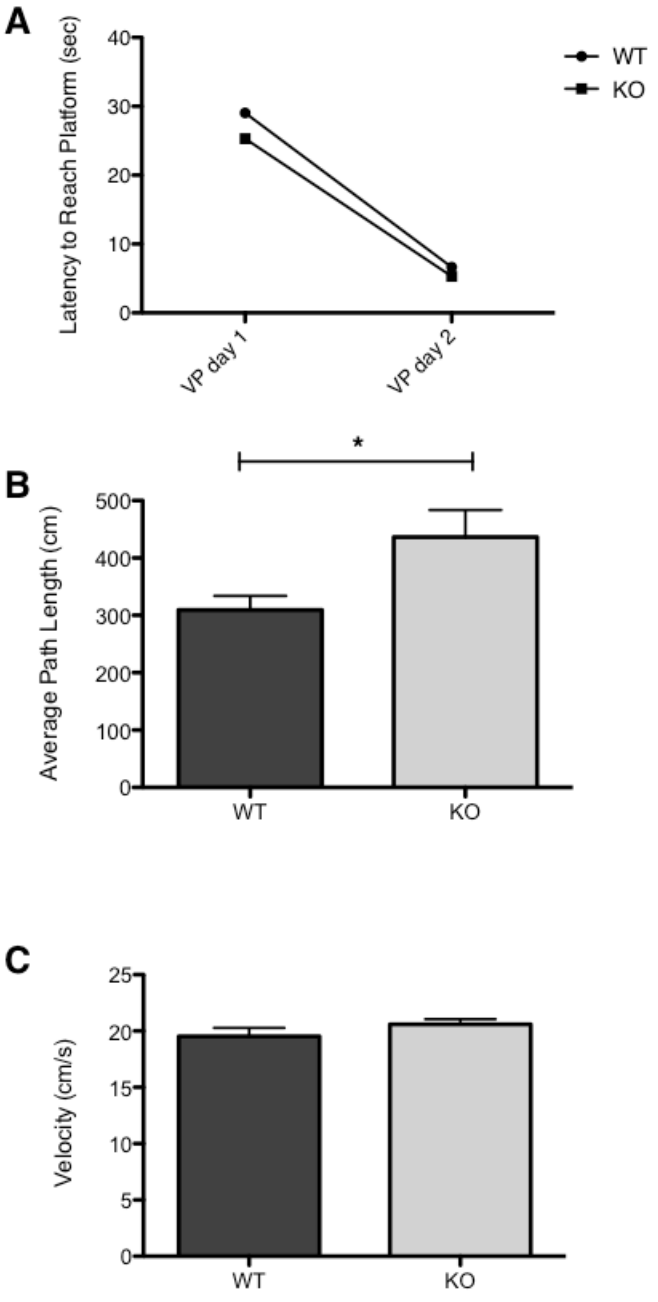
A
Latency to Reach Platform (sec)
40
30
20
10
0
VP day 1
VP day 2
WT
KO
B
*
Average Path Length (cm)
500
400
300
200
100
0
WT
KO
C
Velocity (cm/s)
25
20
15
10
5
0
WT
KO

To parse the discrepancies in hidden platform performance between wild-type and GluK4 knockout mice, I compared the search strategies that they used to locate the platform based on the schema elaborated by Brody and Holtzman (Brody and Holtzman, 2006). Search strategies were classified as follows: spatial strategies, where mice swam directly to the escape platform or to the area surrounding the platform and searched intently in that region; non-spatial systematic strategies, where mice did not swim directly to the platform but instead scanned the pool without spatial bias until they found the platform; and strategies based on repetitive looping, where mice swam circularly at a fixed distance from the pool walls without spatial bias (Figure 4.4).

Both wild-type and knockout mice favored non-spatial systematic strategies on day 1 of the hidden platform trials, presumably because they had not yet learned the position of the platform (Figure 4.5c). Wild-type mice decreased their reliance on non-spatial systematic strategies over time in favor of spatial strategies, and by day 4 they employed spatial search strategies almost exclusively (Figure 4.5d-f). However, while GluK4 knockout mice also decreased their reliance on non-spatial strategies to some extent, they employed non-spatial systematic strategies more frequently than wild-type mice by day 3, and this difference became very robust by day 4 (Chi-square test for overall difference in search strategy between genotypes, day 3 $p = 0.021$; day 4 $p = 0.001$; Figure 4.5e,f). These findings suggest that the increased path length demonstrated by the GluK4 cohort in the hidden platform test relative to the wild-type cohort is a

function of impaired spatial memory acquisition. While wild-type mice learned to use spatial search strategies over time, GluK4 knockout mice continued to use non-spatial search strategies to locate the platform.

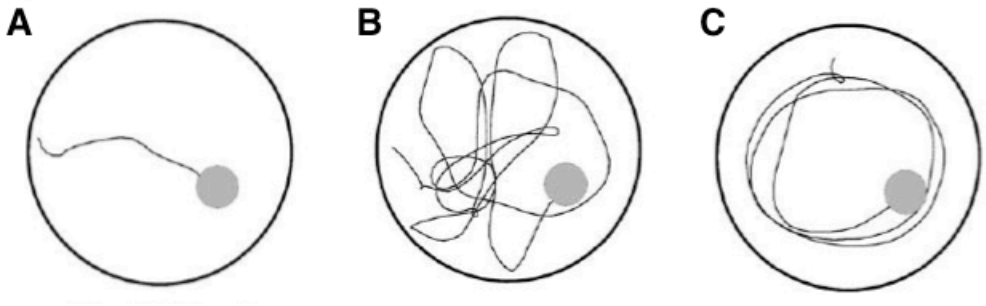

Adapted from Brody et al., 2006

FIGURE 4.4. Schematic of search strategies employed by mice in the MWM. Search strategies were classified as spatial direct **(A)**, non-spatial systematic **(B)**, or repetitive looping **(C)** as a measure of MWM performance and, hence, of spatial learning and memory.

FIGURE 4.5. GluK4 knockout mice use less efficient search strategies than wild-type mice to locate the hidden platform in the MWM. Representative search strategies are shown from wild-type **(A)** and GluK4 knockout mice **(B)** to locate the hidden platform. **(C, D)** Wild-type (n = 13) and GluK4 knockout mice (n = 12) both employed non-spatial systematic strategies on day 1 of the hidden platform trials. **(E, F)** Wild-type mice decreased their reliance on non-spatial systematic strategies in favor of spatial strategies to locate the hidden platform over the course of the trials, while GluK4 knockout mice continued to employ non-spatial systematic strategies. The overall difference in search strategy between wild-type and GluK4 knockout search strategy was significant on days 3 and 4 ($p = 0.021$; $p = 0.001$, respectively).

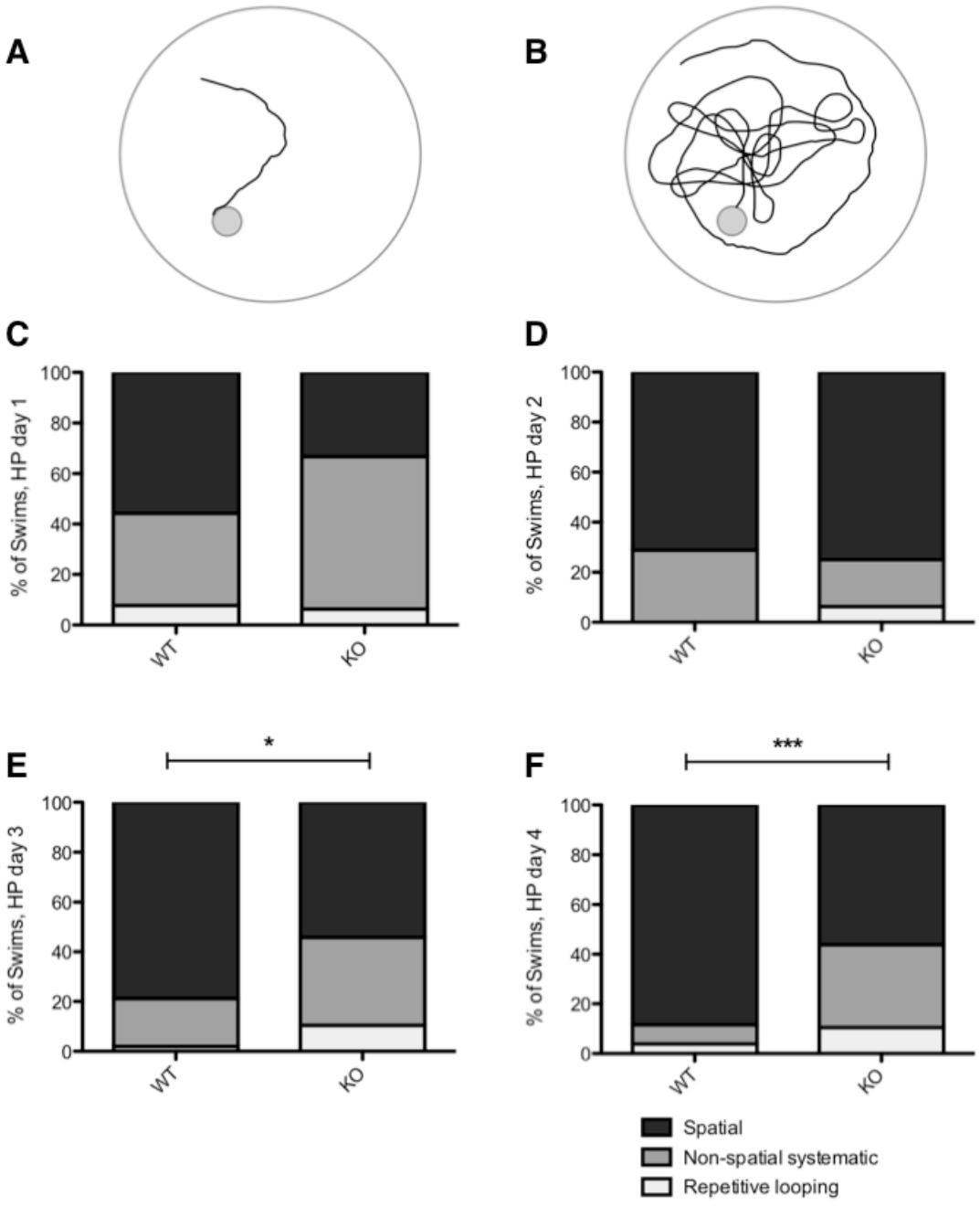
A
B
C
D
E
F
% of Swims, HP day 1
% of Swims, HP day 2
% of Swims, HP day 3
% of Swims, HP day 4
100
80
60
40
20
0
WT
KO
*
***
Spatial
Non-spatial systematic
Repetitive looping

To further assess the role of GluK4 in spatial memory, I performed a probe trial following hidden platform training in which the escape platform was removed from the pool altogether. Animals that have learned to navigate to the platform should spend more time in the quadrant of the pool (target quadrant) in which the platform was previously located during the hidden platform trials than in the other quadrants of the pool. A two-way ANOVA with Bonferroni *post-hoc* analysis for time spent in each quadrant revealed a significant effect of quadrant ($F = 25.63$, $p < 0.0001$), with a significant difference between genotypes in the time spent in the target quadrant ($p < 0.05$), indicating that GluK4 knockout mice showed decreased preference for the target quadrant when compared with knockout mice (Figure 4.6).

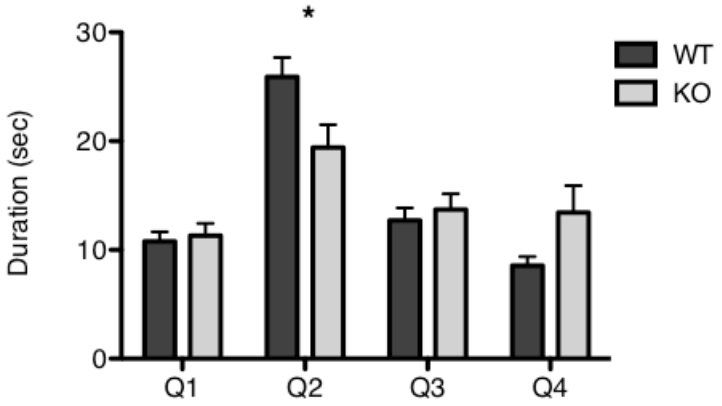

FIGURE 4.6. MWM probe trial performance is impaired in GluK4 knockout mice. Wild-type (n = 13) and GluK4 knockout mice (n = 12) differed significantly in their preference for the target quadrant, Q2 ($p < 0.05$), suggesting that GluK4 knockout mice had not learned the location of the hidden platform and, thus, had impaired spatial memory recall. Bars represent mean ± SEM. Q1-4, quadrant 1-4.

It is possible that the impaired probe trial performance in the GluK4 knockout cohort is an effect of impaired spatial memory acquisition, as in the hidden platform trials. It is also possible that this impairment stems from the combined effects of impaired spatial memory acquisition, consolidation, and/or recall. Because memory acquisition is impaired in these mice, and memory acquisition precedes memory consolidation and recall, it is difficult to disambiguate the individual contributions of each phase of memory formation to the memory deficits induced by GluK4 ablation. Nevertheless, these experiments highlight the key role of GluK4 in spatial memory.

CHAPTER 5: GLUK4 IN MOOD AND NEUROPSYCHIATRIC DISORDERS

Based on associational studies in humans implicating GluK4 in bipolar disorder and schizophrenia (Pickard et al., 2006; 2008), as well as a concurrent behavioral study in which GluK2 knockout animals were shown to be less anxious, more risk-taking, and less despairing than wild-type animals (Shaltiel et al., 2008), I sought to investigate the behavioral phenotype of GluK4 knockout animals.

GluK4 Knockout Mice Display Reduced Despair in the Forced Swim Test

First, I performed a forced swim test to assess depressive behavior in wild-type *versus* GluK4-deficient animals. Each mouse was placed in beaker of water from which it was unable to escape, and its mobility over time was recorded and scored. Immobility in this task is widely considered to be a manifestation of despair (Porsolt et al., 1977). I found that knockout mice spent less time immobile over the course of the trial (wild-type mean percent time spent immobile ± SEM = 41.55 ± 2.88%, n = 6; knockout mean percent time spent immobile ± SEM = 20.82 ± 6.73% n = 5; Student's T-test, $p = 0.0145$). A two-way ANOVA of mobility scored in 1-minute time bins revealed that genotype, time, and the interaction of genotype and time were all significant ($F = 9.29$, $p = 0.0138$; $F = 13.34$, $p < 0.0001$; and $F = 3.46$, $p = 0.0100$, respectively; Figure 5.1). These results are again consistent with those observed in GluK2 knockout mice, and, moreover, suggest that GluK4 may play a modulatory role in baseline affect and mood.

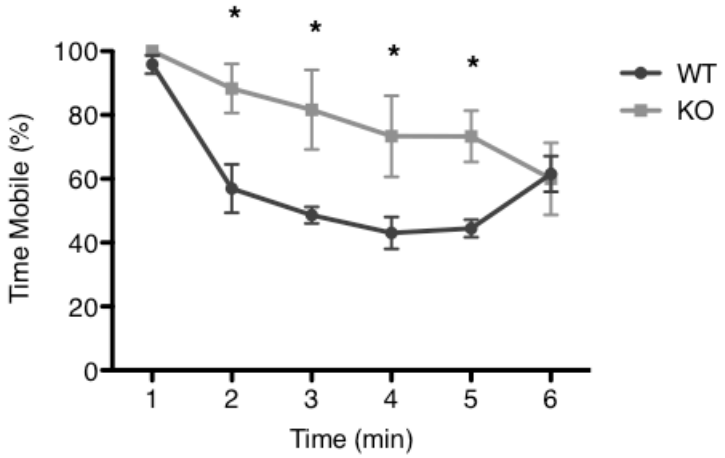

FIGURE 5.1. GluK4 knockout mice show decreased despair-type manifestations in forced swim test. GluK4 knockout mice (n = 5) were consistently more mobile than wild-type mice (n = 6) over the course of a 6-minute forced swim test ($p = 0.0138$). Bars represent mean ± SEM. * $p < 0.05$.

GluK4 Knockout Mice Demonstrate Reduced Anxiety, But Increased Locomotion, in the Open Field Test

To assess anxiety and risk-taking behavior, wild-type and GluK4 knockout animals were observed in an open field test. In this task, mice are allowed to freely investigate an open, evenly lit field, and typically demonstrate robust thigmotaxis. I found that, while both wild-type and GluK4 knockout mice preferred the periphery to the center of the field, knockout mice spent proportionally more time in the center than wild-type mice did (wild-type, n = 13; GluK4 knockout, n = 12; Student's T-test, p = 0.007, Figure 5.2a). Knockout mice also entered the center more frequently than wild-type mice (Student's T-test, p = 0.004; Figure 5.2b).

Additionally, knockout mice showed marked hyperactivity relative to the wild-type mice in the open field. The knockout mice traveled greater total distances (Student's T-test, p = 0.0004; Figure 5.2c) over the course of the assay at higher average velocities than wild-type mice (wild-type mean velocity in cm/second ± SEM = 6.92 ± 0.42; knockout mean velocity in cm/second ± SEM = 9.75 ± 0.54; Student's T-test, p = 0.0004).

FIGURE 5.2. GluK4 knockout mice show decreased aversion to center zone, and increased locomotion in short / lit open field. (A) Though both wild-type (n = 13) and GluK4 knockout mice (n = 12) preferred the periphery to the center zone of the open field during a 5-minute trial, the GluK4 knockout mice spent proportionally more time in the center zone of the open field (and, thus, proportionally less time in the periphery of the open field) than wild-type mice ($p = 0.007$), suggesting that GluK4 knockout mice have decreased basal levels of anxiety relative to wild-type mice. **(B)** GluK4 knockout mice entered the center zone more frequently than wild-type mice over the course of the trial ($p = 0.004$). **(C)** GluK4 knockout mice traveled greater distances over the course of the trial than wild-type mice, suggesting that GluK4 knockout mice may be hyperactive ($p = 0.0004$). Bars represent mean ± SEM.

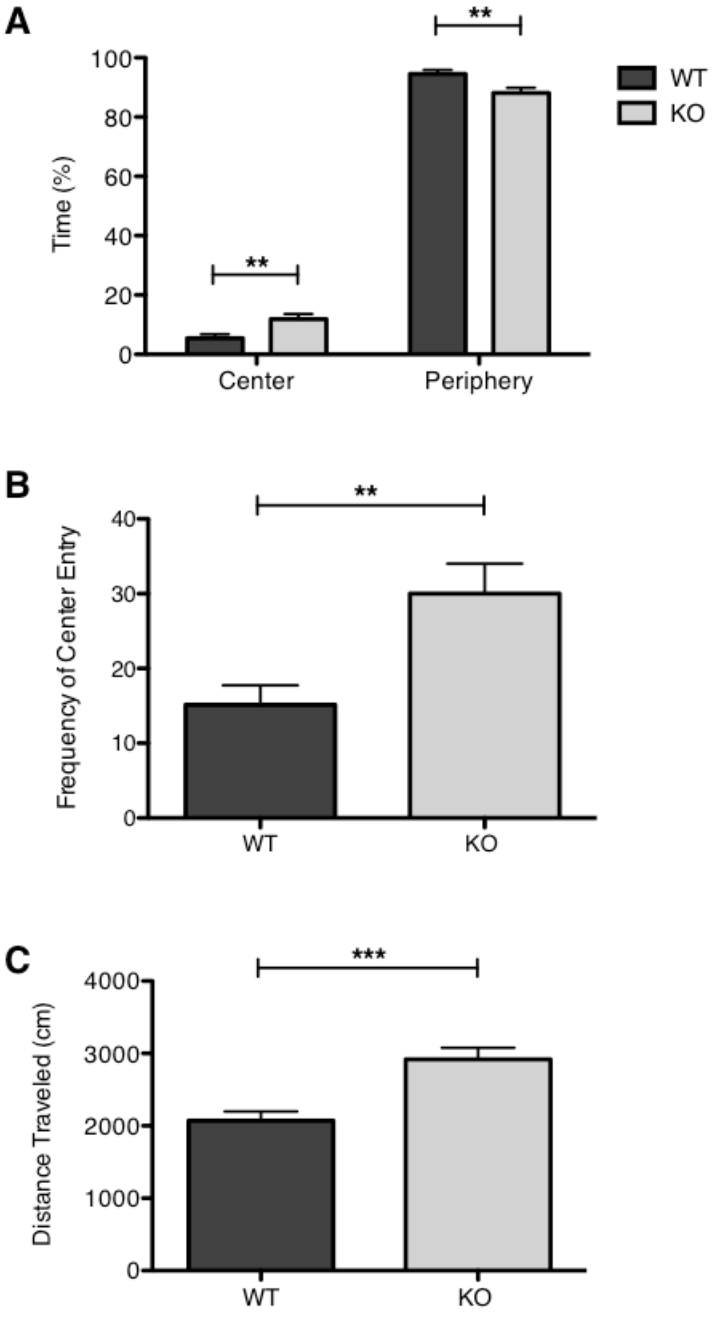
A
**
100
80
60
40
20
0
Time (%)
**
Center
Periphery
WT
KO
B
**
40
30
20
10
0
Frequency of Center Entry
WT
KO
C
***
4000
3000
2000
1000
0
Distance Traveled (cm)
WT
KO

Because hyperactivity could confound the interpretation of the differences between wild-type and GluK4 knockout mice in center zone preference and center zone entries, making it difficult to disambiguate the relative contributions of anxiety and locomotion, I tested separate cohorts of wild-type and GluK4 knockout mice in a second open field paradigm where the primary anxiogenic stimulus – light – was removed. The observation period was also extended to an hour to assess whether mice habituated to the open field environment. Thus, in this second paradigm (long / dark), I investigated whether hyperlocomotion was a function of anxiety or the novelty of the open field environment, rather than a constant feature of GluK4 knockout mouse behavior.

I found that the distance traveled by wild-type and GluK4 knockout mice decreased over time as the mice habituated to the environment. However, GluK4 knockout mice consistently traveled greater distances throughout the 1-hour observation period than wild-type mice, despite demonstrating habituation (Two-way ANOVA: effect of genotype, $F = 8.435$, $p = 0.0076$; effect of time, $F = 31.26$, $p < 0.0001$; wild-type $n = 15$, knockout $n = 12$; Figure 5.3a). Hyperlocomotion in GluK4 knockout animals was therefore independent of the novelty of the environment.

The number of center entries per time bin decreases progressively throughout the trial, in a similar fashion to total distance traveled. However, a two-way ANOVA revealed that the number of center entries in the GluK4 knockout cohort

is significantly higher than in the wild-type cohort (effect of genotype, $F = 5.42$, $p = 0.0283$; Figure 5.3b). Meanwhile, GluK4 mice appeared to spend more time in the center zone than wild-type mice, though the data for each time point were variable, and the difference was not quite significant by two-way ANOVA (effect of genotype, $F = 4.00$, $p = 0.0564$; Figure 5.3c). There was also a significant effect of time on the percent of time spent in the center zone: both wild-type and GluK4 knockout animals appear to have spent more time in the center zone as the trial progressed ($F = 3.47$, $p = 0.0002$).

FIGURE 5.3. GluK4 mice show decreased aversion to center zone, and increased locomotion in long / dark open field. (A) The distance traveled by GluK4 knockout mice (n = 12) was consistently greater than that traveled by wild-type mice (n = 15; p = 0.0076). Nevertheless, both wild-type and GluK4 knockout cohorts habituate to the open field environment over the course of the 1-hour trial. **(B)** The frequency of center zone entry is greater in GluK4 knockout mice than in wild-type mice (0.0283). **(C)** The proportion of time spent in the center zone is different, though not quite significantly (p = 0.0564), between wild-type and GluK4 knockout mice over the course of the trial. Bars represent mean ± SEM.

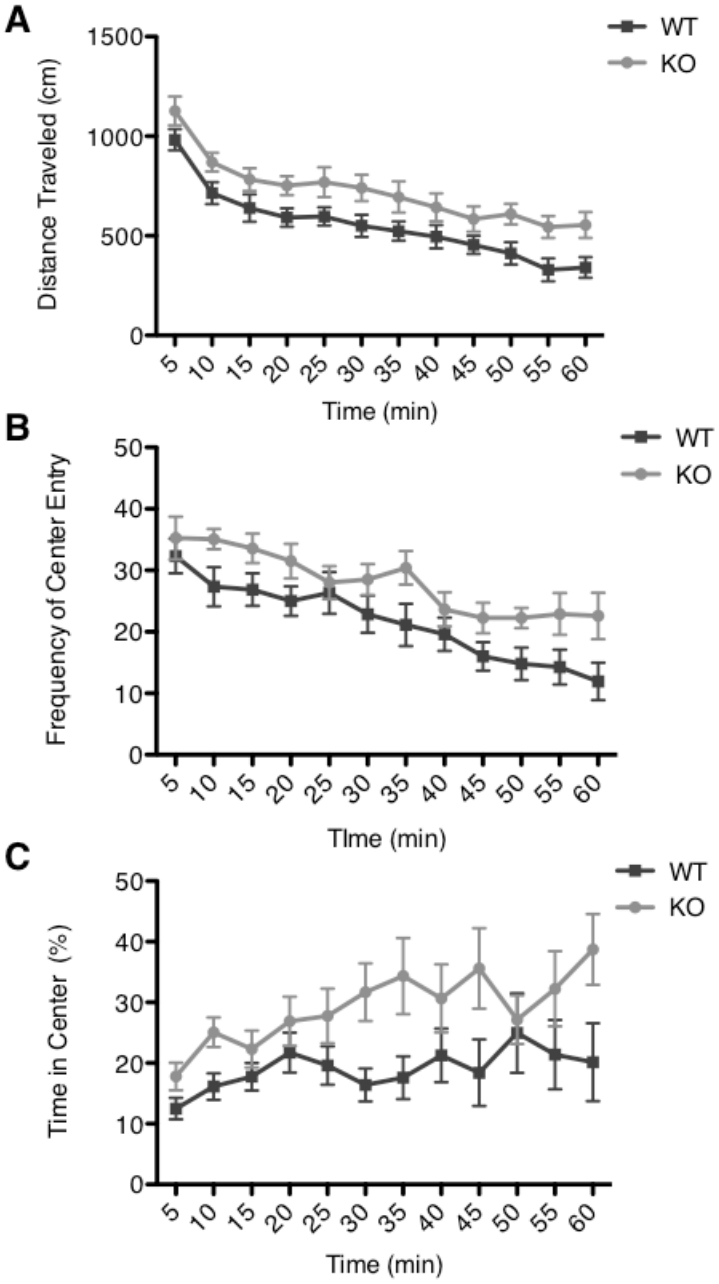
A
WT
KO
Distance Traveled (cm)
1500
1000
500
0
5 10 15 20 25 30 35 40 45 50 55 60
Time (min)
B
WT
KO
Frequency of Center Entry
50
40
30
20
10
0
5 10 15 20 25 30 35 40 45 50 55 60
TIme (min)
C
WT
KO
Time in Center (%)
50
40
30
20
10
0
5 10 15 20 25 30 35 40 45 50 55 60
Time (min)

Together, these results suggest several interpretations. One possibility is that hyperlocomotion accounts for the differences in center entries and percent time spent in center in both the first (short / lit) and the second (long / dark) open field paradigms, and that there is no difference in basal anxiety levels between wild-type and GluK4 knockout mice. Another possibility is that in the first paradigm, it is the open area of the field itself that is serving as the primary anxiogenic stimulus, independently of the ambient illumination. Thus, the fact that wild-type and GluK4 knockout mice differed in center zone preference in both the first and second paradigms could still be attributed to basal differences in anxiety. This would also explain why the time spent in the center zone in the second paradigm increased in both wild-type and knockout cohorts: as they became more familiar with the environment, the center zone may have become less anxiogenic.

GluK4 Ablation Affects PPI and the Acoustic Startle Response

PPI is a cross-species indicator of sensorimotor gating, and involves a suppression of the startle response evoked by a loud tone when that tone is immediately preceded by a weaker tone (Geyer et al., 1990). Under normal conditions, PPI is thought to be a precognitive means of preventing sensory overload (van den Buuse, 2010). Meanwhile, impaired PPI is widely considered to be an endophenotype of schizophrenia – a disorder characterized by cognitive disorganization and an inability to distinguish between salient and non-salient environmental cues (Perry and Braff, 1994). The cellular basis of PPI is complex and involves many brain structures and neurotransmitter systems, among which

are the hippocampus and glutamate, respectively (Reijmers et al., 1995; Koch, 1996).

To assess the effect of GluK4 ablation on PPI, I evaluated wild-type and GluK4 knockout mice in a multi-block PPI paradigm. First, the startle response to single pulses with intensities ranging from 80 – 120 dB was analyzed. Next, the pulse was preceded by a prepulse, and the pulse intensity was maintained at 120 dB, while the prepulse intensity was varied from 3 to 12 dB above the background white noise level of 65 dB. Finally, the prepulse and pulse were maintained at 6 dB (above background) and 120 dB, respectively, and the ISI between the prepulse and the pulse was varied from 25 to 500 milliseconds.

The overall response to single acoustic pulses of varying intensity was significantly different between wild-type and GluK4 knockout mice (two-way ANOVA, effect of genotype, $F = 7.12$, $p = 0.0132$; wild type n = 15, knockout n = 12; Figure 5.4a). *Post-hoc* analysis of the individual pulse intensities revealed that the response to 80, 90, and 100 dB pulses was largely the same between genotypes, but that GluK4 knockout mice displayed significantly reduced startle intensities relative to wild-type mice at 110 dB ($p < 0.01$) and 120 dB ($p < 0.0001$).

PPI was measured as a percentage, representing the ratio of the magnitude of the startle response (Vmax) evoked by a pulse following a prepulse, over the

magnitude of the average baseline startle response to a single 120 dB pulse. Overall, the percent PPI was also significantly reduced in GluK4 knockout mice compared to wild-type mice (two-way ANOVA, effect of genotype, $F = 8.52$, $p = 0.0073$; Figure 5.4b), indicating that GluK4 mice do not effectively inhibit the startle response following a prepulse. Post-hoc analysis indicated that this effect was significant at a prepulse intensity of 6 dB ($p < 0.01$) and 12 dB ($p < 0.001$) above background. Varying the ISI between the prepulse and the pulse did not yield a significant difference between wild-type and GluK4 knockout mice (two-way ANOVA, effect of genotype, $F = 2.34$, $p = 0.1387$; Figure 5.4c).

FIGURE 5.4. The acoustic startle response and PPI are impaired in GluK4 knockout mice. (A) GluK4 knockout mice (n = 15) showed a decreased reaction relative to wild-type mice (n = 12) to acoustic pulses of varying intensity ($p = 0.0132$). **(B)** %PPI was decreased in GluK4 knockout mice ($p = 0.0073$), suggesting impaired sensorimotor gating. **(C)** Varying the ISI did not result in significant differences in %PPI between wild-type and GluK4 knockout mice ($p = 0.1387$). Bars represent mean ± SEM. ** $p < 0.01$, *** $p < 0.001$

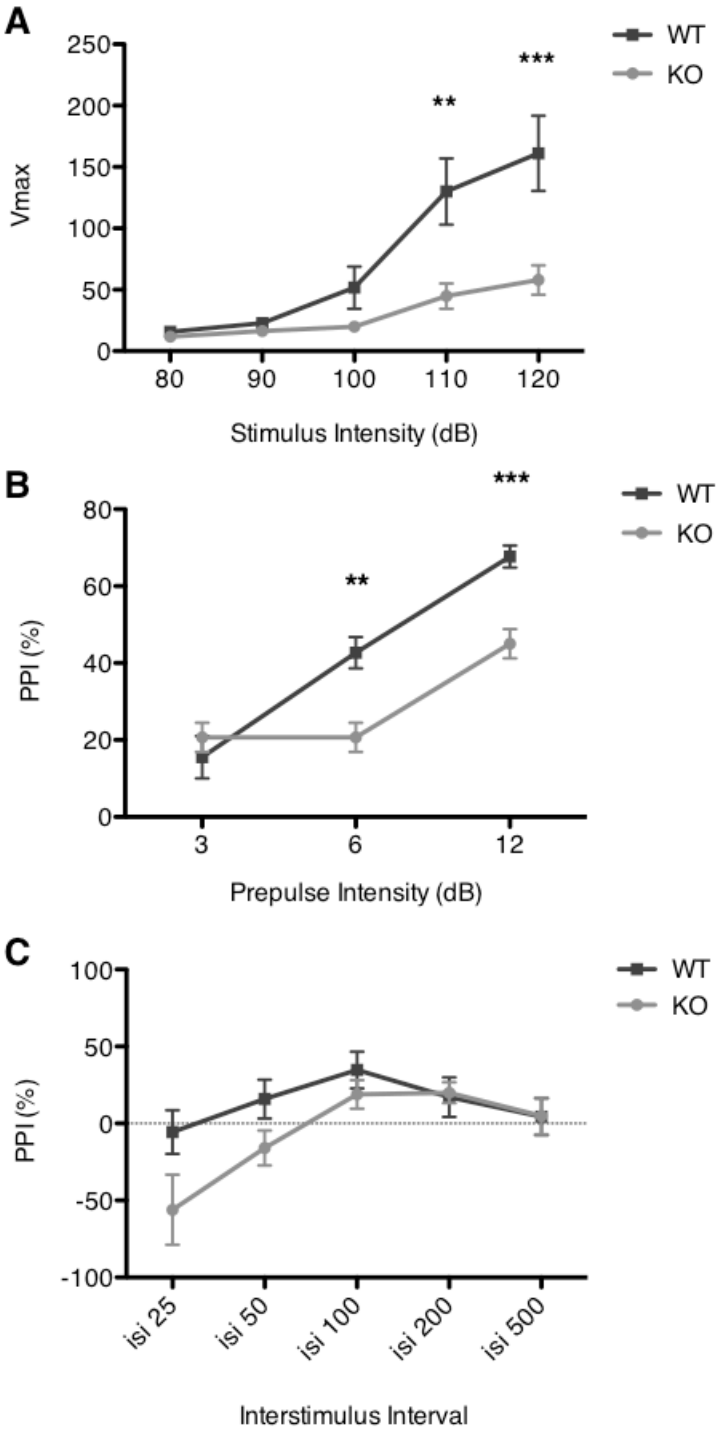
A
WT
KO
250
200
150
100
50
0
Vmax
**
***
80
90
100
110
120
Stimulus Intensity (dB)
B
WT
KO
80
60
40
20
0
PPI (%)
**
***
3
6
12
Prepulse Intensity (dB)
C
WT
KO
100
50
0
-50
-100
PPI (%)
isi 25
isi 50
isi 100
isi 200
isi 500
Interstimulus Interval

Taken together, these results indicate that GluK4 knockout mice show deficits in PPI, as well as the acoustic startle response to a single pulse. The deficit in PPI indicates that GluK4 plays an essential role in sensorimotor gating, and reinforces the hypothesis that impaired GluK4 function or expression contributes to the pathogenesis of schizophrenia. Furthermore, the deficit in the acoustic startle response observed in GluK4 knockout mice suggests a more general difference in emotionality and arousal between wild-type and knockout mice, as the acoustic startle response is modulated by corticotropin releasing factor, a hormone that has been implicated in anxiety disorder and major depression (Risbrough et al., 2003). Thus, the deficit in the acoustic startle response dovetails with the decreased anxiety- and depressive-like behaviors in GluK4 knockout mice that I observed in the open field test and forced swim test, respectively.

CHAPTER 6: GLUK4 IN EXCITOTOXIC NEURODEGENERATION

GluK4 Mediates Kainate-induced Neurodegeneration in the CA3 Region of the Hippocampus

The hippocampus as a whole, and the CA3 region in particular, is exceptionally vulnerable to excitotoxic neurodegeneration due to its high concentration of ionotropic glutamate receptors (Nadler, 1981; Ben-Ari, 1985). The CA3 also corresponds to the region of highest GluK4 expression within the brain (Darstein et al., 2003). To determine the effect of GluK4 deficiency on excitotoxicity, I performed IH stereotaxic kainate injections on wild-type and GluK4 knockout animals. 24 hours after surgery, animals were perfused with saline and PFA, and their brains were removed and sliced on a microtome. Staining the resulting sections with FJC, a marker of degenerating neurons (Schmued et al., 2005), revealed that kainate resulted in extensive cell death in the CA1, CA3, and hilar regions of the hippocampus in wild-type animals (Figure 6.1a, b). However, the CA3 region appeared to be largely spared in GluK4 knockout animals (Figure 6.1e, f). Because it was possible that the lack of FJC staining in the CA3 region of GluK4 knockout sections was actually the result of cell death so severe that the cells in that region had already been degraded, I co-stained the sections with DAPI to assess the general morphology and integrity of the remaining cells. In GluK4 knockout tissue, cells within the CA3 region appeared to be intact and densely packed, while in wild-type tissue, they appeared to be pyknotic and sparsely distributed (Figure 6.1c, d, g, h). Thus, the CA3 region was indeed neuroprotected following kainate injection in GluK4 knockout animals.

I then used stereological methods to quantify the density of FJC staining, and thereby compare the relative extent of neurodegeneration in wild-type *versus* GluK4 knockout hippocampal tissue. As I had observed in my preliminary investigations, I found that GluK4 deficiency resulted in significantly reduced kainate-induced cell death in the CA3 region (Student's T-test, $p = 0.0271$), but not in the CA1, CA2, or dentate gyrus (Figure 6.1i). These results indicate that GluK4 activation is primarily responsible for excitotoxic cell death within the CA3.

FIGURE 6.1. GluK4 ablation attenuates kainate-induced neurodegeneration in the CA3. FJC- **(A, B)** and DAPI- **(C, D)** stained tissue from of KA-treated wild-type animals revealed neurodegeneration throughout the hippocampus. **(B)** and **(D)** correspond to enlargements of the indicated regions of **(A)** and **(C)**, respectively, and demonstrate extensive neurodegeneration in the CA3 region of the hippocampus. FJC- **(E, F)** and DAPI- **(G, H)** stained tissue from KA-treated GluK4 knockout animals revealed decreased neurodegeneration relative to wild-type animals, specifically in the CA3 region of the hippocampus **(F, H)** where GluK4 expression is most concentrated. **(F)** and **(H)** represent enlargements of indicated regions of **(E)** and **(G)**, respectively. **(I)** Stereological quantification of neurodegeneration, corresponding to mean area of FJC staining, demonstrated specific neuroprotection of the CA3 region in GluK4 knockouts ($p = 0.0271$). Bars represent mean ± SEM.

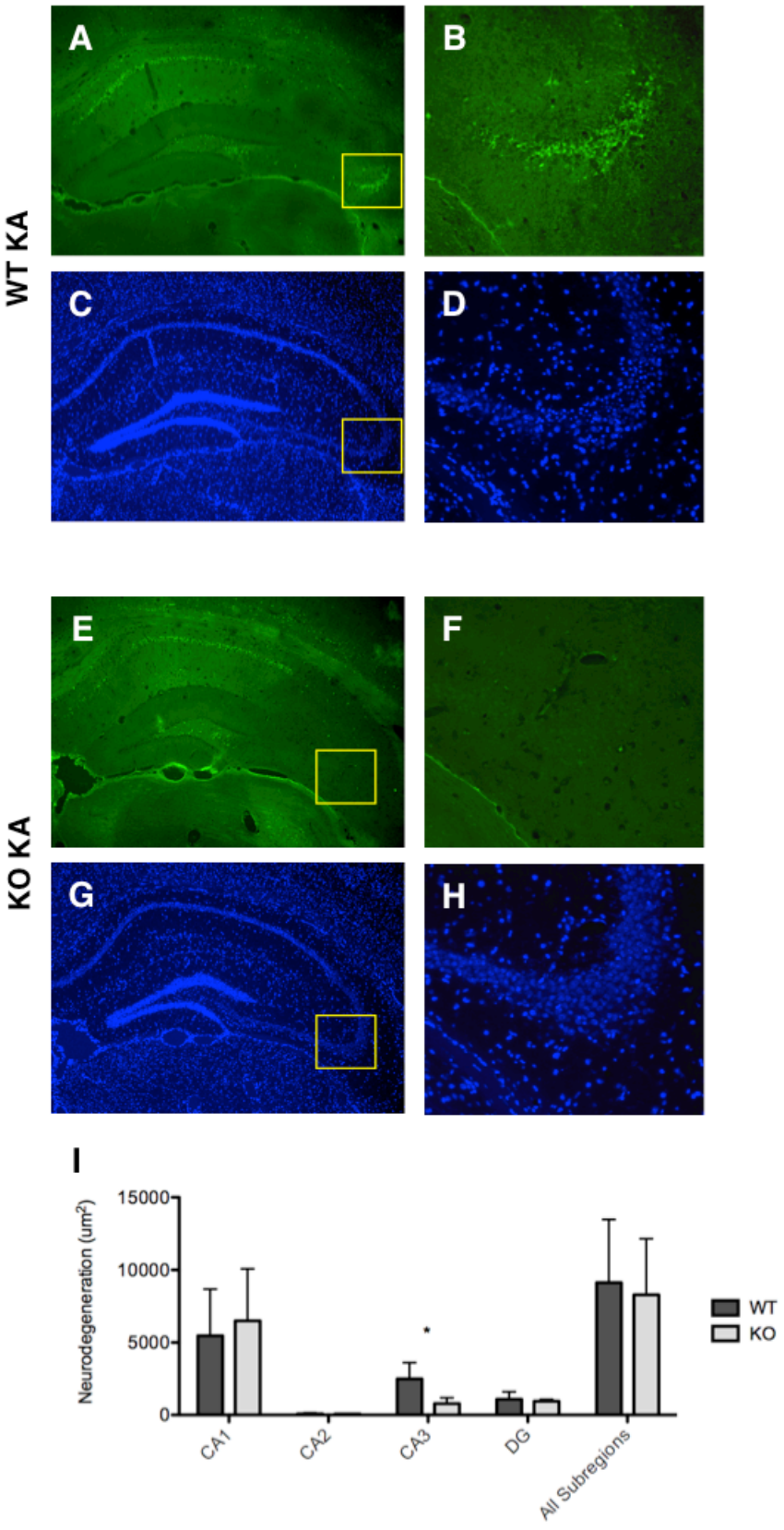
WT KA
A
B
C
D
KO KA
E
F
G
H
I
Neurodegeneration (um²)
15000
10000
5000
0
*
CA1
CA2
CA3
DG
All Subregions
WT
KO

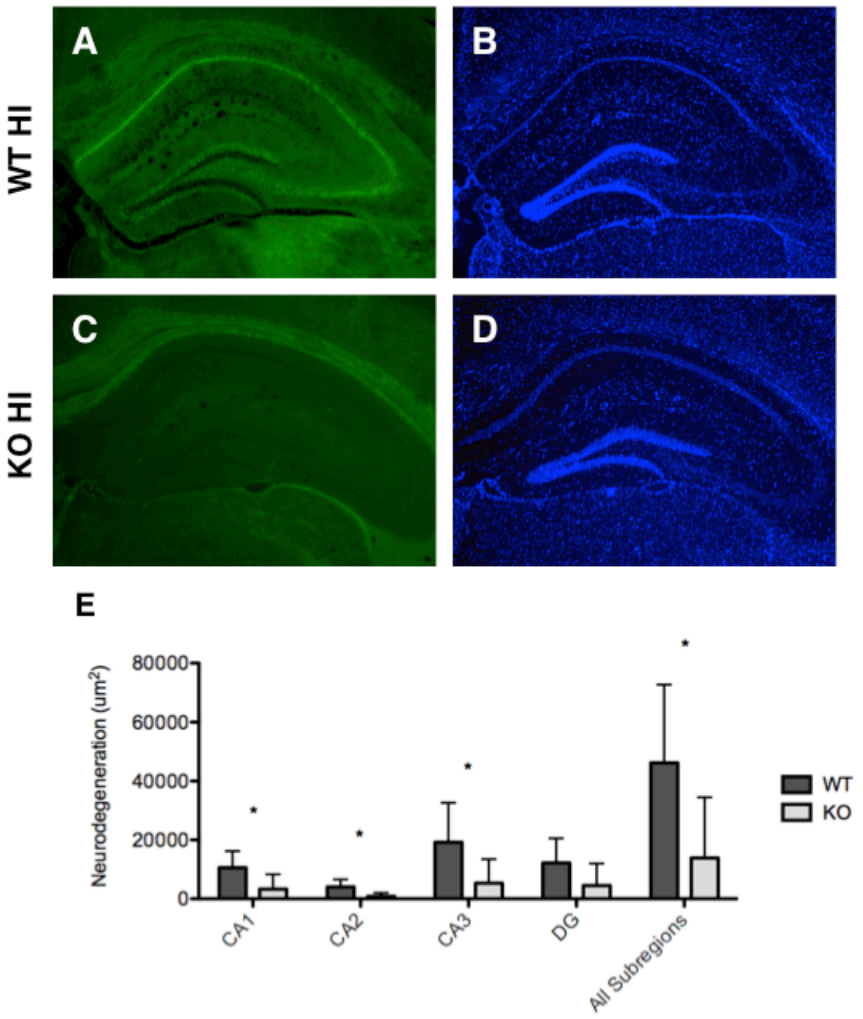

FIGURE 6.2. GluK4 ablation attenuates ischemia-induced neurodegeneration throughout the hippocampus. HI resulted in extensive neurodegeneration throughout the hippocampus of wild-type animals as indicated by FJC (A) and DAPI (B) staining. FJC staining for neurodegeneration (C) was strongly reduced in GluK4 knockout animals, and DAPI staining (D) showed intact cells throughout all subregions of the hippocampus. (E) Stereological quantification of neurodegeneration reflects neuroprotection throughout the hippocampus in GluK4 knockout animals relative to wild-type animals after HI ($p = 0.0405$), particularly in the CA1 ($p = 0.0371$), CA2 ($p = 0.0187$), and CA3 ($p = 0.0189$) subregions. Bars represent mean ± SEM.

GluK4 Orchestrates Widespread Hippocampal Neurodegeneration Following HI

To further explore the role of GluK4 in neurodegeneration in a clinically relevant context, Anna Kruyer, a fellow student in my laboratory with whom I worked closely on many of the experiments described herein, compared neurodegeneration in wild-type and GluK4 knockout mice following transient-global ischemia (HI), a murine model of stroke. Mice were subjected to unilateral transection of the left common carotid artery, followed by 45 minutes of hypoxia. Using the same stereological methods to assess cell death as in the stereotaxic kainate injections described above, Anna found that HI resulted in extensive cell death in all hippocampal subregions. However, GluK4-deficient animals showed dramatically reduced neurodegeneration throughout the hippocampus relative to wild-type animals (Student's T-test, $p = 0.0405$), particularly in the CA1 (Student's T-test, $p = 0.0371$), CA2 (Student's T-Test, $p = 0.0187$) and CA3 subregions (Student's T-Test, $p = 0.0189$) (Figure 6.2). The robust neuroprotection afforded by GluK4 ablation suggests that GluK4 plays a role in initiating the molecular cascades that lead to neurodegenerative cell death.

CHAPTER 7: MOLECULAR MECHANISMS OF GLUK4-MEDIATED NEURODEGENERATION

The neuroprotection observed in GluK4 knockout mice following administration of kainate or HI suggested that GluK4 was critical to the activation of cell death pathways. To elucidate the role of GluK4 in the molecular cascades leading to neurodegeneration, I designed a microarray assay in which I compared mRNA expression levels from kainate- versus PBS-injected wild-type and knockout samples. Enriched genes were further analyzed to extrapolate enriched molecular pathways. I chose to employ the kainate-mediated model of neurodegeneration over the HI-mediated model because the nature of the insult – kainate – is specific to kainate receptors and the extent of damage is highly reproducible between animals.

Microarray Design

Using the same IH injection protocol as I had to perform the stereology experiments described above, I bilaterally injected wild-type and GluK4 knockout mice with kainate or PBS. 24 hours after injection, hippocampi from both hemispheres were isolated, and one from each animal was further microdissected to isolate the CA3, as the neuroprotective effect of GluK4 ablation is restricted to the CA3 in the kainate-mediated model of neurodegeneration. However, the CA3 region is difficult to isolate and yields far less mRNA than whole hippocampus samples. To preclude the possibility that the CA3 samples might under-represent the molecular changes induced by kainate injection by

yielding insufficient or poor-quality mRNA, I included both CA3 and whole hippocampus samples in the microarray design. In sum, I tested the effects of treatment (kainate versus PBS), genotype (wild-type versus GluK4 knockout), and tissue (whole hippocampus versus CA3). All conditions included in the microarray are outlined in Table 7.1.

TABLE 7.1. Microarray conditions.

Genotype	Injection	Tissue Type
Wild-type	PBS	Whole hippocampus
Wild-type	PBS	CA3
GluK4 Knockout	PBS	Whole hippocampus
GluK4 Knockout	PBS	CA3
Wild-type	Kainate	Whole hippocampus
Wild-type	Kainate	CA3
GluK4 Knockout	Kainate	Whole hippocampus
GluK4 Knockout	Kainate	CA3

Microarray Sample Quality Control

All RNA samples were purified after extraction, and bioanalyzed to assess the RNA integrity number (RIN) of each sample. Any samples where the RIN fell below 8 were re-purified.

To ensure that CA3 samples were free, or as free as possible, of contamination from neighboring subregions, I performed one-step RT-PCR on CA3 mRNA samples using primers that were designed to amplify Nov and Dsp, genes specific to the CA1 and DG subregions, respectively. Reactions for each region-specific primer set were optimized for cycle number and RNA concentration. PCR products were then analyzed semi-quantitatively for Nov and Dsp levels,

and samples that yielded the lowest expression of each – i.e., were least contaminated – were selected for further experiments (Figures 7.1 and 7.2).

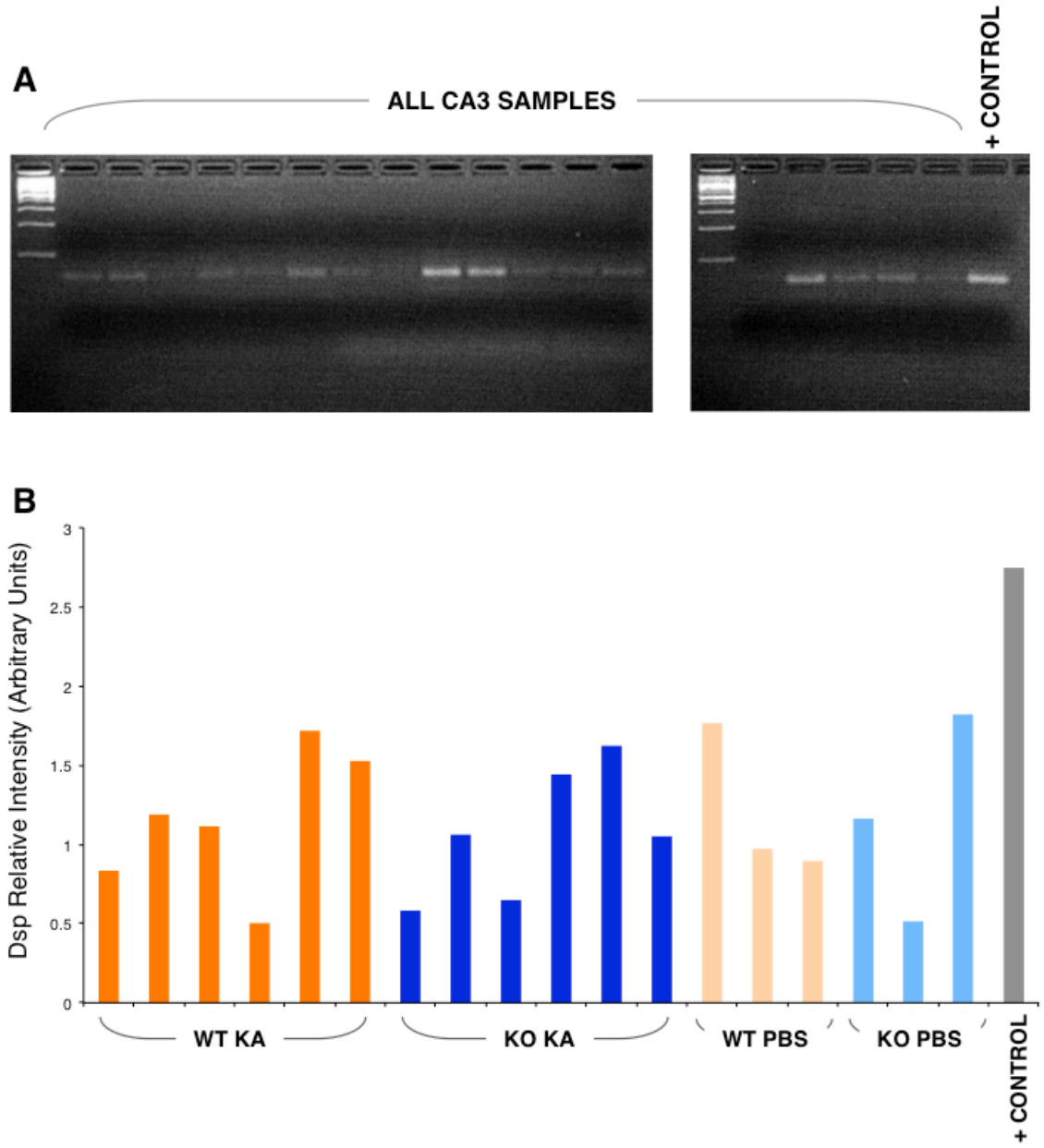

FIGURE 7.1. Assessing contamination of microarray CA3 samples by DG tissue. (A) Representative gels of one-step RT-PCR assays for the DG marker Dsp show varying levels of DG contamination in CA3 samples. A DG sample was run as a positive control in the last lane. **(B)** Semiquantitative analysis of Dsp expression was used to select the least-contaminated CA3 samples from each condition. KA, kainate-injected samples; PBS, PBS-injected samples; + control, pure DG mRNA used as template instead of CA3 mRNA.

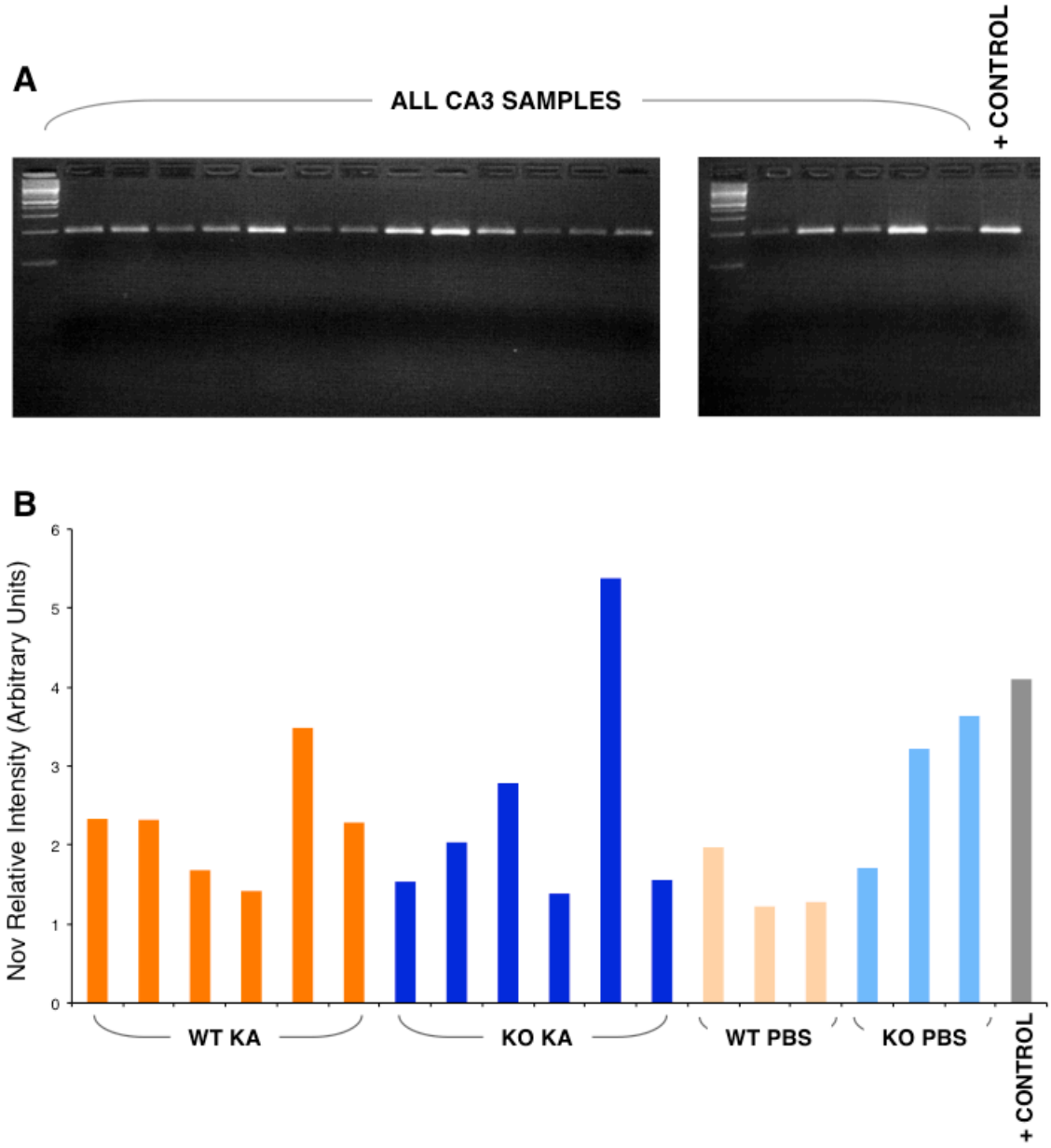

FIGURE 7.2. Assessing contamination of microarray CA3 samples by CA1 tissue. (A) Representative gels of one-step RT-PCR assays for the CA1 marker Nov show varying levels of CA1 contamination in CA3 samples. A CA1 sample was run as a positive control in the last lane. **(B)** Semiquantitative analysis of Nov expression was used to select the least-contaminated CA3 samples from each condition. + control, pure CA1 mRNA used as template instead of CA3 mRNA.

Additionally, all CA3 and whole hippocampus samples were analyzed to determine whether the samples that were supposed to receive kainate had actually received it. FJC staining of kainate-injected tissue will occasionally reveal that kainate has not been properly administered, perhaps as a result of air bubbles in the injection syringe or defects in the injection pump. Thus, expression levels of Hsp27, a heat shock protein that has been shown to be highly up-regulated following IP kainate injection (Brecht et al., 2005), were assessed by one-step RT-PCR as a positive indicator of kainate injection. Hsp27 has the added advantage of being neuroprotective in excitotoxic conditions, as transgenic mice that overexpress Hsp27 are neuroprotected in the context of MCAO, indicating that it may still be up-regulated in GluK4 CA3 samples despite resistance of cells in that region to kainate-induced neurodegeneration. Hsp27 was indeed observed in both kainate-injected wild-type and GluK4 knockout tissue, and expression levels were indistinguishable using semi-quantitative analysis (Figure 7.3). Ultimately, all kainate-injected samples had received kainate.

FIGURE 7.3. Assessing Hsp27 expression as a measure of successful kainate injection. (A) Levels of Hsp27, a neuroprotective gene that is highly up-regulated in the context of excitotoxicity, were assessed in kainate- and PBS-injected samples using one-step RT-PCR. Kainate- and PBS-injected samples were interspersed in these gels, with the exception of the last gel in which only kainate-injected samples were run. **(B)** Semiquantitative analysis revealed that all samples that were supposed to receive kainate had actually received it.

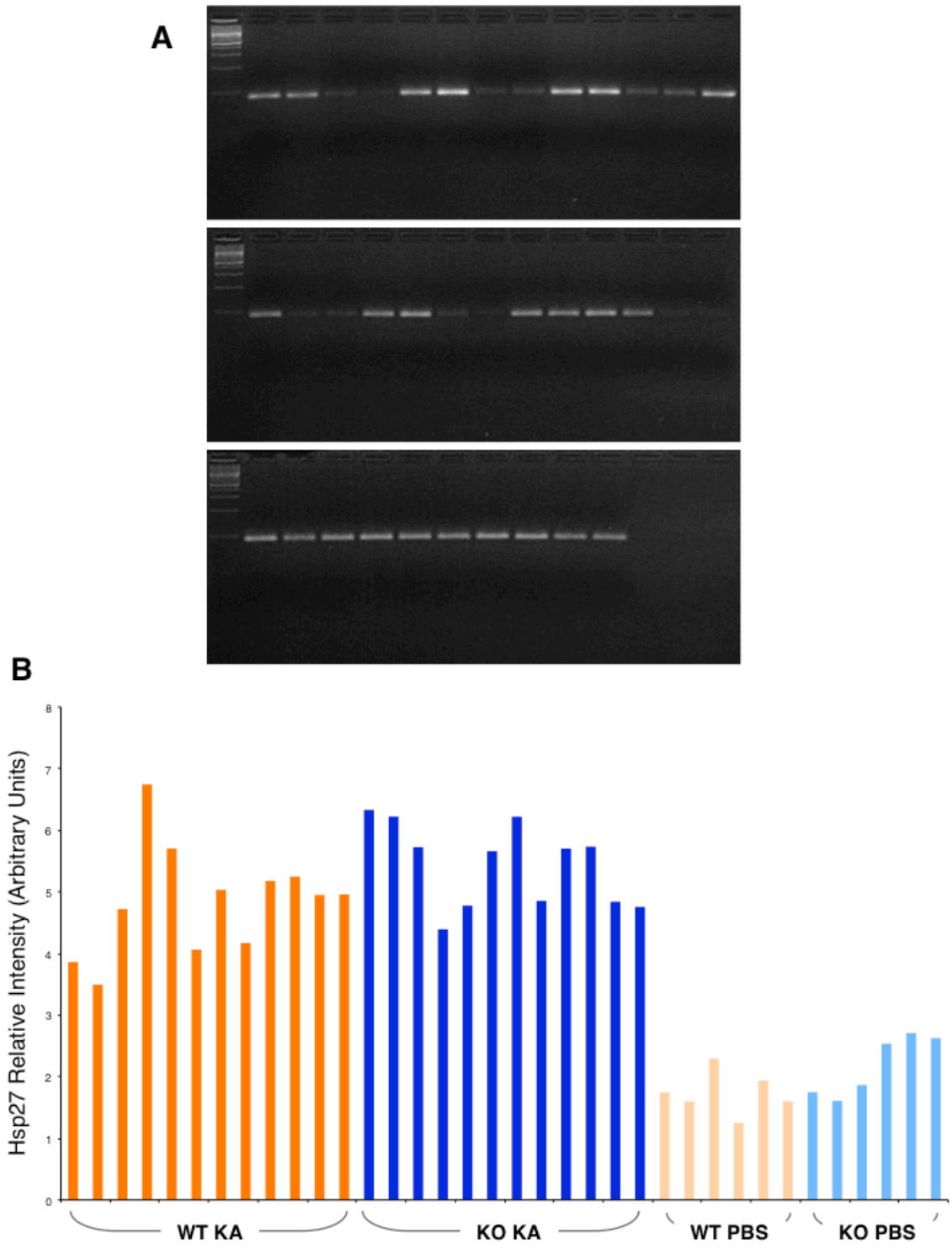
A
B
Hsp27 Relative Intensity (Arbitrary Units)
0
1
2
3
4
5
6
7
8
WT KA
KO KA
WT PBS
KO PBS

Three samples from each of the eight conditions outlined in Table 7.1 were pooled and submitted to the Genomics Core Facility at The Rockefeller University, where they were then labeled, hybridized to the individual wells of an Illumina Expression BeadChip, and scanned. Raw gene expression signals were thresholded as described in materials and methods.

Gene Enrichment in CA3 Versus *Whole Hippocampus Samples*

For all conditions examined, whole hippocampus samples yielded fewer enriched genes than CA3 samples. For instance, the list of genes up-regulated by 2-fold or greater in wild-type CA3 tissue following kainate injection included 559 genes, while the same list in whole hippocampus tissue included only 336 genes. One reason for this difference may be that CA3-specific changes in gene regulation were counterbalanced by a lack of change, or perhaps changes in the opposite direction, in the same genes in other regions of the hippocampus. Thus, whole hippocampus samples were excluded from further analysis, and all of the results reported here are from CA3 samples.

Gene Enrichment Following Kainate Injection in Wild-type Versus *GluK4 Knockout Samples*

To determine the effects of kainate on gene expression, the fold-change in gene expression levels in the kainate condition relative to the PBS condition was calculated for each genotype. The resulting wild-type and GluK4 knockout gene lists were then compared to determine the effects of kainate on gene expression

between genotypes. Only genes with a fold-change greater than |2| in the kainate condition relative to the PBS condition for each genotype were included in this analysis. 3 gene lists emerged: genes that were exclusively up-regulated in wild-type tissue, i.e., up-regulated by 2-fold or more in wild-type tissue but not GluK4 knockout tissue following kainate injection, relative to PBS (320 genes altogether); genes that were exclusively up-regulated in GluK4 knockout tissue (74 genes); and genes that were up-regulated in both wild-type and GluK4 knockout tissue (239 genes) (Figure 7.4). The top 30 genes in the wild-type-exclusive and GluK4 knockout-exclusive lists are outlined in Tables 7.2 and 7.3.

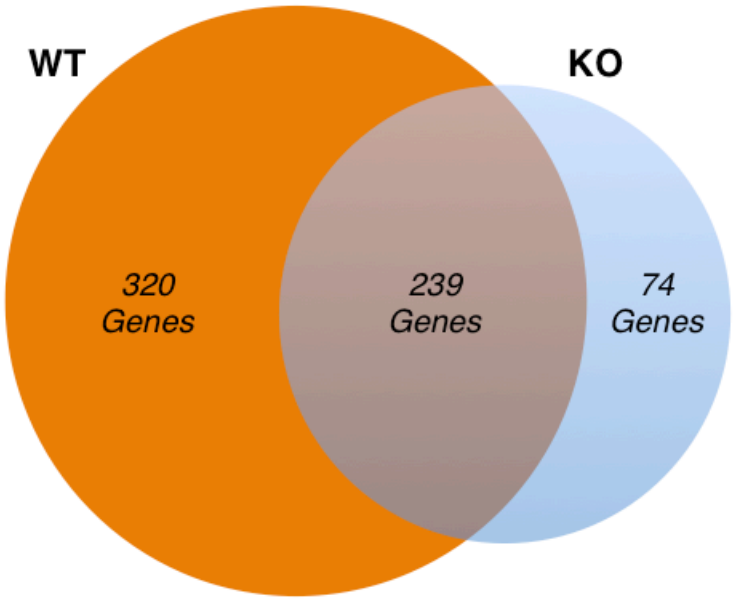

FIGURE 7.4. Schematic Venn diagram of gene enrichment in wild-type *versus* GluK4 knockout samples after kainate injection. 320 genes were exclusively enriched by |2|-fold or more following kainate injection (relative to PBS injection) in wild-type samples (orange); 74 genes were exclusively enriched in GluK4 knockout samples (blue); and 239 genes were enriched in both.

TABLE 7.2. Genes enriched in wild-type samples following kainate.

Gene Name	Symbol	Fold-change in wild-type following kainate, relative to PBS	Fold-change in knockout following kainate, relative to PBS
β-actin	Actb	**-50.522327**	-1.2285179
growth hormone	Gh	**17.440138**	1.1244828
prolactin	Prl	**7.5980372**	-1.0499934
purkinje cell protein 2 (L7)	Pcp2	**6.7068973**	1.4683733
solute carrier family 13 (sodium/sulfate symporters), member 4	Slc13a4	**6.142569**	-1.9992677
sulfatase 1	Sulf1	**5.927293**	-1.0554414
prolactin receptor	Prlr	**5.5717325**	-1.3291636
decorin	Dcn	**5.001785**	1.7570093
matrix Gla protein	Mgp	**4.4215**	1.5079937
retinol dehydrogenase 5	Rdh5	**4.349441**	-1.2431543
insulin-like growth factor 2	Igf2	**4.2631984**	-1.9494125
insulin-like growth factor binding protein 2	Igfbp2	**4.242587**	-1.1547633
nuclear receptor co-repressor 1	Ncor1	**-4.0182915**	1.1821797
solute carrier family 17 (sodium-dependent inorganic phosphate cotransporter), member 6	Slc17a6	**4.0027905**	1.4765645
lectin, galactose binding, soluble 1	Lgals1	**3.896389**	1.9174436
gap junction protein, β-2	Gjb2	**3.4975474**	1.3912534
interferon-induced protein with tetratricopeptide repeats 3	Ifit3	**3.49664**	1.3959935
interferon, α-inducible protein 27	Ifi27	**3.4579968**	1.1008872
tubulin, α-1c	Tuba6	**3.4517848**	1.6111073
rap guanine nucleotide exchange factor (GEF)-like 1	Rapgefl1	**-3.4238975**	-1.9603293
tubulin, β-2b	Tubb2b	**3.2463224**	1.39096
leucine rich repeat containing 4B; similar to Leucine rich repeat containing 4B	LOC100045241	**-3.2053182**	-1.5128021
lectin, galactoside-binding, soluble, 3 binding protein	Lgals3bp	**3.2032213**	1.2697843
ubiquitin specific peptidase 18; similar to ubiquitin specific protease UBP43	LOC100048346	**3.1747127**	1.701681
chemokine (C-C motif) ligand 2	Ccl2	**3.154905**	1.9624745
protein kinase C, γ	Prkcc	**-3.1515055**	-1.9287628
predicted gene 12141; heat shock protein 1 (chaperonin)	Hspd1	**3.1073248**	1.2092633
I830012O16Rik RIKEN cDNA I830012O16 gene	LOC667370	**3.1015675**	1.7340547
vesicle amine transport protein 1 homolog-like (T. californica)	Vat1l	**3.0500953**	-1.2528175
predicted gene 5778; similar to heterogeneous nuclear ribonucleoprotein A2/B1; heterogeneous nuclear ribonucleoprotein A2/B1	Hnrnpa2b1	**3.043459**	1.1359648

TABLE 7.3. Genes enriched in GluK4 knockout samples following kainate

Gene Name	Symbol	Fold-change in knockout following kainate, relative to PBS	Fold-change in wild-type following kainate, relative to PBS
similar to α-lactalbumin; lactalbumin, α	Lalba	**3.6236696**	1.1536819
sclerostin domain containing 1	Sostdc1	**-3.3527162**	1.4620374
inositol 1,4,5-trisphosphate 3-kinase A	Itpka	**-3.2814567**	-1.9674851
glycine dehydrogenase	Gldc	**-3.1782527**	-1.9073267
acyl-CoA thioesterase 11	Acot11	**-3.0526004**	-1.673179
tyrosinase-related protein 1	Tyrp1	**3.0267994**	1.3415347
cysteine and glycine-rich protein 3	Csrp3	**3.000433**	1.3494827
Ca2+-dependent activator protein for secretion 2	Cadps2	**-2.7261322**	-1.7462686
fibrinogen C domain containing 1	Fibcd1	**-2.6653936**	-1.2815868
pleckstrin and Sec7 domain containing 2	Psd2	**-2.6561596**	-1.3567331
chromagranin A	Chga	**2.6017258**	1.8398476
B-cell linker	Blnk	**2.5908782**	1.6979231
glycine decarboxylase	Gldc	**-2.5458357**	-1.817069
sulfotransferase family 1A, phenol-preferring, member 1	Sult1a1	**-2.5454924**	-1.2607372
serine peptidase inhibitor, Kazal type 8	Spink8	**-2.520413**	-1.592723
similar to calponin 3, acidic; predicted gene 4815; calponin 3, acidic	LOC100047856	**2.508167**	1.8010483
strawberry notch homolog 2 (Drosophila)	Sbno2	**2.5037324**	1.9636917
solute carrier family 7 (cationic amino acid transporter, ψ+ system), member 10	Slc7a10	**-2.4803817**	-1.3164182
polymerase (DNA-directed), δ 4	Pold4	**2.44297**	1.8516624
multiple EGF-like-domains 11	Megf11	**2.4371126**	1.8443365
glucosaminyl (N-acetyl) transferase 2, I-branching enzyme	Gcnt2	**2.425731**	1.7545487
lin-7 homolog B (C. elegans)	Lin7b	**-2.39229**	-1.9965154
activin A receptor, type IC	Acvr1c	**2.3459048**	1.6499034
phosphoatidic acid phosphatase type 2B	Ppap2b	**-2.3409045**	-1.7861793
ST6 (α-N-acetyl-neuraminyl-2,3-β-galactosyl-1,3)-N-acetylgalactosaminide a-2,6-sialyltransferase 4	St6galnac4	**2.3217778**	1.772647
chromogranin A	Chga	**2.3211932**	1.7686646
solute carrier family 39 member 12	Slc39a12	**-2.3190215**	-1.4546387
VGF nerve growth factor inducible	Vgf	**2.3179793**	1.6363449
B-cell leukemia/lymphoma 3	Bcl3	**2.3033428**	1.9761575
interferon γ induced GTPase	Igtp	**2.2822418**	1.8902932

DAVID Analysis of Enriched Molecular Pathways Indicates Enrichment of the JNK Pathway in Kainate-treated Wild-type Samples

The list of genes exclusively up-regulated following kainate treatment in wild-type, but not GluK4 knockout tissue, represents the genes that are enriched in a GluK4-dependent manner. To gain insight into the molecular pathways in which GluK4 might participate to mediate neurodegeneration, this list was analyzed using the Database for Annotation, Visualization and Integrated Discovery (DAVID), a program that compares gene lists against various pathway databases and extracts statistically over-represented (i.e., enriched) pathways (Huang et al., 2007).

Using the DAVID program, the list of genes exclusively enriched in wild-type tissue was compared against the Kyoto Encyclopedia of Genes and Genomes (KEGG) database. Significantly enriched pathways ($p < 0.05$) are outlined in Table 7.4. The biological relevance of some of these pathways, such as the type II diabetes mellitus pathway, to GluK4-mediated excitotoxicity is not immediately clear. However, among the significantly enriched pathways, the Mitogen Activated Protein Kinase (MAPK) signaling pathway is of particular interest: while it includes many auxiliary pathways and governs diverse physiological processes, including proliferation, differentiation, and inflammation, it also mediates apoptosis through the subset of MAPK proteins that comprise the JNK pathway (Schaeffer and Weber, 1999).

TABLE 7.4. KEGG pathways exclusively enriched in wild-type samples following kainate

KEGG Pathway	p Value	Genes
Homeostasis/Energy Metabolism		
Type II diabetes mellitus	0.0011	MAPK1, HK1, MAPK10, PRKCE, ABCC8, PRKCD
GnRH signaling pathway	0.0047	MAPK1, ADCY9, PTK2B, JUN, MAPK10, CAMK2A, PRKCD
Glycerolipid metabolism	0.0400	LPL, DGKB, DGKZ, MGLL
Neurotransmission		
Neuroactive ligand-receptor interaction	0.0030	TSPO, THRA, GRIA2, PRLR, NPY2R, GRIK5, GRIA3, NPY1R, GRM1, PRL, GH, F2R
Long-term potentiation	0.0053	MAPK1, GRIA2, PPP3R1, GRM1, CAMK2A, PRKCC
Long-term depression	0.0060	MAPK1, GNAO1, GRIA2, GRIA3, GRM1, PRKCC
Gap junction	0.0125	MAPK1, TUBB2B, ADCY9, GRM1, PRKCC, TUBB4
Calcium signaling pathway	0.0346	ADCY9, PTK2B, RYR3, PPP3R1, GRM1, CAMK2A, PRKCC, F2R
Hemovascular function		
Vascular smooth muscle contraction	0.0128	KCNMA1, MAPK1, ADCY9, ACTA2, PRKCE, PRKCD, PRKCC
Cell death		
MAPK signaling pathway	0.0270	MAPK1, DUSP1, JUN, PPP3R1, FGF10, HSPA1A, FGF13, MAPK10, PRKCC, HSPA8
Immunity		
Natural killer cell mediated cytotoxicity	0.0473	ICAM1, MAPK1, PTK2B, PPP3R1, FCGR4, PRKCC

There is strong evidence to suggest that the JNK pathway mediates excitotoxic neurodegeneration, as outlined in Chapter 1: mice deficient in JNK3, the neuronal isoform of JNK, are resistant to neurodegeneration following MCAO and IP kainate injection (Brecht et al., 2005), and JNK pathway-inhibiting compounds are neuroprotective (Bogoyevitch et al., 2004). There is also evidence linking JNK pathway activation and kainate receptors: MLK3, an earlier initiator of the JNK pathway kinase cascade, can form a complex with GluK2 and PSD95 that results in MLK3-autophosphorylation and, subsequently, JNK pathway activation

(Tian et al., 2005; Jiang et al., 2007). These findings, in conjunction with the enrichment of the MAPK pathway in wild-type but not GluK4 knockout tissue, suggested that GluK4 might mediate excitotoxic neurodegeneration through the JNK pathway.

Performing the same DAVID analysis with the list of genes exclusively enriched in GluK4 knockout tissue after kainate – genes that might play a neuroprotective role in the context of excitotoxicity – yielded no significantly enriched pathways.

GSEA Analysis Reveals Selective Enrichment of Cell Death Pathways in Kainate-treated Wild-type Samples

The DAVID program does not take into account the relative enrichment (i.e., fold-change values) of the genes within a given list, merely the gene names, when extrapolating enriched pathways. While this low stringency can be considered an advantage in the sense that it facilitates pathway discovery, it is also a disadvantage in the sense that it may over- or underestimate the importance of a given pathway by giving weight to the number – rather than the magnitude of regulation – of genes within a given list that coincide with a given pathway. Furthermore, DAVID cannot distinguish between significantly up-regulated versus significantly down-regulated pathways, thereby clouding downstream interpretations of biological relevance.

To address these issues, I performed a second round of analysis using GSEA software. GSEA can incorporate the magnitude – and, to some extent, the direction – of regulation of the genes within the list to generate a set of proposed pathways in which those genes might participate (Subramanian et al., 2005). GSEA was run from two distinct gene lists: all genes probed in the microarray from 1. wild-type, and 2. GluK4 knockout tissue, ranked by fold-change after kainate administration relative to their respective PBS baseline. These lists were then compared against the Biocarta pathway database to assess positively enriched (up-regulated) and negatively enriched (down-regulated) pathways.

As with DAVID analysis, the set of positively enriched pathways that is exclusive to the wild-type condition (Table 7.5) gives insight into the molecular actions of GluK4 downstream of kainate administration. While the relevance of some of the enriched pathways to GluK4-mediated neurodegeneration is not immediately apparent (for instance, the erythrocyte pathway), there is a clear enrichment of cell-death-mediating pathways. These include, in order from most to least statistically significant, the p53 hypoxia pathway, which involves the induction of apoptosis through p53; the caspase pathway, which involves the induction of apoptosis through the caspase proteolytic cascade; the death receptor pathway, which involves the induction of apoptosis through DR3 and DR4/5 receptors; the D4-GDI pathway, which involves the induction of apoptosis through D4-GDI, a molecule that regulates the cytoskeletal changes associated with apoptosis through the Rho family of GTPases; the Fas pathway, which involves the

induction of apoptosis through the cell-surface expressed Fas receptor; and the ceramide pathway, which involves the induction of apoptosis through ceramide, a lipid signaling molecule.

TABLE 7.5. Biocarta pathways exclusively enriched in wild-type samples following kainate

Biocarta Pathway	P Value	Genes (with Core Enrichment)
Cell Death		
p53 hypoxia Pathway	0.019	CDKN1A, HSP1A1, GADD45A, IGFBP3, CSNK1D
Caspase Pathway	0.019	ARHGDIB, LMNA, LMNB1, CASP8, CASP1, CASP4, CASP9, LMNB2, BIRC, CASP3, CASP7, CASP2, CASP6, APAF1, BIRC3, PRF1
Death Receptor Pathway	0.018	LMNA, FADD, CASP8, RELA, MAP3K14, NFKB1, TNFRSF10B, RIPK1, NFKBIA, TRAF2, CASP9, BIRC4, CASP3, CASP7, CASP6, APAF1, BIRC3
D4-GDI Pathway	0.020	not reported by GSEA
Fas Pathway	0.058	not reported by GSEA
Ceramide Pathway	0.050	not reported by GSEA
Cell Survival and Proliferation		
IGF-1 Pathway	0.041	FOS, JUN, SHC1
Nerve Growth Factor Pathway	1.627	not reported by GSEA
Immunity		
Toll-like Receptor Pathway	0.017	FOS, CD14, TLR2, JUN, MAP2K3, MYD88, RELA, TLR7, TIRAP, MAP3K14, NFKB1, LY96, NFKBIA, TLR4, IRAK1, TLR6, TRAF6
Natural Killer T-Cell Polarization Pathway	0.000	CCL4, CCL3, CCR5
IL6 Cytokine Pathway	0.020	FOS, STAT, JUN, CEBPB, SHC1
B Lymphocyte Pathway	0.051	not reported by GSEA
Homeostasis/Energy Metabolism		
Insulin Pathway	0.034	FOS, JUN, SHC1
Hemovascular Function		
Intrinsic Prothrombin Activation Pathway	0.017	F2R, PROS1, SERPING1, COL4A4, COL4A5, COL4A1, F5, COL4A2, COL4A6, FGA, FGG, SERPINC1, KLKB1
Erythrocyte Differentiation Pathway	0.034	not reported by GSEA

Amongst the pathways that were positively enriched in the GluK4 knockout samples (Table 7.6), the EPO NFkB pathway stands out a potential modulator of cell survival in the CA3. Aside from its role in the production of erythrocytes,

erythropoietin (EPO) promotes neuroprotection in murine models of stroke by activating a variety of downstream signaling pathways, including the NFkB pathway (van der Kooij et al., 2008). This finding suggests that GluK4 may directly suppress the neuroprotective functions of EPO in the context of kainate-induced excitotoxicity, or, perhaps more plausibly, that pathways downstream of GluK4 activation modulate EPO production. Establishing the molecular pathway(s) that lead(s) to the up-regulation of the EPO NFκB following kainate administration in the absence of GluK4 was outside the scope of this thesis, but may warrant future investigation.

Very few pathways were negatively enriched either the wild-type or GluK4 knockout samples. Two pathways mediating immunity – the MEF2D pathway, and the NK Cells pathway – were down-regulated in wild-type samples. In GluK4 samples, down-regulated pathways included the Bad cell death pathway, the CK1 cell signaling pathway that is involved in dopamine signaling, and the Glycolysis and Kreb pathways, both of which regulate homeostasis and energy metabolism. The down-regulation of these pathways leads to many hypothesis as to their role in GluK4-mediated neurodegeneration. Down-regulation of the Bad cell death pathway in GluK4 knockout tissue may be of particular interest, as it parallels the up-regulation of pro-apoptotic pathways in wild-type tissue.

TABLE 7.6. Biocarta pathways exclusively enriched in GluK4 knockout samples following kainate

Biocarta Pathway	P Value	Genes (with Core Enrichment)
IMMUNITY		
Tcr Pathway	0.051	Not reported by GSEA
Il2 Pathway	0.048	Not reported by GSEA
Tid Pathway	0.053	Not reported by GSEA
Cd40 Pathway	0.037	DUSP 1, NFKBIA, RELA, NFKB1, TRAF6, CHUK, IKBKG, MAP3K14
41bb Pathway	0.019	JUN, NFKBIA, RELA, MAP4K5, NFKB1, IFNG, TNFSF9, CHUK, ATF2
CELL SURVIVAL		
Rela Pathway	0.000	TNFRSF1A, NFKBIA, RELA, RIPK1, NFKB1, FADD, TRAF6, TNF, CHUK, IKBKG
EPO NFkB Pathway	0.036	CDKN1A, NFKBIA, RELA, NFKB1, ARNT, JAK2, GRIN1, EPOR
HEMOVASCULAR FUNCTION		
Vegf Pathway	0.000	NOS3, ELAVL1, EIF1A, FLT1, PXN, EIF2B4, PTK2, SHC1, ARNT, EIF2B2, PRKCA, EIF2S2, PIK3CA
No1 Pathway	0.000	CHRNA1, CAV1, PRKG2, NOS3, TNNI1, ACTA1, FLT1
CELL DEATH		
Tnf Stress Pathway	0.000	MAP2K3, JUN, TNFRSF1A, NFKBIA, RELA, RIPK1, NFKB1, TNF, CRADD, CHUK, IKBKG, MAP3K14
SIGNAL TRANSDUCTION		
Ps1 Pathway	0.000	NOTCH1, ADAM17, BRTC, TCF1, CTNNB1, APC, DVL1, PSEN1, FDZ1

Surprisingly, the MAPK pathway was positively enriched in both the wild-type and GluK4 knockout conditions, though more so in the wild-type than in the knockout condition (wild-type, p = 0.000; GluK4 knockout, p = 0.036; see Appendix 1). This finding suggests several interpretations. One possibility is that the up-regulation of the MAPK pathway in GluK4 knockout tissue is more limited than in wild-type tissue, and that it may be statistically, but not biologically significant. Another possibility is that that MAPK pathway activation serves different functions in wild-type versus GluK4 knockout conditions – that it may promote neurodegeneration

in the wild-type condition and neuroprotection in the GluK4 knockout condition. As discussed above, the MAPK pathway is comprised of several auxiliary pathways, each with multiple, wide-ranging functions including cell proliferation in addition to apoptosis. While GSEA does identify the specific genes within each pathway that are enriched for a given condition (wild-type versus GluK4 knockout), the overlap in genes between the various auxiliary pathways makes it difficult to assess which pathways are enriched. Thus, it is difficult to determine from these data whether the JNK pathway is involved in either condition.

Biochemical Analysis of JNK Pathway Activation Suggests Biphasic Role of GluK4

To better understand the interaction between GluK4 and the JNK pathway, I investigated the phosphorylation states of JNK pathway components by Western blot in kainate-injected wild-type and GluK4 knockout CA3 tissue. I hypothesized that analysis of the JNK pathway at the protein level would yield a more accurate – and more physiologically relevant – representation of JNK pathway activation than analysis at the mRNA level, as JNK pathway activation is dependent upon kinase-mediated phosphorylation of proteins.

The JNK pathway is activated by the phosphorylation of a MAPK kinase kinase, such as MLK3, which in turn phosphorylates MAPK kinase 4 or 7 (Hirai et al., 1997; Nagata et al., 1998). I found that phosphorylated MAPK kinase 4 (MKK4) was significantly up-regulated in wild-type CA3 samples following kainate

treatment as compared to PBS treatment, but remained unchanged in CA3 samples from GluK4 knockout mice (Student's T-test, p = 0.003; Figure 7.5a)

MAPK kinases perpetuate the kinase cascade by phosphorylating one of three JNK isoforms: JNK 1, 2, or 3. While JNK 1 and JNK 2 are expressed systemically, JNK 3 is primarily expressed in neurons (Gupta et al., 1996; Martin et al., 1996). Though native JNK1 and JNK 2/3 expression remained unchanged after kainate administration (Figure 7.5b), I observed an increase, though not statistically significant, in wild-type levels of phosphorylated JNK 2/3 after kainate treatment (Student's T-test, p = 0.087; Figure 7.5c). However, the increase in phosphorylated JNK 2/3 levels in kainate-treated wild-type samples relative to kainate-treated GluK4 knockout samples was statistically significant (Student's T-test, p=0.007; Figure 7.5c). Phosphorylated JNK 1 expression remained unchanged in all conditions (Figure 7.5c).

Phosphorylated JNK isoforms regulate the activity of activator protein 1 (AP-1), a transcription factor that modulates various cellular processes including apoptosis (Whitmarsh and Davis, 1996). AP-1 assembles as a homo- or heterodimer from a number of DNA-binding bZip proteins, including c-Jun, activating transcription factor 2 (ATF2), and c-Fos. Native cJun, phosphorylated cJun, and phosphorylated ATF-2 were all up-regulated in kainate-treated wild-type samples relative to PBS-treated samples (Student's T-test, p = 0.002, p = 0.011, and p = 0.004, respectively), but remained unchanged between kainate- and PBS-treated

GluK4 knockout samples (Figure 7.5d - f). Though c-Fos expression was not significantly different between kainate- and PBS-treated wild-type samples, it was down-regulated in kainate-treated GluK4 knockout samples relative to PBS-treated GluK4 knockout samples and kainate-treated wild-type samples (Student's T-test, $p = 0.001$ and $p = 0.053$, respectively; Figure 7.5g). Surprisingly, phosphorylated ATF-2, c-Jun, phosphorylated c-Jun, and c-Fos levels were all constitutively higher in PBS-treated GluK4 knockout samples than in PBS-treated wild-type samples (Student's T-test, $p = 0.044$, $p = 0.048$, $p = 0.038$, and $p = 0.053$, respectively; Figure 7.5d - g).

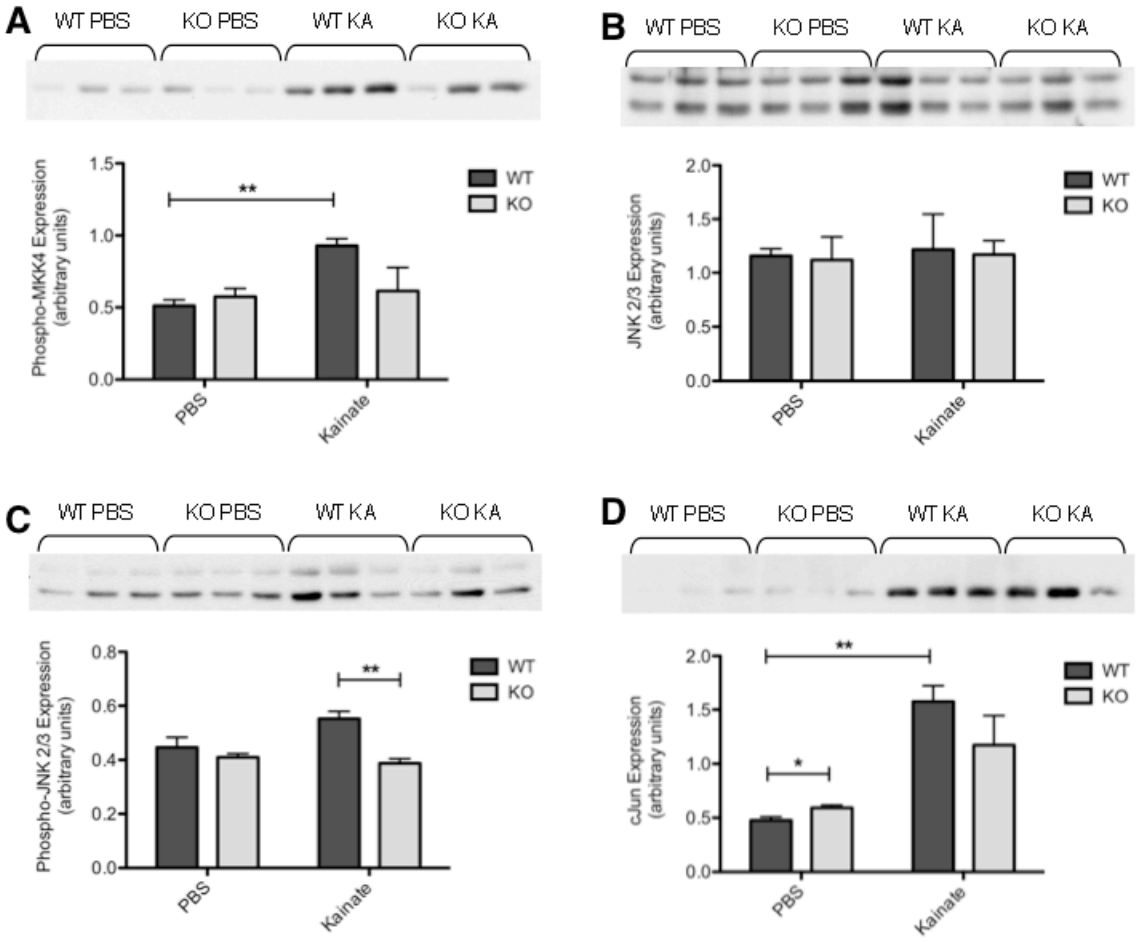

Figure 7.5. GluK4 ablation results in decreased JNK pathway activation following kainate, but increased JNK pathway activation at baseline. (A) The active form of one of the earliest kinases in the JNK pathway, MKK4, was up-regulated in wild-type CA3 tissue after KA treatment relative to PBS treatment, but not in GluK4 CA3 tissue. **(B)** The native neuronal isoform of JNK (JNK 2/3, 54 kDa, top band) remained unchanged between genotypes after PBS or KA treatment. The bottom band represents the JNK 1 isoform (46 kDa), which is expressed globally. **(C)** Despite the fact that the native form of JNK 2/3 remained unchanged in all conditions, the phosphorylated (activated) form of JNK 2/3 is up-regulated in KA-treated wild-type tissue relative to KA-treated GluK4 knockout tissue. **(D)** The native form of cJun, a member of the AP-1 transcription factor complex that is activated downstream of JNK, was up-regulated in wild-type tissue following KA treatment relative to PBS treatment. The increase in cJun expression between PBS- and KA treated GluK4 knockout tissue was not significant, due to variability between samples. Basal c-Jun expression was higher in PBS-treated GluK4 knockout tissue than in PBS-treated wild-type tissue.

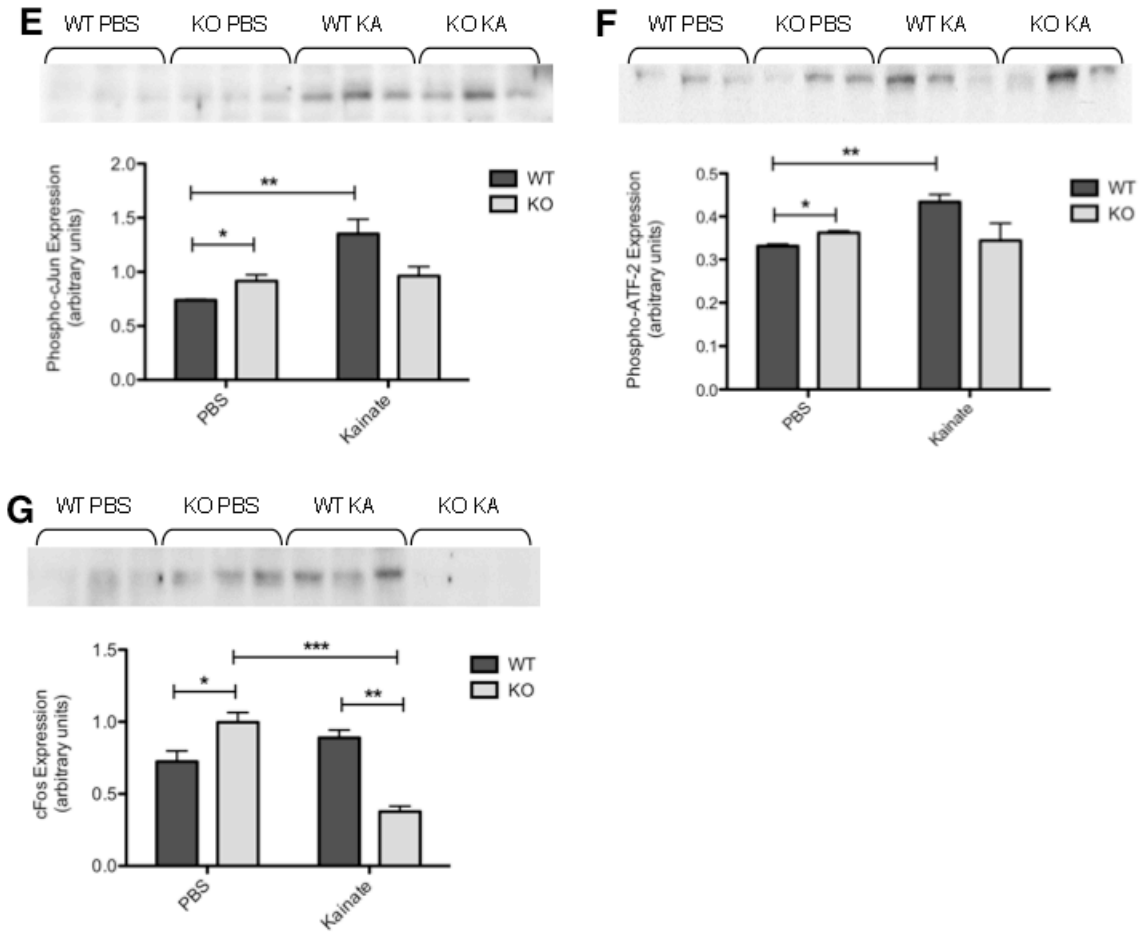

Figure 7.5, continued. (E) The phosphorylated (activated) form of cJun was up-regulated in KA- versus PBS- treated wild-type tissue but not GluK4 knockout tissue. However, phosphorylated c-Jun expression was higher after PBS treatment in GluK4 knockout tissue than in wild-type tissue. **(F)** Phorphorylated ATF-2, another member of the AP-1 complex, followed a similar expression pattern to phosphorylated cJun. Phosphorylated ATF-2 was up-regulated in up-regulated in KA- versus PBS- treated wild-type tissue but not GluK4 knockout tissue, though its expression was higher after PBS treatment in GluK4 knockout tissue than in wild-type tissue. **(G)** cFos is also a member of the AP-1 transcription complex. Its expression was strongly down-regulated between KA-treated wild-type and GluK4 knockout tissue, and between PBS- and KA-treated GluK4 knockout tissue. As with the other members of the AP-1 complex, c-Fos expression was increased at baseline in PBS-treated GluK4 knockout versus wild-type tissue. Bars represent mean ± SEM. *$p < 0.05$, **$p < 0.01$, ***$p < 0.001$.

Collectively, these data suggest that GluK4 can regulate JNK pathway activity in a biphasic, context-dependent manner. In the context of excitotoxicity, GluK4 appears to be essential to the activation of the JNK pathway throughout its various kinase tiers, which further suggests that GluK4 acts on one or more of the early components of the pathway to initiate neurodegeneration. In non-pathological contexts, GluK4 seems to play a role in suppressing JNK pathway activation.

CHAPTER 8: GLUK4 IN KAINATE-INDUCED SEIZURES

Mesial temporal lobe epilepsy (mTLE) is one of the most common forms of epilepsy, and is characterized by recurrent focal seizures that originate in populations of hyperexcitable, hypersynchronous cells in the hippocampus (Falconer et al., 1964). In most affected patients, mTLE arises in tandem with lesions or alterations in neuronal connectivity that are the result of previous neuronal insults, including trauma, encephalitis, and ischemia (Engel, 1993; Camilo and Goldstein, 2004). Approximately 70% of patients with mTLE also develop hippocampal sclerosis, which is characterized by neurodegeneration, astrogliosis, and a form of synaptic reorganization in the dentate gyrus known as mossy fiber sprouting (Babb and Brown, 1986).

Kainate, in addition to being a potent excitotoxin, is also an epileptogenic compound that reproduces many of the hallmarks of mTLE in animals: recurring motor seizures, hippocampal neurodegeneration, and mossy fiber sprouting (Vincent and Mulle, 2009). In this model, animals are typically injected IP with kainate and monitored for seizure activity for 2 – 4 hours thereafter. Seizure severity is normally scored by hand and ranked using a metric developed by Racine (Racine, 1972).

I hypothesized that GluK4 might play a role in the kainate model of mTLE based on several lines of evidence. Mice deficient in GluK2, the kainate receptor subunit with which GluK4 co-precipitates in the CA3, are resistant to kainate-

induced seizures (Mulle et al., 1998). Meanwhile, rats that were injected IH with a viral vector that transduced GluK2 experienced seizures 4 hours after injection (Telfeian et al., 2000). Furthermore, GluK4 expression is highest in the CA3, and this region has been shown to be an epicenter of seizurogenic activity (Avoli and Barbarosie, 1999). Synchronized discharges that originate within the network of glutamatergic collaterals of the CA3, and subsequently spread throughout the hippocampal subfields, are thought to underlie interictal spiking, a pathological EEG pattern that may predict or precipitate epileptic seizures (Avoli et al., 2006). While the anesthetics administered during the IH kainate injections prevented motor seizures in the experiments described above (see Chapter 6), the neuroprotection afforded by GluK4 ablation in this paradigm suggested that GluK4 knockout mice might also have altered susceptibility to kainate-induced seizures.

Additionally, GluK4-mediated seizures could explain the robust difference in neurodegeneration following HI between wild-type and knockout animals. HI has been shown to result in spontaneous motor seizures within 72 hours of surgery in unanesthetized adult animals, and the occurrence of HI-induced seizures correlated with the severity of HI-induced neurodegeneration (El-Hayek et al., 2011). Though seizures were not specifically evaluated in Anna's HI experiments described above (see Chapter 6) they were often observed in passing. Thus, HI could induce seizures that originate in GluK4-expressing cell populations of the

CA3, then propagate throughout brain and produce widespread neuronal cell death in wild-type, but not GluK4 knockout animals.

High, Incremental Doses of Kainate Suggest Decreased Seizure Susceptibility In GluK4 Knockout Mice

To explore the role of GluK4 in seizure generation, wild-type and GluK4 knockout animals were injected IP with an initial dose of 30 mg/kg kainate, followed by two 15 mg/kg doses at 45 minute intervals. Seizures were scored using a modified version of Racine's scale (see Chapter 2, p. 39). This dosing scheme resulted in high mortality: 3 of 9 animals (33.33%) died. Nevertheless, seizure scores from the remaining animals (wild-type, n = 3; GluK4 knockout, n = 3) suggested that GluK4 knockout mice might be more resistant to kainate-induced seizures than wild-type mice. Though the high variability and low *n* in the seizure score data precluded any significant results by two-way ANOVA (effect of genotype, $F = 2.67$, $p = 0.1776$; Figure 8.1a), GluK4 knockout mice were almost entirely unaffected by the initial 30 mg/kg dose of kainate (time (t) = 0 minutes), while wild-type mice showed low-grade seizures. Following the next injection (15 mg/kg; t = 45 minutes), both wild-type and GluK4 knockout animal scores escalated, and animals of both genotypes showed intermittent high-grade seizures (level 4 - 5). Following the last injection (15 mg/kg; t = 90 minutes), wild-type animals showed sustained high-grade seizures, plateauing at level 5, while GluK4 knockout animals showed sustained mid-grade seizures, plateauing at level 3.

Increased Seizure Activity in GluK4 Knockout Mice at Low Doses of Kainate

Because the above dosing scheme resulted in high mortality, and because the difference in seizure scores between wild-type and GluK4 knockout mice appeared to be most pronounced after the first injection, I lowered the dose of kainate administered using several dosing schemes. An initial dose of 15 mg/kg kainate followed by two doses of 5 mg/kg at 10 minute intervals yielded no significant difference in seizure sensitivity by two-way ANOVA (wild-type n = 2, GluK4 knockout n = 3; effect of genotype, $F = 0.02$, $p = 0.9018$; Figure 8.1b) or appreciable trend to suggest that a difference might exist: both wild-type and Glu4 knockout mice plateaued at level 4 seizures. Similar results were observed with an initial dose of 15 mg/kg, followed by a single dose of 5 mg/kg after 20 minutes (wild-type n = 3, GluK4 knockout, n = 3; two-way ANOVA, effect of genotype, $F = 1.25$, $p = 0.3262$; Figure 8.1c), though seizure scores in GluK4 knockout animals did not seem to increase as steadily as in wild-type animals. Finally, a single injection of 15 mg/kg without subsequent injections did not yield significant results by two-way ANOVA (wild-type n = 4; GluK4 knockout n = 2; effect of genotype, $F = 3.69$, $p = 0.1270$; Figure 8.1d). At this dose, GluK4 knockout mice appeared more sensitive to the effects of kainate, though the low *n* and high variability again made results difficult to interpret.

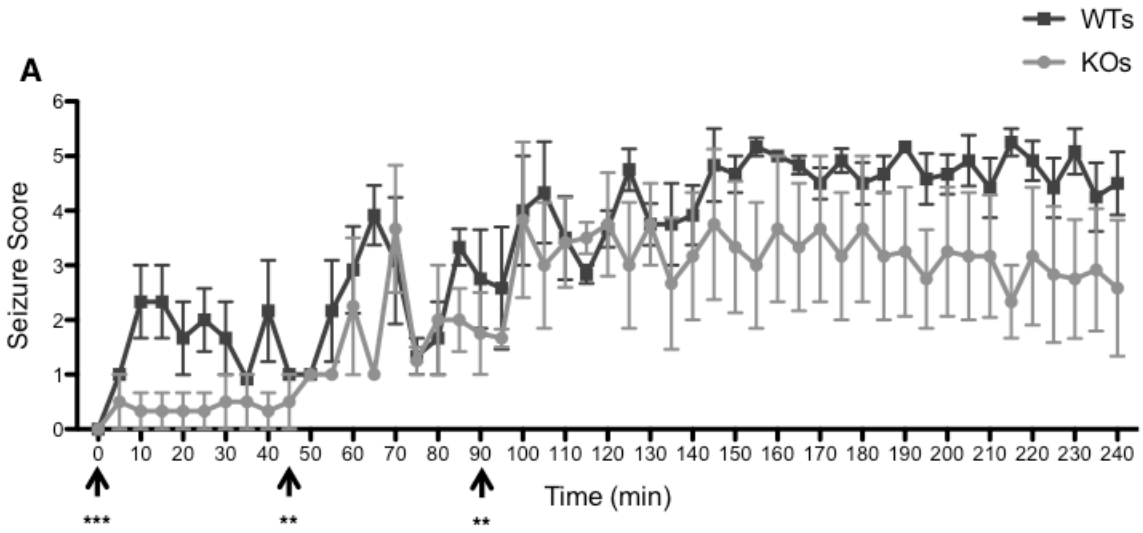
A
WTs
KOs
Seizure Score
Time (min)
***
**
**

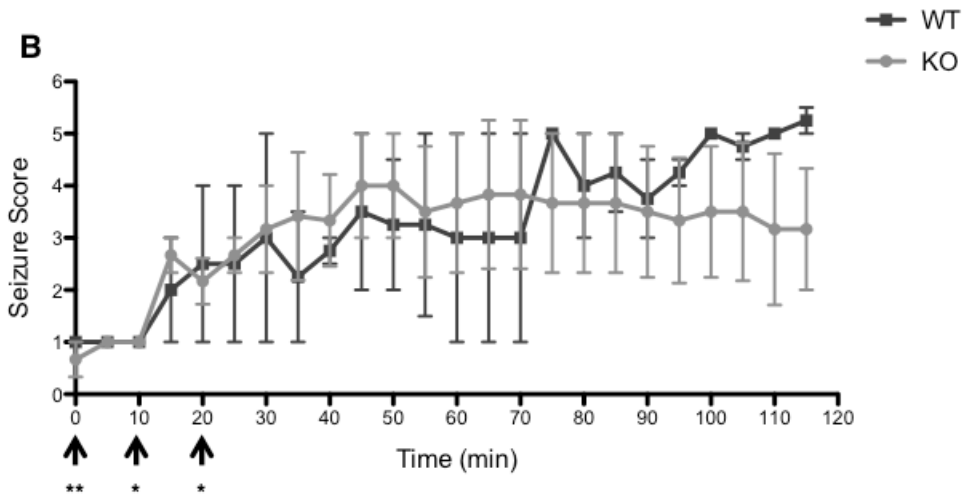
B
WT
KO
Seizure Score
Time (min)
**
*
*

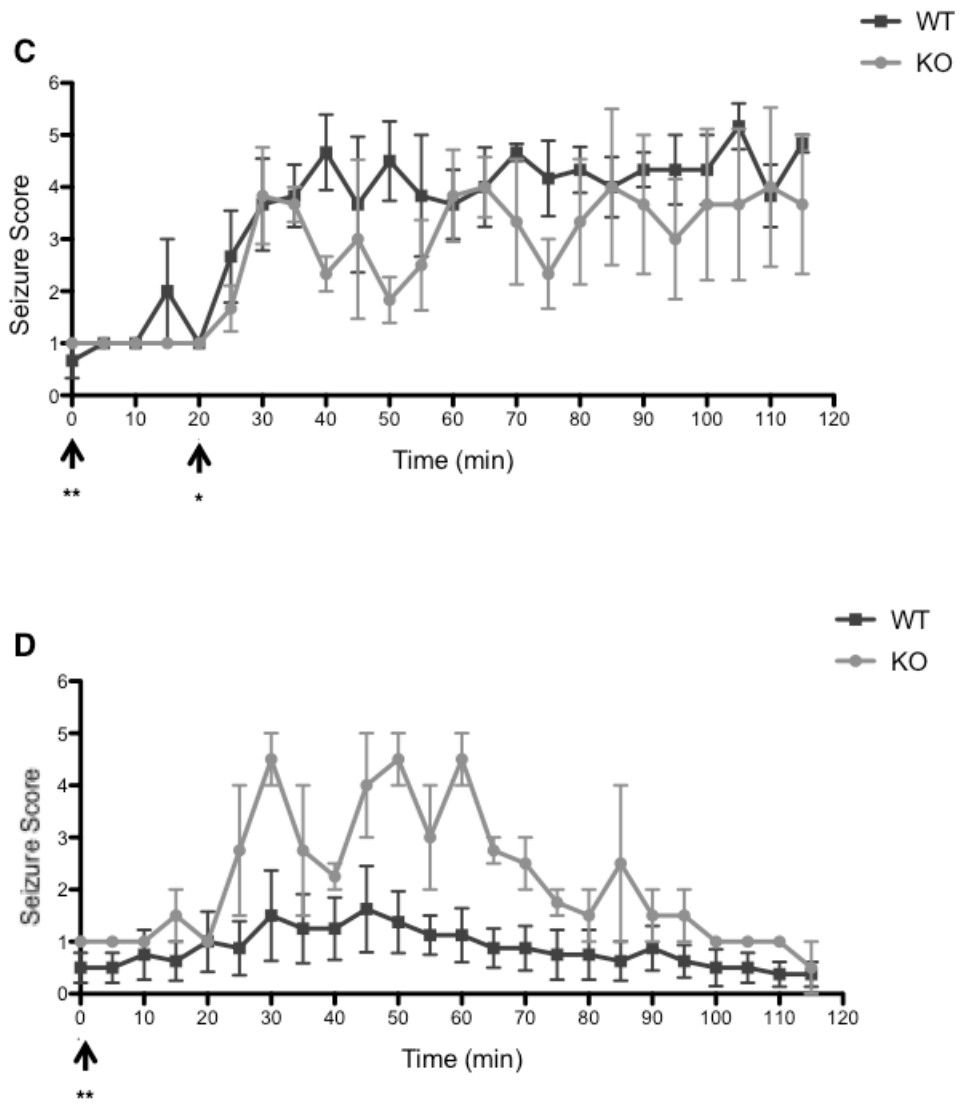

FIGURE 8.1. GluK4 knockout mice trend towards altered seizure susceptibility. (A) GluK4 knockout mice showed a decrease, though not significant, in susceptibility to high incremental doses of IP kainate relative to wild-type mice ($p = 0.1776$). **(B)** A low-dose incremental injection scheme did not reveal differences in seizure activity between wild-type and GluK4 knockout mice ($p = 0.9081$). **(C)** A second low-dose incremental injection scheme failed to reveal a difference between genotypes ($p = 0.3262$). **(D)** Surprisingly, single injections of a low dose of kainate reveal a trend towards increased seizure susceptibility in GluK4 knockout animals. Arrows indicate injection time points. *** = 30 mg/kg kainate; ** = 15 mg/kg kainate; * = 5 mg/kg kainate.

Though none of the results obtained were significant, there appeared to be two trends in the data: at very high doses of kainate (initial injection of 30 mg/kg, followed by 2 injections of 15 mg/kg), GluK4 knockout mice appear to be less sensitive to kainate-induced seizures that wild-type mice; at very low doses of kainate (single injection of 15 mg/kg), GluK4 knockout mice may be more sensitive to kainate-induced seizures than wild-type mice. Further experiments would be needed to confirm these findings, but they suggest nevertheless that the role of GluK4 in kainate-induced seizures may be dose-dependent.

CHAPTER 9: DISCUSSION

Like the other ionotropic glutamate receptors, NMDA and AMPA receptors, post-synaptic kainate receptors initiate EPSCs upon ligand binding. However, kainate receptors are unique in that they also modulate neurotransmitter release in a bi-directional manner when expressed pre-synaptically. Furthermore, kainate receptors have been found to alter inhibitory transmission at GABAergic terminals, as well as to serve non-canonical, metabotropic functions (Rodríguez-Moreno and Sihra, 2011). Ultimately, through their complex and diverse functions, kainate receptors are responsible for fine-tuning the excitability of neuronal networks within the CNS, and for preventing aberrant excitatory transmission. Here, I have presented evidence that loss of a single kainate receptor subunit, GluK4, disrupts this tenuous balance, and uncovers a crucial role for GluK4 in diverse neurological processes.

Persistent GRIK4 *mRNA Expression in GluK4 Knockout Animals*

To study the function of GluK4 in the CNS, I generated a global GluK4 knockout mouse line by crossing mice in which exon 16 of *GRIK4* was floxed, with transgenic mice in which cre was expressed in the germline. I found through an exhaustive investigation of GluK4 expression in the GluK4 knockout line that GluK4 was effectively ablated at the protein level, rendering these mice functional knockouts. However, *GRIK4* mRNA was missing the region corresponding to exon 16 but was otherwise intact in GluK4 knockout animals, and expressed at normal levels.

There are several potential explanations for the observation that *GRIK4* mRNA persists in GluK4 knockout animals, but GluK4 protein does not. One possibility is that the absence of exon 16 renders *GRIK4* mRNA unstable in a way that discourages translation, or decreases translational efficiency to a point where GluK4 protein is undetectable by western blot. Another possibility is that GluK4 protein is indeed generated from the altered *GRIK4* mRNA present in GluK4 knockout mice, but that the protein is inherently unstable without the p-loop region corresponding to exon 16 and therefore gets ubiquitinated or otherwise flagged for degradation. Because no GluK4 protein was detected by western blot, GluK4 degradation in this scenario would need to occur fairly quickly after translation, or else turnover of GluK4 is so slow that it doesn't accumulate quickly – it can persist at levels below the threshold for western blot detection before it gets degraded. One means of testing this hypothesis would be to generate a mouse where floxed *GRIK4* is fused to a reporter gene, with the caveat that the reporter could further destabilize or interfere with the structure of the cre-excised (referred to hereafter as "mutant") form of GluK4 protein. The presence of the reporter could then be assessed in a quantitative, GluK4-independent assay that is more sensitive than western blotting.

Alternatively, mutant GluK4 may be stable, but it may somehow fail a cellular checkpoint in the process of kainate receptor assembly, and therefore get targeted for destruction. There have been several previous reports of critical checkpoints during kainate receptor assembly. Within the endoplasmic reticulum

(ER), high affinity GluK5 subunits are probed for their ability to properly bind glutamate before they, and any receptor complex in which they participate, can be trafficked to the plasma membrane (Valluru et al., 2005). Coatomer protein complex I (COPI) and 14.3.3ζ proteins also interact with GluK5 to regulate GluK5 trafficking. COPI interacts with the ER retention motif in GluK5 to promote sequestration of GluK5 within the ER, and this association is reduced upon the assembly of GluK5 with GluK2 (Vivithanaporn et al., 2006). As the association between GluK5 and COPI is reduced, the association between GluK5 and 14.3.3ζ is increased, and 14.3.3ζ promotes the forward trafficking of heteromeric kainate receptors containing GluK5 to the plasma membrane (Vivithanaporn et al., 2006). These findings in GluK5 suggest that similar mechanisms may exist to regulate the inclusion of GluK4 in functional kainate receptor subunits, and that misfolding of GluK4 or the absence of the p-loop may compromise the ability of mutant GluK4 to pass critical checkpoints.

Finally, it is possible that mutant GluK4 protein is stable and does not get degraded at all, but is truncated or folded in such a way that it cannot be detected by either of the antibodies used in my western blotting assays. One means of addressing this issue would be to generate a range of custom antibodies directed against all regions of GluK4 and to run western blots using denaturing conditions to ensure that the altered secondary structure of mutant GluK4 did not obscure the antibody binding regions.

Memory Deficits in GluK4 Knockout Animals

Because GluK4 ablation results in aberrant mossy fiber LTP (Catches et al., 2012), I hypothesized that GluK4 may play a role in learning and memory, both of which are LTP-dependent processes. I compared the performance of wild-type and GluK4 knockout mice in various hippocampus-dependent learning tasks to assess the nature and extent of the memory deficits induced by GluK4 ablation, and found that working memory was intact in GluK4 knockout mice, but that fear memory and spatial memory were impaired. These findings are consistent with previous studies which have highlighted the importance of the CA3 – the hippocampal region where GluK4 expression is most concentrated – to associative learning processes such as fear conditioning (Daumas et al., 2004) and the MWM (Steffenach et al., 2002; Stupien et al., 2003; Florian and Roullet, 2004).

One caveat to my findings could be that, while GluK4 knockout mice showed decreased freezing behavior relative to wild-type mice during successive tone-shock pairings on the first day of fear conditioning, and I have interpreted this deficit to be an indication of impaired fear memory acquisition, it is possible to attribute this deficit to other sources. The decreased freezing behavior observed in GluK4 knockout mice in response to the foot shock may be akin to their decreased response to the acoustic startle – that is, a reflection of decreased arousal or attention rather than learning. Thus, wild-type and GluK4 knockout mice may have sensed the footshock with equal intensity, as the incremental

hotplate test indicated that both genotypes have equivalent pain thresholds, but GluK4 knockout mice may have attached less emotional valence to the experience.

Another possibility is that the decrease in freezing behavior is a reflection of the basal hyperactivity observed in GluK4 animals during the open field tasks. This seems unlikely, however, as basal freezing behavior within the fear conditioning chamber was not significantly different between wild-type and GluK4 mice during the acclimatization period preceding the tone-shock pairings on day 1. Furthermore, freezing behavior did not differ between wild-type and GluK4 knockout animals in the contextual or cued paradigms on day 2, although the argument could be made that hyperactivity in the GluK4 knockout animals may have masked a true deficit in freezing behavior and, thus, in learning and memory. Nevertheless, one means of addressing this issue would be to measure behavioral outputs of fear that were not dependent on movement, such as ultrasonic vocalizations or hypertension.

Basal hyperactivity in the GluK4 knockout line may have also been a confounding factor in the MWM results, and could explain why knockout mice took longer trajectories to reach the hidden platform during the hidden platform trials. However, the increase in distance traveled during these trials was not accompanied by an increase in swimming velocity relative to wild-type animals, while the increase in distance traveled during the open field test was, suggesting

that increased velocity is a feature of hyperactivity in GluK4 knockout animals. Furthermore, visual platform performance did not differ between GluK4 knockout and wild-type animals. The increase in the distance traveled by the GluK4 knockout cohort during the hidden platform trials is therefore more likely to be a product of impaired cognitive processes rather than hyperactivity.

The learning and memory deficits in GluK4 knockout mice may provide further evidence for a role of GluK4 in human neuropsychiatric disorders: cognitive function, and particularly declarative and working memory, are consistently impaired in individuals with schizophrenia (Stone et al., 1998). Additionally, the number of synapses between mossy fibers and CA3 pyramidal neuronal spines is reduced in schizophrenic patients (Kolomeets et al., 2007), which may result in reduced excitatory transmission in this region and thereby parallel the effects of GluK4 ablation.

Ultimately, further research into the role of GluK4 in memory is warranted in humans. A previous study on the relationship between GluK4 and hippocampal activation has shown that patients who carry a deletion variant of *GRIK4* that increases *GRIK4* mRNA expression demonstrate greater hippocampal activation during a facial processing task than patients who carry the normal *GRIK4* allele (Whalley et al., 2009b; 2009a). To elucidate the effects of GluK4 on memory in humans, this experimental paradigm could be modified so that the test subjects were performing a hippocampus-dependent memory task.

Another future line of research could be to investigate the effects of GluK4 ablation in CA3 networks outside of the mossy fiber pathway. The majority of excitatory synapses within the CA3 originate from pyramidal cells that form recurrent collaterals onto neighboring pyramidal cells to form a self-contained network of excitatory input within the CA3 (Ishizuka et al., 1990). It has been proposed that modification of synaptic strength within this autoassociative network contributes to hippocampus-dependent memory (Gardner-Medwin, 1976). Recurrent collaterals within the CA3 project to the stratum oriens and stratum radiatum of the CA3 (Ishizuka et al., 1990), and GluK4 is expressed (albeit weakly) in the stratum radiatum (Darstein et al., 2003), suggesting that GluK4 may contribute to memory forming process through its actions at mossy fiber synapses as well as at recurrent CA3 synapses. GluK4-mediated activity at both types of synapses may in fact be interdependent, as the mnemonic functions of the autoassociative CA3 network rely in part on mossy fiber input (McNaughton and Morris, 2002). Assessing the electrophysiological properties of this autoassociative network in GluK4 knockout mice might further elucidate the role of GluK4 in memory.

Altered Behavior and Mood in GluK4 Knockout Animals, and Implications for Human Neuropsychiatric Disorders

The behavioral phenotype of GluK4 knockout mice strongly suggests that GluK4 regulates mood. I observed decreased anxiety- and depressive-type behavior in GluK4 knockout mice in the open field and forced swim tests, respectively.

Furthermore, the fact that GluK4 mice exhibit a decreased acoustic startle response compared to wild-type mice is an indication that basal levels of arousal and emotionality differ between the genotypes. The acoustic startle response is regulated by corticotropin releasing factor, which activates the hypothalamic-pituitary-adrenal axis in response to stress, and contributes to anxiety and depression disorders (Risbrough et al., 2003). These findings are consistent with a previous study in which *GRIK4* mRNA expression was significantly up-regulated following chronic restraint stress, and was shown to be regulated by the adrenal steroid corticosterone (Hunter et al., 2009). Furthermore, an allelic variant of *GRIK4* is associated with the outcome of selective serotonin reuptake inhibitor treatment in patients with major depressive disorder (Paddock et al., 2007). Thus, the anxiolytic, antidepressant effects of GluK4 ablation suggest that GluK4 may be involved in regulating baseline affect and mood, and that aberrant GluK4 expression may contribute to anxiety and depression in humans.

As with the memory assays described above, hyperlocomotion in GluK4 knockout animals may be a confounding factor in the interpretation of the open field and forced swim results because the scored behaviors in these experiments are dependent upon mobility. However, there are several lines of evidence to suggest that the differences in anxiety and depressive-type behaviors between wild-type and GluK4 knockout mice are valid. In both open field paradigms (short / lit, and long / dark), GluK4 mice showed an overall preference for the periphery of the open field over the center, much as wild-type mice did. This observation

indicates that, despite being hyperlocomotive, GluK4 mice nevertheless exhibited directed motor behaviors – they were not randomly moving through the open field. The difference between wild-type and GluK4 knockout mice in their preference for the center of the field can therefore be attributed to the fact that the GluK4 knockout mice perceived the center zone to be less aversive than the wild-type mice do.

Furthermore, a concurrent study of GluK4 knockout mouse behavior that supports many of our findings has recently been published (Catches et al., 2012). The authors employed several non-locomotor tests that bypass the issue of hyperlocomotion in GluK4 knockout mice. They demonstrated, using a novelty-induced suppression of feeding test, that GluK4 knockout mice are less anxious than wild-type mice: GluK4 knockout mice exhibit a shorter latency to consume food placed in a novel, anxiogenic environment than wild-type mice do. The authors also demonstrated, using a sucrose preference test, that GluK4 knockout mice are less prone to depressive type behaviors: GluK4 knockout mice exhibit a greater preference for a 1% sucrose solution than wild-type mice do, presumably because they derive greater pleasure from this stimulus than wild-type mice do, and, by extension, are less depressive.

Finally, hyperlocomotion is often considered in animal models of psychological disorders to be a reflection or behavioral correlate of psychomotor agitation, an endophenotype of both bipolar disorder and schizophrenia (van den Buuse,

2010). According to the dopamine hypothesis of schizophrenia, psychomotor agitation and other positive symptoms of schizophrenia can be attributed to excess dopaminergic activity, and, indeed, drugs that enhance dopamine neurotransmission such as amphetamine induce hyperactivity in rodents (van den Buuse, 2010). Meanwhile, the glutamate hypothesis of schizophrenia postulates that the positive symptoms of schizophrenia are related to insufficient glutamatergic activity, and NMDA receptor antagonists such as MK-801 and phencyclidine also induce hyperactivity in rodents, as does GluK2 ablation (Shaltiel et al., 2008; Gunduz-Bruce, 2009). Thus, hyperlocomotion in GluK4 knockout mice may be a relevant phenotype to the understanding of the role of GluK4 in neuroaffective disorders.

The involvement of GluK4 in schizophrenia and bipolar disorder is further supported by data from the PPI assays. Compared to wild-type mice, GluK4 knockout mice showed decreased inhibition of the acoustic startle response when the startle-inducing tone was preceded by a weaker tone. Deficits in PPI are common in patients with schizophrenia, and have also been observed in patients with bipolar disorder during periods of acute psychotic mania (Perry et al., 2001). The relationship between PPI and psychosis is not fully understood. However, PPI deficits may be a reflection of the fact that psychotic patients are unable to discriminate between trivial and salient stimuli within their environment, and are therefore subjected to constant cognitive overload as they respond to each with equal measure (Perry and Braff, 1994; Geyer et al., 2002). While

psychosis and cognitive overload are difficult to model definitively in animals, GluK4 ablation at the very least phenocopies a human correlate of these dysfunctions by inducing PPI impairments in GluK4 knockout mice.

The results obtained in the open field and forced swim trials may be relevant to psychological disorders, as the basal decreases in anxiety and despair in GluK4 knockout animals may parallel the dramatic mood elevation and increased risk-taking behavior that are characteristic of bipolar disorder (Belmaker, 2004). Taken together with the cognitive and sensorimotor gating impairments observed in GluK4 knockout animals, and the ample evidence from human studies implicating GluK4 in bipolar disorder and schizophrenia, my findings suggest that aberrant GluK4 expression may explain certain facets of these diseases.

My findings in GluK4 knockout animals are also largely congruent with those observed by other groups in GluK2 knockout animals (Ko et al., 2005; Shaltiel et al., 2008). Like GluK4 knockout mice, GluK2 knockout mice are less anxious, more risk-taking, and show fewer manifestations of despair than wild-type mice. However, GluK2 knockout mice display hyperaggression in resident-intruder assays, while I was unable to observe any behavioral markers of aggression in GluK4 knockout mice in a pilot study of the same test (data not shown). GluK2 knockout mice also show significant reduction in fear memory recall, as indicated by decreased freezing times relative to wild-type mice in both contextual and cued fear conditioning paradigms (Ko et al., 2005), while I found only impaired

acquisition of fear memory in GluK4 knockout mice. The discrepancies observed between GluK2 and GluK4 knockout behavior suggest the possibility that GluK2 and GluK4 may co-assemble to regulate anxiety, risk-taking, and despair, but that GluK2 and GluK4 may assemble with other kainate receptor subunits to regulate aggression and fear memory retrieval in the case of GluK2, and fear memory acquisition in the case of GluK4.

GluK4-mediated Excitotoxic Neurodegeneration, and Regulation of the JNK Pathway

Excitoxicity is responsible for the widespread cell death that underlies many of the debilitating aspects of neurodegenerative diseases such as ischemic stroke. It is triggered by the excessive stimulation of glutamate receptors, whereupon large influxes of calcium into neurons instigate a host of cytotoxic events, including mitochondrial dysfunction, nitric oxide and free radical production, and activation of cell death pathways (reviewed in (Lau and Tymianski, 2010)). Depending on the nature and the magnitude of the insult, affected neurons ultimately undergo apoptotic, necrotic, or programmed cell death (Wang et al., 2005; 2005; Tokuhara et al., 2007).

I observed that the CA3 region of the hippocampus in GluK4 knockout animals is protected against neurodegeneration following kainate-induced excitotoxicity. To elucidate the pathways downstream of GluK4 activation that lead to neurodegeneration, I compared the transcriptomes of wild-type and GluK4

knockout CA3 tissue after kainate or vehicle injection. I found that the MAP kinase pathway, as well as other apoptotic cell death pathways, were up-regulated in wild-type, but not GluK4 knockout tissues following kainate injection, suggesting that these pathways may interact with GluK4 to mediate cell death. Biochemical analysis of the JNK pathway, a subset of the MAP kinase pathway that is known to mediate excitotoxic cell death (Bogoyevitch et al., 2004), revealed that the JNK pathway was activated in wild-type tissue, but not GluK4 tissue, following kainate administration. Furthermore, basal JNK pathway activation was higher in GluK4 knockout tissue than in wild-type tissue. Together, these results suggest a biphasic role for GluK4 in the modulation of the JNK pathway: under basal conditions, GluK4 serves to suppress JNK pathway activations, while under excitotoxic conditions, GluK4 serves to activate the JNK pathway.

Several scenarios present themselves as to how GluK4 and the JNK pathway interact. One possibility is that GluK4 interacts with the JNK pathway directly by participating in heteromeric receptor complexes with GluK2, and, by extension, the GluK2 / PSD-95 / MLK3 signaling complex that activates the JNK pathway (Tian et al., 2005). GluK4 may also participate in other non-canonical, metabotropic actions that indirectly induce the JNK pathway. The JNK pathway has many upstream effectors, including G-proteins (Yang et al., 2006), and kainate receptors are known to couple with G-proteins to mediate various cellular signaling events, such as pre-synaptic glutamate and GABA release (Rodríguez-

Moreno and Sihra, 2011; Sihra and Rodríguez-Moreno, 2011). It is also possible that GluK4 subserves a purely ionotropic function in the initiation of excitotoxic cell death by either fluxing calcium directly into post-synaptic cells, or by triggering excess glutamate release from presynaptic cells and thereby activating any or all forms of post-synaptic ionotropic glutamate receptors, which then flux calcium into post-synaptic cells. Calcium ions can initiate a large number of signal transduction pathways, and elevated intracellular calcium levels have been shown to induce JNK pathway activation in macrophages (Kim and Sharma, 2004).

The means by which JNK pathway activation results in cell death remains controversial (Lin, 2003). JNK may indirectly activate caspase-dependent cell death pathways, either through the intermediary of mitochondrial cytochrome c-dependent pathways (Tournier et al., 2000) or TNFa-dependent pathways (Chang et al., 2006). Nevertheless, GSEA analysis of my microarray results indicated that several cell death pathways were up-regulated in wild-type but not GluK4 knockout tissue following kainate administration. One can speculate that these pathways are downstream of JNK activation, although proving this hypothesis would be challenging. Repeating the microarray experiment with an extra condition, where mice were treated with a JNK pathway inhibitor such as D-JNKI1 or sp600125 in addition to kainate or vehicle to determine whether the same cell death pathways were differentially regulated between wild-type and

GluK4 knockout mice in the absence of JNK activity, would be a first step in establishing a link between JNK and downstream cell death pathways.

In contrast to the regionalized neuroprotection that I observed in GluK4 knockout mice following kainate-induced excitotoxicity, the neuroprotection observed following HI extended throughout the hippocampus. One explanation for this phenomenon could be that, in the context of HI, GluK4 activates cell death pathways other than, or in addition to, the JNK pathway. These pathways may be more pervasive than the JNK pathway, or they may incite alternative forms of cell death. Another possibility is that the neurodegeneration resulting from HI may stem from GluK4-mediated seizures. While avertin, the long-acting anesthetic used during the IH kainate injection procedure, may have precluded seizure activity in the IH kainate paradigm, the short-acting isofluorane anesthetic used in the HI procedure would have permitted it. Indeed, Anna observed sporadic seizures in HI-treated animals, though she was blind to the genotype of the affected animals at the time. The potential role of GluK4 in seizures is further discussed below.

Finally, the microarray experiment generated a vast collection of data, and following up on each potentially relevant lead was outside the scope of my thesis. However, there are several microarray results that may warrant further investigation. For instance, biochemical analysis of the cell death pathways that emerged from GSEA analysis as being differentially regulated in wild-type and

GluK4 knockout tissue following kainate administration may provide insight into the relationship between GluK4, JNK pathway activation, and cell death pathways. Furthermore, there were a handful of genes that were differentially regulated between wild-type and GluK4 knockout tissue at baseline (i.e., after vehicle injection). One such gene, transmembrane protein 25 (Tmem25), was down-regulated 45.03-fold in GluK4 knockout samples relative to wild-type samples. Very little is known about the function of Tmem25, other than the fact that it is a member of the immunoglobulin superfamily (Katoh and Katoh, 2004), and that it may be a biomarker for breast cancer (Doolan et al., 2009). However, a preliminary search of the online Allan Mouse Brain Atlas (Allan Institute for Brain Science) indicates that Tmem25 expression is highly concentrated within the CA3 region of the hippocampus, which, again, is an area of highly concentrated GluK4 expression. Furthermore, the fact that Tmem25 is a transmembrane protein (Katoh and Katoh, 2004) whose expression is heavily influenced by the presence or absence of GluK4 suggests that it may serve as an auxiliary protein for GluK4, perhaps aiding in GluK4 trafficking.

The microarray experiment may ultimately be worth repeating, with the following modifications: 1. using individual, rather than pooled, biological replicates to facilitate downstream analysis; 2. excluding whole hippocampus samples; 3. including samples injected with both kainate or vehicle plus a JNK inhibitor; 4. including un-injected samples from each genotype to better understand basal differences between wild-type and GluK4 knockout transcriptomes; and 5.

including samples from mice that had been sacrificed at a series of time points following kainate or vehicle injection to assess the time-course of GluK4-mediated pathway activation.

Parsing the Role of GluK4 in Kainate-Induced Seizures

To investigate the role of GluK4 in mTLE and seizures, I injected wild-type and GluK4 knockout mice IP with kainate using several dosing schemes. While none of the dosing schemes yielded significant results, there appeared to be two trends in the data: at very high doses of kainate GluK4 knockout mice appeared to be less sensitive to kainate-induced seizures than wild-type mice, while at very low doses of kainate GluK4 knockout mice appeared to be more sensitive. These results again suggest a biphasic role for GluK4 in the regulation of synaptic activity.

One reason for the dose-dependent effects of kainate on seizure activity in GluK4 knockout mice could be that lower doses of kainate preferentially activate GluK4-containing presynaptic autoreceptors, which are somewhat more abundant than postsynaptic receptors (Darstein et al., 2003), and that these receptors may serve to prevent neurotransmitter release and curb excitatory transmission (Frerking et al., 2001). Meanwhile, higher doses of kainate may activate facilitatory post-synaptic receptors to a greater extent than lower doses do, and the excitatory post-synaptic receptor response may outweigh the inhibitory presynaptic receptor response.

Though results were not significant for any of the dosing schemes evaluated, there are several variables which may have obfuscated a true difference in kainate sensitivity between wild-type and GluK4 knockout animals. One of the major drawbacks of this experiment is the scoring method: seizure scores must be evaluated by hand, as there is no suitable video tracking software (to my knowledge) to automate scoring, and the scores are therefore subjective. To address this issue, all experiments were live-scored by two independent observers, and the scores from both observers were then averaged. Nevertheless, the Racine scale used for scoring leaves room for ambiguity, particularly because seizure severity does not always increase in a linear manner from levels 0 – 6. In some cases, it was difficult to score seizure events definitively.

A second drawback of this paradigm is that it is relatively low-throughput. I found that the maximum number of mice that could be tested at once was 6; beyond that, it was difficult to keep track of the behavior of individual mice, and to inject them swiftly. Coupled with the fact that there was high inter-animal variability in kainate sensitivity within genotypes, perhaps due to differences in kainate metabolism and bioavailability, the low *n* may have contributed to the lack of significant results. While in some instances I did try repeating experiments and combining the results, I found that there was high variability within genotypes between experimental days. This may have been due to differences in the time of day at which experiments were initiated, as circadian rhythms could, in theory,

affect kainate metabolism. Another possibility is that the kainate solutions injected on different experimental days were inconsistent: kainate was mixed fresh daily from powder, and the powder often originated from separate lots (though it was always produced by the same manufacturer, Tocris). Finally, the within-genotype differences across experimental days may have been, once again, an artifact of inter-animal differences in kainate metabolism and bioavailability.

Were these experiments to be continued, they would require much larger cohorts, and either a means of scoring all the animals simultaneously, e.g. by video-recording the trials and scoring 6 animals at a time from the recordings, or a means of spreading the experiment across several days such that the time of day that the animals were tested was consistent, and the kainate used was always from the same batch. It might also be beneficial to evaluate other, more objective measures of seizure severity, such as electroencephalographic recordings (Hatazaki et al., 2007). Finally, another potential avenue of investigation could be to compare seizure severity in wild-type versus GluK4 knockout mice following HI.

Coda

The GluK4 kainate receptor subunit has, arguably, been overlooked in previous studies of kainate receptor function. Because of its restricted expression pattern relative to other subunits, its contribution to overall network activity was assumed to be less influential than that of the other subunits, and its signaling properties were largely extrapolated from those of GluK5 (Huettner, 2003). However, from the work described in this thesis, the wide-ranging impact of GluK4 – and of its absence – on mood, memory, and excitotoxicity, has come into focus.

APPENDIX 1. Biocarta pathways enriched in both wild-type and GluK4 knockout samples following kainate administration

Biocarta Pathway	WT P Value	WT Genes (with Core Enrichment)	KO P Value	KO Genes (with Core Enrichment)
OXITATIVE STRESS				
VITCB PATHWAY	0.000	SLC23A2, P4HB, COL4A4, COL4A5, COL4A1, COL4A2, SCL2A1, COL4A6, COL4A3, SLC23A1, SLC2A3	0.020	COL4A2, COL4A1, P4HB, SLC2A1, SLC23A1, SLC23A2
ARENRF2 PATHWAY	0.000	FOS, JUN, MAFF, NFE2L2, MAFG	0.000	FOS, JUN, MAFF, MAFK, CREB1, FXYD2, PRKCA
FREE PATHWAY	*0.056*	*Not reported by GSEA*	*0.043*	*Not reported by GSEA*
IMMUNITY				
CCR5 PATHWAY	0.000	CCL4, FOS, CCL2, JUN, CCR5	0.000	CCL4, FOS, CCL2, JUN, CC45
MONOCYTE PATHWAY	0.000	CD44, ICAM1, PECAM1, ITGB1, SELP	0.000	CD44, ICAM1, PECAM1, SELP, ITGB1
IL22BP PATHWAY	0.000	SOCS3, STAT3, STAT1, STAT5A	0.020	SOCS3, STAT3, JAK3, JAK1, IL22RA1, STAT1, STAT5A
CLASSIC PATHWAY	0.000	C4B, C3, C1QA, C1QB, C2	0.019	Not reported by GSEA
IL1R PATHWAY	0.038	JUN, MAP2K3, MYD88, IL1RAP, RELA, IL1A, IL1B, MAP3K14, NFKB1, IL1RN, NFKBIA, IRAK3, TGFB3, IRAK1, TRAF6, IL1R1, MAP3K7IP1, TNF, TOLLIP, MAP3K7, MAP3K1	0.000	MAP2K3, JUN, MYD99, NFKBIA, IL1B, IL1RAP, RELA, TGFB3, TOLLIP, NFKB1, IRAK3, MAP3K7, TRAF6, IL1A, TNF, CHUK
IL2RB PATHWAY	0.000	SOCS3, FOS	0.000	SOCS3, FOS, JAK3, JAK1, NMI, PTPN6, STAT5A, BCL2L1, RPS6KB1, BCL2, SHC1, IL2RG, MYC
IL10 PATHWAY	0.019	STAT3, HMOX1, BLVRB, STAT1, STAT5A, IL1A, BLVRA	0.000	STAT3, HMOX1, JAK1, STAT1, STAT5A, BLVRA, BVLRB, IL1A, TNF
COMP PATHWAY	0.018	C4B, C3, C1QA, C1QB, MASP2	0.037	Not reported by GSEA
ETS PATHWAY	0.035	FOS, CSF1, JUN, ETS2	0.019	FOS, JUN, CSF1, ETS1, ETS2, E2F4
CDMAC PATHWAY	0.016	FOS, JUN, RELA, NFKB1, NFKBIA	0.037	FOS, JUN, NFKBIA, RELA, NFKB1, CUZD1, TNF, MYC, PRKCA
LAIR PATHWAY	0.000	ICAM1, C3, VCAM1, IL1A, ITGB1, SELP	0.000	C3, ICAM1, SELP, ITGB1, IL1A, TNF
BCR PATHWAY	0.036	FOS, JUN, BLNK, SHC1, VAV1, NFATC4	0.052	Not reported by GSEA
TNFR2 PATHWAY	0.020	Not reported by GSEA	0.039	Not reported by GSEA

APPENDIX 1, *Continued*

Biocarta Pathway	WT P Value	WT Genes (with Core Enrichment)	KO P Value	KO Genes (with Core Enrichment)
CELL SIGNALING				
CELL2CELL PATHWAY	0.055	PECAM1, CTNNA1, ACTN1, CTNNB1, BCAR1, ACTN3, PXN, CSK, VCL, PTK2	0.000	PECAM1, PXN, ACTN1, CTNNA1, PTK2, CTNNB1, CTNNA2, CSK, BCAR1, VCL
PAIN				
DREAM PATHWAY	0.000	FOS, JUN, CREM	0.019	FOS, JUN, PRKAR2A, CREM, CREB1
CELL PROLIFERATION AND DIFFERENTIATION				
Promoting				
TPO PATHWAY	0.000	FOS, STAT3, JUN, SHC1, STAT1, STAT5A	0.053	FOS, STAT3, JUN, STAT1, STAT5A, SHC1, PRKCA, JAK2, PIK3CA
PDGF PATHWAY	0.000	FOS, STAT3, JUN, SHC1, STAT1, STAT5A	0.019	FOS, STAT3, JUN, JAK1, STAT1, STAT5A, SHC1, SRF, PRKCA, PIK3CA
EGF PATHWAY	0.020	FOS, STAT3, JUN, SHC1, STAT1, STAT5A	0.020	FOS, STAT3, JUN, JAK1, STAT1, STAT5A, SHC1, SRF, PRKCA, PIK3CA
MET PATHWAY	0.019	FOS, STAT3, JUN, DOCK1, ACTA1, ITGB1, RAP1B	0.000	FOS, STAT3, JUN, DOCK1, ACTA1, PXN, GAB1, ITGB1
IL3 PATHWAY	0.000	FOS, SHC1, STAT5A, PTPN6	0.034	Not reported by GSEA
KERATINOCYTE PATHWAY	0.036	Not reported by GSEA	0.019	FOS, MAP2K3, JUN, TNFRSF1A, ETS1, PRKCD, NFKBIA, ETS2, RELA, RIPK1, PRKCH, NFKB1, MAP2K7, SP1, TNF, BCL2, CHUK, PRKCA
Inhibiting				
P53 PATHWAY	0.000	CDKN1A, GADD45A, CDK2, TIMP3, CCND1, PCNA, BAX	0.019	CKDN1A, GADD45A, CDK2, MDM2, PCNA, CCND1, TIMP3, BCL2
HEMOVASCULAR FUNCTION				
TPO PATHWAY	0.000	FOS, STAT3, JUN, SHC1, STAT1, STAT5A	0.053	FOS, STA3, JUN, STAT1, STAT5A, SHC1, PRKCA, JAK2, PIK3CA
CARDIAC EGF PATHWAY	0.000	FOS, JUN, RELA, EDN1, NFKB1, EDNRB, ADAM12, EGFR	0.019	FOS, JUN, RELA, NFKB1, ADAM12, EDN1, MYC, PRKCA
EPO PATHWAY	0.032	FOS, JUN, SHC1, STAT5A, PTPN6	0.047	Not reported by GSEA

APPENDIX 1, *Continued*

Biocarta Pathway	WT P Value	WT Genes (with Core Enrichment)	KO P Value	KO Genes (with Core Enrichment)
CELL DEATH				
MAPK PATHWAY	**0.000**	FOS, JUN, MAP2K3, MAPKAPK2, MAPKAPK3, SHC1, PRS6KA1, STAT1, MAP3K8, RELA, MAPK6, MAPK9, MAX, MAP3K6, MAP3K14, NFKB1, RIPK1, NFKBIA, TRAF2, MAPK4, MAPK12, MAPK7	**0.036**	FOS, MAPK23, JUN, MAPKAPK2, MAP3KA, MAPK6, MAP3K6, NFKBIA, RPS6KA1, MAPKAPK3, MAPK11, RELA, MAP4K5, MAP4K4, TGFB3, RIPK1, NFKB1, STAT1, MAP2K7, SP1, MAPK12, RPS6KB1, MEF2C, MAP3K7, RPS6KA3, TGFBR1, RPS6KB2, SHC1, CHUK, CREB1, MYC
FREE PATHWAY	0.056	Not reported by GSEA	0.043	Not reported by GSEA
TNFR1 PATHWAY	0.036	Not reported by GSEA	0.000	JUN, TNFRSF1A, LMNA, ARHGDIB, LMNB1, CASP8, RIPK1, FADD, MAP3K7, TNF, CRADD, BAG4, LMNB2
CELL SURVIVAL				
NFKB PATHWAY	0.000	MYD88, TNFRSF1A, FADD, RELA, IL1A, MAP3K14, NFKB1, RIPK1, TLR4, IRAK1, TRAF6, IL1R1, MAP3K7IP1, TNF, MAP3K7, MAP3K1	0.000	MYD99, TNFRSF1A, NFKBIA, RELA, RIPK1, TLR4, NFKB1, FADD, MAP3K7, TRAF6, IL1A, TNF, CHUK, IKBKG, MAP3K14
HSP27 PATHWAY	0.000	HSPB1, MAPKAPK2, FAS, MAPKAPK3, ACTA1, IL1A	0.000	HSPB1, FAS, MAPKAPK2, MAPKAPK3, ACTA1, IL1A, TNF, BCL2
MAPK PATHWAY	0.000	FOS, JUN, MAP2K3, MAPKAPK2, MAPKAPK3, SHC1, PRS6KA1, STAT1, MAP3K8, RELA, MAPK6, MAPK9, MAX, MAP3K6, MAP3K14, NFKB1, RIPK1, NFKBIA, TRAF2, MAPK4, MAPK12, MAPK7	0.036	FOS, MAPK23, JUN, MAPKAPK2, MAP3KA, MAPK6, MAP3K6, NFKBIA, RPS6KA1, MAPKAPK3, MAPK11, RELA, MAP4K5, MAP4K4, TGFB3, RIPK1, NFKB1, STAT1, MAP2K7, SP1, MAPK12, RPS6KB1, MEF2C, MAP3K7, RPS6KA3, TGFBR1, RPS6KB2, SHC1, CHUK, CREB1, MYC
P38 MAPK PATHWAY	0.031	CDKN1A, GADD45A, CDK2, IMP3, CCND1, PCNA, BAX	0.000	HSPB1, MAPKAPK2, DDIT3, HMGN1, TGFB3, RIPK1, CDC42, STAT1, MEF2C, MAP3K7, TGFBR1, SHC1, CREB1, MYC, ATF2, HSPB2

APPENDIX 1, *Continued*

Biocarta Pathway	WT P Value	WT Genes (with Core Enrichment)	KO P Value	KO Genes (with Core Enrichment)
GSK3 PATHWAY	0.000	CD14, LBP, MYD88, CCND1, RELA, FZD1, TIRAP, NFKB1, LY96, CTNNB1, TLR4	0.000	CD14, MYD88, TIRAP, RELA, TLR4, TOLLIP, NFKB1, LEF1, CCND1, CTNNB1, APC, PIK3CA, LY96, DVL1
SODD PATHWAY	0.000	TNFRSF1A, FADD, CASP9, RIPK1, TRAF2	0.038	TNFRSF1A, CASP8, RIPK1, FADD, TNF, BAG4
TNFR1 PATHWAY	*0.036*	*Not reported by GSEA*	*0.000*	*JUN, TNFRSF1A, LMNA, ARHGDIB, LMNB1, CASP8, RIPK1, FADD, MAP3K7, TNF, CRADD, BAG4, LMNB2*
OTHER				
MTA3 PATHWAY	0.000	HSPB1, TUBA6, GREB1	0.000	HSPB1, GREB1, TUBA6
NTHI PATHWAY	0.017	TLR2, DUSP1, MAP2K3, MYD88, TGFBR2, RELA, IL1B, MAP3K14, NFKB1, NFKBIA	0.019	TLR2, MAP2K3, MYD88, DUSP1, NFKBIA, TGFBR2, IL1B, MAPK11, RELA, NFKB1, MAP3K7, TNF, TGFBR1, CHUK
RNA PATHWAY	0.017	DNAJC3, RELA, EIF2S2, MAP3K14, NFKB1, NFKBIA	0.000	NFKBIA, RELA, NFKB1, DNAJC3, CHUK, IF2S2, MAP3K14, EIF2S1
RANKL PATHWAY	0.019	FOS, RELA, NFKB1, IFNAR2, TRAF6, TNFSF11, TNFRSF11A	0.000	FOS, RELA, NFKB1, TRAF6, TNFRSF11A
HIVNEF PATHWAY	0.036	ARHGDIB, LMNA, TNFRSF1A, FADD, LMNB1, CDC2L1, CASP8, RELA, MAP3K14, NFKB1, RIPK1, NFKBIA, GSN, TRAF2, CASP9, MAP2K7, LMNB2, BIRC4, CASP3, TNF, MDM2, MAP3K1, CASP7, CASP2, PTK2, CASP6, APAF1, BIRC3	0.000	TNFRSF1A, LMNA, ARHGDIB, LMNB1, PRKCD, NFKBIA, CDC2L1, RELA, CASP8, RIPK1, NFKB1, MAP2K7, MDM2, FADD, PTK2, TNF, CRADD, BCL2, CHUK, BAG4, LMNB2, MAP3K14, GSN
GLEEVEC PATHWAY	0.019	FOS, JUN, STAT1, STAT5A	0.000	Not reported by GSEA

REFERENCES

Allan Institute for Brain Science Allan Mouse Brain Atlas. Http://Mouse.Brain-Map.org.

Amaral, D.G., and Witter, M.P. (1989). The three-dimensional organization of the hippocampal formation: a review of anatomical data. Neuroscience *31*, 571–591.

Avoli, M., and Barbarosie, M. (1999). Interictal-ictal interactions and limbic seizure generation. Rev. Neurol. (Paris) *155*, 468–471.

Avoli, M., Biagini, G., and de Curtis, M. (2006). Do interictal spikes sustain seizures and epileptogenesis? Epilepsy Curr *6*, 203–207.

Babb, T.L., and Brown, W.J. (1986). Neuronal, dendritic, and vascular profiles of human temporal lobe epilepsy correlated with cellular physiology in vivo. Adv Neurol *44*, 949–966.

Belmaker, R.H. (2004). Bipolar disorder. N. Engl. J. Med. *351*, 476–486.

Ben-Ari, Y. (1985). Limbic seizure and brain damage produced by kainic acid: mechanisms and relevance to human temporal lobe epilepsy. Neuroscience *14*, 375–403.

Bettler, B., Boulter, J., Hermans-Borgmeyer, I., O'Shea-Greenfield, A., Deneris, E.S., Moll, C., Borgmeyer, U., Hollmann, M., and Heinemann, S. (1990). Cloning of a novel glutamate receptor subunit, GluR5: expression in the nervous system during development. Neuron *5*, 583–595.

Bliss, T.V., and Collingridge, G.L. (1993). A synaptic model of memory: long-term potentiation in the hippocampus. Nature *361*, 31–39.

Bogoyevitch, M.A., Boehm, I., Oakley, A., Ketterman, A.J., and Barr, R.K. (2004). Targeting the JNK MAPK cascade for inhibition: basic science and therapeutic potential. Biochim Biophys Acta *1697*, 89–101.

Bortolotto, Z.A., Lauri, S., Isaac, J.T.R., and Collingridge, G.L. (2003). Kainate receptors and the induction of mossy fibre long-term potentiation. Philosophical Transactions of the Royal Society B: Biological Sciences *358*, 657–666.

Brecht, S., Kirchhof, R., Chromik, A., Willesen, M., Nicolaus, T., Raivich, G., Wessig, J., Waetzig, V., Goetz, M., Claussen, M., et al. (2005). Specific pathophysiological functions of JNK isoforms in the brain. Eur J Neurosci *21*, 363–377.

Brody, D.L., and Holtzman, D.M. (2006). Morris water maze search strategy analysis in PDAPP mice before and after experimental traumatic brain injury. Exp Neurol *197*, 330–340.

Brown, T.H., Kairiss, E.W., and Keenan, C.L. (1990). Hebbian synapses: biophysical mechanisms and algorithms. Annu Rev Neurosci *13*, 475–511.

Camilo, O., and Goldstein, L.B. (2004). Seizures and epilepsy after ischemic stroke. Stroke *35*, 1769–1775.

Castillo, P.E., Malenka, R.C., and Nicoll, R.A. (1997). Kainate receptors mediate a slow postsynaptic current in hippocampal CA3 neurons. Nature *388*, 182–186.

Catches, J.S., Xu, J., and Contractor, A. (2012). Genetic ablation of the GluK4 kainate receptor subunit causes anxiolytic and antidepressant-like behavior in mice. Behav Brain Res *228*, 406–414.

Chang, L., Kamata, H., Solinas, G., Luo, J.-L., Maeda, S., Venuprasad, K., Liu, Y.-C., and Karin, M. (2006). The E3 ubiquitin ligase itch couples JNK activation to TNFalpha-induced cell death by inducing c-FLIP(L) turnover. Cell *124*, 601–613.

Contractor, A., Sailer, A.W., Darstein, M., Maron, C., Xu, J., Swanson, G.T., and Heinemann, S.F. (2003). Loss of kainate receptor-mediated heterosynaptic facilitation of mossy-fiber synapses in KA2-/- mice. J Neurosci *23*, 422–429.

Cossart, R., Tyzio, R., Dinocourt, C., Esclapez, M., Hirsch, J.C., Ben-Ari, Y., and Bernard, C. (2001). Presynaptic kainate receptors that enhance the release of GABA on CA1 hippocampal interneurons. Neuron *29*, 497–508.

Coussen, F., and Mulle, C. (2006). Kainate receptor-interacting proteins and membrane trafficking. Biochem Soc Trans *34*, 927–930.

Darstein, M., Petralia, R.S., Swanson, G.T., Wenthold, R.J., and Heinemann, S.F. (2003). Distribution of kainate receptor subunits at hippocampal mossy fiber synapses. J Neurosci *23*, 8013–8019.

Daumas, S., Halley, H., and Lassalle, J.-M. (2004). Disruption of hippocampal CA3 network: effects on episodic-like memory processing in C57BL/6J mice. Eur J Neurosci *20*, 597–600.

Doolan, P., Clynes, M., Kennedy, S., Mehta, J.P., Germano, S., Ehrhardt, C., Crown, J., and O'Driscoll, L. (2009). TMEM25, REPS2 and Meis 1: favourable prognostic and predictive biomarkers for breast cancer. Tumour Biol. *30*, 200–209.

El-Hayek, Y.H., Wu, C., Chen, R., Al-Sharif, A.R., Huang, S., Patel, N., Du, C., Ruff, C.A., Fehlings, M.G., Carlen, P.L., et al. (2011). Acute postischemic seizures are associated with increased mortality and brain damage in adult mice. Cereb Cortex *21*, 2863–2875.

Engel, J. (1993). Update on surgical treatment of the epilepsies. Summary of the Second International Palm Desert Conference on the Surgical Treatment of the Epilepsies (1992). pp. 1612–1617.

Falconer, M.A., Serafetinides, E.A., and Corsellis, J.A. (1964). Etiology and Pathogenesis of Temporal Lobe Epilepsy. Arch. Neurol. *10*, 233–248.

Fernandes, H.B., Catches, J.S., Petralia, R.S., Copits, B.A., Xu, J., Russell, T.A., Swanson, G.T., and Contractor, A. (2009). High-Affinity Kainate Receptor Subunits Are Necessary for Ionotropic but Not Metabotropic Signaling. Neuron *63*, 818–829.

Florian, C., and Roullet, P. (2004). Hippocampal CA3-region is crucial for acquisition and memory consolidation in Morris water maze task in mice. Behav Brain Res *154*, 365–374.

Fogarty, D., Perez-Cerda, F., and Matute, C. (2000). KA1-like kainate receptor subunit immunoreactivity in neurons and glia using a novel anti-peptide antibody. Brain Res Mol Brain Res *81*, 164–176.

Frerking, M., and Ohliger-Frerking, P. (2002). AMPA receptors and kainate receptors encode different features of afferent activity. J Neurosci *22*, 7434–7443.

Frerking, M., Schmitz, D., Zhou, Q., Johansen, J., and Nicoll, R.A. (2001). Kainate receptors depress excitatory synaptic transmission at CA3-->CA1 synapses in the hippocampus via a direct presynaptic action. J Neurosci *21*, 2958–2966.

Gardner-Medwin, A.R. (1976). The Recall of Events through the Learning of Associations between their Parts. Proceedings of the Royal Society B: Biological Sciences *194*, 375–402.

Geyer, M.A., McIlwain, K.L., and Paylor, R. (2002). Mouse genetic models for prepulse inhibition: an early review. Mol Psychiatry *7*, 1039–1053.

Geyer, M.A., Swerdlow, N.R., Mansbach, R.S., and Braff, D.L. (1990). Startle response models of sensorimotor gating and habituation deficits in schizophrenia. Brain Res Bull *25*, 485–498.

Gunduz-Bruce, H. (2009). The acute effects of NMDA antagonism: from the rodent to the human brain. Brain Res Rev *60*, 279–286.

Gupta, S., Barrett, T., Whitmarsh, A.J., Cavanagh, J., Sluss, H.K., Dérijard, B., and Davis, R.J. (1996). Selective interaction of JNK protein kinase isoforms with transcription factors. Embo J *15*, 2760–2770.

Hampson, D.R., Huie, D., and Wenthold, R.J. (1987). Solubilization of kainic acid binding sites from rat brain. J Neurochem *49*, 1209–1215.

Hatazaki, S., Bellver-Estelles, C., Jimenez-Mateos, E.M., Meller, R., Bonner, C., Murphy, N., Matsushima, S., Taki, W., Prehn, J.H.M., Simon, R.P., et al. (2007). Microarray profile of seizure damage-refractory hippocampal CA3 in a mouse model of epileptic preconditioning. Neuroscience *150*, 467–477.

Herb, A., Burnashev, N., Werner, P., Sakmann, B., Wisden, W., and Seeburg, P.H. (1992). The KA-2 subunit of excitatory amino acid receptors shows widespread expression in brain and forms ion channels with distantly related subunits. Neuron *8*, 775–785.

Hirai, S.I., Katoh, M., Terada, M., Kyriakis, J.M., Zon, L.I., Rana, A., Avruch, J., and Ohno, S. (1997). MST/MLK2, a member of the mixed lineage kinase family, directly phosphorylates and activates SEK1, an activator of c-Jun N-terminal kinase/stress-activated protein kinase. J Biol Chem *272*, 15167–15173.

Hollmann, M., Maron, C., and Heinemann, S. (1994). N-glycosylation site tagging suggests a three transmembrane domain topology for the glutamate receptor GluR1. Neuron *13*, 1331–1343.

Huang, D.W., Sherman, B.T., and Lempicki, R.A. (2008). Systematic and integrative analysis of large gene lists using DAVID bioinformatics resources. Nat Protoc *4*, 44–57.

Huang, D.W., Sherman, B.T., Tan, Q., Collins, J.R., Alvord, W.G., Roayaei, J., Stephens, R., Baseler, M.W., Lane, H.C., and Lempicki, R.A. (2007). The DAVID Gene Functional Classification Tool: a novel biological module-centric algorithm to functionally analyze large gene lists. Genome Biol *8*, R183.

Huettner, J.E. (2003). Kainate receptors and synaptic transmission. Progress in Neurobiology *70*, 387–407.

Hughes, R.N. (2004). The value of spontaneous alternation behavior (SAB) as a test of retention in pharmacological investigations of memory. Neurosci Biobehav Rev *28*, 497–505.

Hughes, T.E. (1994). Transmembrane topology of the glutamate receptors. A tale of novel twists and turns. J Mol Neurosci *5*, 211–217.

Hunsaker, M.R., Tran, G.T., and Kesner, R.P. (2009). A behavioral analysis of the role of CA3 and CA1 subcortical efferents during classical fear conditioning. Behav Neurosci *123*, 624–630.

Hunsberger, J.G., Bennett, A.H., Selvanayagam, E., Duman, R.S., and Newton, S.S. (2005). Gene profiling the response to kainic acid induced seizures. Brain Res Mol Brain Res *141*, 95–112.

Hunter, R.G., Bellani, R., Bloss, E., Costa, A., McCarthy, K., and McEwen, B.S. (2009). Regulation of Kainate Receptor Subunit mRNA by Stress and Corticosteroids in the Rat Hippocampus. PLoS ONE *4*, e4328.

Ishizuka, N., Weber, J., and Amaral, D.G. (1990). Organization of intrahippocampal projections originating from CA3 pyramidal cells in the rat. J Comp Neurol *295*, 580–623.

Jacob, C.P., Koutsilieri, E., Bartl, J., Neuen-Jacob, E., Arzberger, T., Zander, N., Ravid, R., Roggendorf, W., Riederer, P., and Grünblatt, E. (2007). Alterations in expression of glutamatergic transporters and receptors in sporadic Alzheimer's disease. J. Alzheimers Dis. *11*, 97–116.

Jiang, H.-X., Guan, Q.-H., Pei, D.-S., and Zhang, G.-Y. (2007). Functional cooperation between KA2 and GluR6 subunits is involved in the ischemic brain injury. J Neurosci Res *85*, 2960–2970.

Katoh, M., and Katoh, M. (2004). Identification and characterization of human TMEM25 and mouse Tmem25 genes in silico. Oncol. Rep. *12*, 429–433.

Kesner, R.P. (2007). Behavioral functions of the CA3 subregion of the hippocampus. Learn Mem *14*, 771–781.

Kim, J., and Sharma, R.P. (2004). Calcium-mediated activation of c-Jun NH2-terminal kinase (JNK) and apoptosis in response to cadmium in murine macrophages. Toxicol. Sci. *81*, 518–527.

Knight, H.M., Walker, R., James, R., Porteous, D.J., Muir, W.J., Blackwood, D.H.R., and Pickard, B.S. (2011). GRIK4/KA1 protein expression in human brain and correlation with bipolar disorder risk variant status. American Journal of Medical Genetics Part B, Neuropsychiatric Genetics : the Official Publication of the International Society of Psychiatric Genetics.

Ko, S., Zhao, M.-G., Toyoda, H., Qiu, C.-S., and Zhuo, M. (2005). Altered behavioral responses to noxious stimuli and fear in glutamate receptor 5 (GluR5)- or GluR6-deficient mice. J Neurosci *25*, 977–984.

Koch, M. (1996). The septohippocampal system is involved in prepulse inhibition of the acoustic startle response in rats. Behav Neurosci *110*, 468–477.

Kolomeets, N.S., Orlovskaya, D.D., and Uranova, N.A. (2007). Decreased numerical density of CA3 hippocampal mossy fiber synapses in schizophrenia. Synapse *61*, 615–621.

Köhler, M., Burnashev, N., Sakmann, B., and Seeburg, P.H. (1993). Determinants of Ca2+ permeability in both TM1 and TM2 of high affinity kainate receptor channels: diversity by RNA editing. Neuron *10*, 491–500.

Krystal, J.H., Karper, L.P., Seibyl, J.P., Freeman, G.K., Delaney, R., Bremner, J.D., Heninger, G.R., Bowers, M.B., and Charney, D.S. (1994). Subanesthetic effects of the noncompetitive NMDA antagonist, ketamine, in humans. Psychotomimetic, perceptual, cognitive, and neuroendocrine responses. Arch. Gen. Psychiatry *51*, 199–214.

Lau, A., and Tymianski, M. (2010). Glutamate receptors, neurotoxicity and neurodegeneration. Pflugers Arch *460*, 525–542.

Lein, E.S., Zhao, X., and Gage, F.H. (2004). Defining a molecular atlas of the hippocampus using DNA microarrays and high-throughput in situ hybridization. J Neurosci *24*, 3879–3889.

Leuschner, W.D., and Hoch, W. (1999). Subtype-specific assembly of alpha-amino-3-hydroxy-5-methyl-4-isoxazole propionic acid receptor subunits is mediated by their n-terminal domains. J Biol Chem *274*, 16907–16916.

Lin, A. (2003). Activation of the JNK signaling pathway: breaking the brake on apoptosis. Bioessays *25*, 17–24.

Liu, X.-M., Pei, D.-S., Guan, Q.-H., Sun, Y.-F., Wang, X.-T., Zhang, Q.-X., and Zhang, G.-Y. (2006). Neuroprotection of Tat-GluR6-9c against neuronal death induced by kainate in rat hippocampus via nuclear and non-nuclear pathways. J Biol Chem *281*, 17432–17445.

Lodge, D. (2009). The history of the pharmacology and cloning of ionotropic glutamate receptors and the development of idiosyncratic nomenclature. Neuropharmacology *56*, 6–21.

London, E.D., and Coyle, J.T. (1979). Specific binding of [3H]kainic acid to receptor sites in rat brain. Mol Pharmacol *15*, 492–505.

Lopes da Silva, F.H., and Arnolds, D.E. (1978). Physiology of the hippocampus and related structures. Annu Rev Physiol *40*, 185–216.

Lucas, D., and Newhouse, J. (1957). The toxic effect of sodium L-glutamate on the inner layers of the retina. AMA Arch Ophthalmol *58*, 193–201.

Lucifora, S., Willcockson, H.H., Lu, C.-R., Darstein, M., Phend, K.D., Valtschanoff, J.G., and Rustioni, A. (2006). Presynaptic low- and high-affinity kainate receptors in nociceptive spinal afferents. Pain *120*, 97–105.

Maren, S. (2008). Pavlovian fear conditioning as a behavioral assay for hippocampus and amygdala function: cautions and caveats. Eur J Neurosci *28*, 1661–1666.

Martin, J.H., Mohit, A.A., and Miller, C.A. (1996). Developmental expression in the mouse nervous system of the p493F12 SAP kinase. Brain Res Mol Brain Res *35*, 47–57.

McKhann, G.M., Wenzel, H.J., Robbins, C.A., Sosunov, A.A., and Schwartzkroin, P.A. (2003). Mouse strain differences in kainic acid sensitivity, seizure behavior, mortality, and hippocampal pathology. Neuroscience *122*, 551–561.

McLin, J.P., and Steward, O. (2006). Comparison of seizure phenotype and neurodegeneration induced by systemic kainic acid in inbred, outbred, and hybrid mouse strains. Eur J Neurosci *24*, 2191–2202.

McNaughton, B.L., and Morris, R.G.M. (2002). Hippocampal synaptic enhancement and information storage within a distributed memory system. Trends Neurosci *10*, 408–415.

Melyan, Z., and Lancaster, B. (2004). Metabotropic regulation of intrinsic excitability by synaptic activation of kainate receptors. The Journal of Neuroscience.

Melyan, Z., Wheal, H.V., and Lancaster, B. (2002). Metabotropic-mediated kainate receptor regulation of IsAHP and excitability in pyramidal cells. Neuron *34*, 107–114.

Morris, R.G.M. (2003). Long-term potentiation and memory. Philos Trans R Soc Lond, B, Biol Sci *358*, 643–647.

Mulle, C., Sailer, A., Pérez-Otaño, I., Dickinson-Anson, H., Castillo, P.E., Bureau, I., Maron, C., Gage, F.H., Mann, J.R., Bettler, B., et al. (1998). Altered synaptic physiology and reduced susceptibility to kainate-induced seizures in GluR6-deficient mice. Nature *392*, 601–605.

Nadler, J.V. (1981). Minireview. Kainic acid as a tool for the study of temporal lobe epilepsy. Life Sci. *29*, 2031–2042.

Nagata, K.I., Puls, A., Futter, C., Aspenstrom, P., Schaefer, E., Nakata, T., Hirokawa, N., and Hall, A. (1998). The MAP kinase kinase kinase MLK2 co-localizes with activated JNK along microtubules and associates with kinesin superfamily motor KIF3. Embo J *17*, 149–158.

Nasu-Nishimura, Y., Hurtado, D., Braud, S., Tang, T.T.-T., Isaac, J.T.R., and Roche, K.W. (2006). Identification of an endoplasmic reticulum-retention motif in an intracellular loop of the kainate receptor subunit KA2. J Neurosci *26*, 7014–7021.

Olney, J.W. (1969). Brain lesions, obesity, and other disturbances in mice treated with monosodium glutamate. Science *164*, 719–721.

Oswald, R.E., Ahmed, A., Fenwick, M.K., and Loh, A.P. (2007). Structure of glutamate receptors. Current Drug Targets *8*, 573–582.

Paddock, S., Laje, G., Charney, D., Rush, A.J., Wilson, A.F., Sorant, A.J.M., Lipsky, R., Wisniewski, S.R., Manji, H., and McMahon, F.J. (2007). Association of GRIK4 with outcome of antidepressant treatment in the STAR*D cohort. The American Journal of Psychiatry *164*, 1181–1188.

Palomo, T., Kostrzewa, R.M., Beninger, R.J., and Archer, T. (2008). Schizopsychotic symptom-profiles and biomarkers: beacons in diagnostic labyrinths. Neurotoxicity Research *14*, 79–96.

Perry, W., and Braff, D.L. (1994). Information-processing deficits and thought disorder in schizophrenia. The American Journal of Psychiatry *151*, 363–367.

Perry, W., Minassian, A., Feifel, D., and Braff, D.L. (2001). Sensorimotor gating deficits in bipolar disorder patients with acute psychotic mania. Biological Psychiatry *50*, 418–424.

Pfaffl, M.W., Horgan, G.W., and Dempfle, L. (2002). Relative expression software tool (REST) for group-wise comparison and statistical analysis of relative expression results in real-time PCR. Nucleic Acids Res *30*, e36.

Pickard, B.S., Knight, H.M., Hamilton, R.S., Soares, D.C., Walker, R., Boyd, J.K.F., Machell, J., Maclean, A., McGhee, K.A., Condie, A., et al. (2008). A common variant in the 3'UTR of the GRIK4 glutamate receptor gene affects transcript abundance and protects against bipolar disorder. Proc Natl Acad Sci USA *105*, 14940–14945.

Pickard, B.S., Malloy, M.P., Christoforou, A., Thomson, P.A., Evans, K.L., Morris, S.W., Hampson, M., Porteous, D.J., Blackwood, D.H.R., and Muir, W.J. (2006). Cytogenetic and genetic evidence supports a role for the kainate-type glutamate receptor gene, GRIK4, in schizophrenia and bipolar disorder. Mol Psychiatry *11*, 847–857.

Porsolt, R.D., Bertin, A., and Jalfre, M. (1977). Behavioral despair in mice: a primary screening test for antidepressants. Arch Int Pharmacodyn Ther *229*, 327–336.

Porter, R.H., Eastwood, S.L., and Harrison, P.J. (1997). Distribution of kainate receptor subunit mRNAs in human hippocampus, neocortex and cerebellum, and bilateral reduction of hippocampal GluR6 and KA2 transcripts in schizophrenia. Brain Res *751*, 217–231.

Racine, R.J. (1972). Modification of seizure activity by electrical stimulation. II. Motor seizure. Electroencephalogr Clin Neurophysiol *32*, 281–294.

Reijmers, L.G., Vanderheyden, P.M., and Peeters, B.W. (1995). Changes in prepulse inhibition after local administration of NMDA receptor ligands in the core region of the rat nucleus accumbens. Eur J Pharmacol *272*, 131–138.

Ren, Z., Riley, N.J., Needleman, L.A., Sanders, J.M., Swanson, G.T., and Marshall, J. (2003). Cell surface expression of GluR5 kainate receptors is regulated by an endoplasmic reticulum retention signal. J Biol Chem *278*, 52700–52709.

Risbrough, V.B., Hauger, R.L., Pelleymounter, M.A., and Geyer, M.A. (2003). Role of corticotropin releasing factor (CRF) receptors 1 and 2 in CRF-potentiated acoustic startle in mice. Psychopharmacology (Berl) *170*, 178–187.

Rodriguez-Moreno, A., Herreras, O., and Lerma, J. (1997). Kainate receptors presynaptically downregulate GABAergic inhibition in the rat hippocampus. Neuron *19*, 893–901.

Rodríguez-Moreno, A., and Sihra, T.S. (2011). Metabotropic actions of kainate receptors in the control of glutamate release in the hippocampus. Adv Exp Med Biol *717*, 39–48.

Sakimura, K., Morita, T., Kushiya, E., and Mishina, M. (1992). Primary structure and expression of the gamma 2 subunit of the glutamate receptor channel selective for kainate. Neuron *8*, 267–274.

Schaeffer, H.J., and Weber, M.J. (1999). Mitogen-activated protein kinases: specific messages from ubiquitous messengers. Mol. Cell. Biol. *19*, 2435–2444.

Schmitz, D., Frerking, M., and Nicoll, R.A. (2000). Synaptic activation of presynaptic kainate receptors on hippocampal mossy fiber synapses. Neuron *27*, 327–338.

Schmued, L.C., Stowers, C.C., Scallet, A.C., and Xu, L. (2005). Fluoro-Jade C results in ultra high resolution and contrast labeling of degenerating neurons. Brain Res *1035*, 24–31.

Shaltiel, G., Maeng, S., Malkesman, O., Pearson, B., Schloesser, R.J., Tragon, T., Rogawski, M., Gasior, M., Luckenbaugh, D., Chen, G., et al. (2008). Evidence for the involvement of the kainate receptor subunit GluR6 (GRIK2) in mediating behavioral displays related to behavioral symptoms of mania. Mol Psychiatry *13*, 858–872.

Sharma, A.K., Reams, R.Y., Jordan, W.H., Miller, M.A., Thacker, H.L., and Snyder, P.W. (2007). Mesial temporal lobe epilepsy: pathogenesis, induced rodent models and lesions. Toxicologic Pathology *35*, 984–999.

Sihra, T.S., and Rodríguez-Moreno, A. (2011). Metabotropic actions of kainate receptors in the control of GABA release. Adv Exp Med Biol *717*, 1–10.

Sokolov, B.P. (1998). Expression of NMDAR1, GluR1, GluR7, and KA1 glutamate receptor mRNAs is decreased in frontal cortex of “neuroleptic-free” schizophrenics: evidence on reversible up-regulation by typical neuroleptics. J Neurochem *71*, 2454–2464.

Steffenach, H.-A., Sloviter, R.S., Moser, E.I., and Moser, M.-B. (2002). Impaired retention of spatial memory after transection of longitudinally oriented axons of hippocampal CA3 pyramidal cells. Proc Natl Acad Sci USA *99*, 3194–3198.

Stone, M., Gabrieli, J.D., Stebbins, G.T., and Sullivan, E.V. (1998). Working and strategic memory deficits in schizophrenia. Neuropsychology *12*, 278–288.

Stupien, G., Florian, C., and Roullet, P. (2003). Involvement of the hippocampal CA3-region in acquisition and in memory consolidation of spatial but not in object information in mice. Neurobiol Learn Mem *80*, 32–41.

Subramanian, A., Tamayo, P., Mootha, V.K., Mukherjee, S., Ebert, B.L., Gillette, M.A., Paulovich, A., Pomeroy, S.L., Golub, T.R., Lander, E.S., et al. (2005). Gene set enrichment analysis: a knowledge-based approach for interpreting genome-wide expression profiles. Proc Natl Acad Sci USA *102*, 15545–15550.

Telfeian, A.E., Federoff, H.J., Leone, P., During, M.J., and Williamson, A. (2000). Overexpression of GluR6 in rat hippocampus produces seizures and spontaneous nonsynaptic bursting in vitro. Neurobiol Dis *7*, 362–374.

Tian, H., Zhang, Q.-G., Zhu, G.-X., Pei, D.-S., Guan, Q.-H., and Zhang, G.-Y. (2005). Activation of c-Jun NH2-terminal kinase 3 is mediated by the GluR6.PSD-95.MLK3 signaling module following cerebral ischemia in rat hippocampus. Brain Res *1061*, 57–66.

Tokuhara, D., Sakuma, S., Hattori, H., Matsuoka, O., and Yamano, T. (2007). Kainic acid dose affects delayed cell death mechanism after status epilepticus. Brain Dev. *29*, 2–8.

Tournier, C., Hess, P., Yang, D.D., Xu, J., Turner, T.K., Nimnual, A., Bar-Sagi, D., Jones, S.N., Flavell, R.A., and Davis, R.J. (2000). Requirement of JNK for stress-induced activation of the cytochrome c-mediated death pathway. Science *288*, 870–874.

Valluru, L., Xu, J., Zhu, Y., Yan, S., Contractor, A., and Swanson, G.T. (2005). Ligand binding is a critical requirement for plasma membrane expression of heteromeric kainate receptors. J Biol Chem *280*, 6085–6093.

van den Buuse, M. (2010). Modeling the positive symptoms of schizophrenia in genetically modified mice: pharmacology and methodology aspects. Schizophr Bull *36*, 246–270.

van der Kooij, M.A., Groenendaal, F., Kavelaars, A., Heijnen, C.J., and van Bel, F. (2008). Neuroprotective properties and mechanisms of erythropoietin in in vitro and in vivo experimental models for hypoxia/ischemia. Brain Res Rev *59*, 22–33.

van der Weerd, L., Tariq Akbar, M., Aron Badin, R., Valentim, L.M., Thomas, D.L., Wells, D.J., Latchman, D.S., Gadian, D.G., Lythgoe, M.F., and de Belleroche, J.S. (2010). Overexpression of heat shock protein 27 reduces cortical damage after cerebral ischemia. J Cereb Blood Flow Metab *30*, 849–856.

Vannucci, S.J., Willing, L.B., Goto, S., Alkayed, N.J., Brucklacher, R.M., Wood, T.L., Towfighi, J., Hurn, P.D., and Simpson, I.A. (2001). Experimental stroke in the female diabetic, db/db, mouse. J Cereb Blood Flow Metab *21*, 52–60.

Vignes, M., and Collingridge, G.L. (1997). The synaptic activation of kainate receptors. Nature *388*, 179–182.

Vincent, P., and Mulle, C. (2009). Kainate receptors in epilepsy and excitotoxicity. Neuroscience *158*, 309–323.

Vivithanaporn, P., Yan, S., and Swanson, G.T. (2006). Intracellular trafficking of KA2 kainate receptors mediated by interactions with coatomer protein complex I (COPI) and 14-3-3 chaperone systems. J Biol Chem *281*, 15475–15484.

Wang, Q., Yu, S., Simonyi, A., Sun, G.Y., and Sun, A.Y. (2005). Kainic acid-mediated excitotoxicity as a model for neurodegeneration. Mol Neurobiol *31*, 3–16.

Werner, P., Voigt, M., Keinänen, K., Wisden, W., and Seeburg, P.H. (1991). Cloning of a putative high-affinity kainate receptor expressed predominantly in hippocampal CA3 cells. Nature *351*, 742–744.

Whalley, H.C., Pickard, B.S., McIntosh, A.M., Zuliani, R., Johnstone, E.C., Blackwood, D.H.R., Lawrie, S.M., Muir, W.J., and Hall, J. (2009a). A GRIK4 variant conferring protection against bipolar disorder modulates hippocampal function. Mol Psychiatry *14*, 467–468.

Whalley, H.C., Pickard, B.S., McIntosh, A.M., Zuliani, R., Johnstone, E.C., Blackwood, D.H.R., Lawrie, S.M., Muir, W.J., and Hall, J. (2009b). Modulation of hippocampal activation by genetic variation in the GRIK4 gene. Mol Psychiatry *14*, 465.

Whitmarsh, A.J., and Davis, R.J. (1996). Transcription factor AP-1 regulation by mitogen-activated protein kinase signal transduction pathways. J. Mol. Med. *74*, 589–607.

Wo, Z.G., and Oswald, R.E. (1994). Transmembrane topology of two kainate receptor subunits revealed by N-glycosylation. Proc Natl Acad Sci USA *91*, 7154–7158.

Yan, S., Sanders, J.M., Xu, J., Zhu, Y., Contractor, A., and Swanson, G. (2004). A C-Terminal Determinant of GluR6 Kainate Receptor Trafficking. J Neurosci *24*, 679–691.

Yang, L., Mao, L., Chen, H., Catavsan, M., Kozinn, J., Arora, A., Liu, X., and Wang, J.Q. (2006). A signaling mechanism from G alpha q-protein-coupled metabotropic glutamate receptors to gene expression: role of the c-Jun N-terminal kinase pathway. Journal of Neuroscience *26*, 971–980.